

ABSTRACT

Title of dissertation: PREDICTING WATER TABLE
FLUCTUATIONS USING ARTIFICIAL
NEURAL NETWORK

Chung-Yu Wu, Ph.D., 2008

Dissertation directed by: Professor Adel Shirmohammadi
Fischell Department of Bioengineering

Correctly forecasting groundwater level fluctuations can assist water resource managers and engineers in efficient allocation of the regional water needs. Modeling such systems based on satellite remotely sensed data may be a viable option to predict water table fluctuations. Two types of water table prediction models based on Artificial Neural Network (ANN) technology were developed to simulate the water table fluctuations at two well sites in Maryland. One was based on the relationship between the variations of brightness temperature and water table depth. The other one was based on the relationship between the changes of soil moisture and water table depth. Water table depths recorded at these two wells, brightness temperature retrieved from the Advanced Microwave Scanning Radiometer, and soil moisture data produced by the Land Data Assimilation System were used to train and validate the models. Three models were constructed and they all performed well in predicting water table fluctuations. The root mean square errors of the water table depth

forecasts for 12 months were between 0.043m and 0.047m for these three models. The results of sensitivity test showed that the models were more sensitive to the uncertainty in water table depth than to that in brightness temperature or in soil moisture content. This suggests that for situations where high resolution remotely sensed data is not available, an ANN water table prediction model still can be built if the trend of the time series of the data, such as brightness temperature or soil moisture, over the study site correlates well with the trend of the time series of the ground measurement at the study site. An extension of the study to a regional scale was also performed at 12 available well sites in Piedmont Plateau, Maryland. Hydrologic soil types, LDAS soil moistures, and water table depths at these locations were used in the ANN modeling. The root mean square error of one month long water table depth forecast was 0.142m. However, the accuracy of the monthly forecast decreases with the increase of time. A further study to improve the accuracy of long-term water table fluctuation forecast is recommended.

**PREDICTING WATER TABLE FLUCTUATIONS USING
ARTIFICIAL NEURAL NETWORK**

By

Chung-Yu Wu

Dissertation submitted to the Faculty of the Graduate School of the
University of Maryland, College Park, in partial fulfillment
of the requirements for the degree of
Doctor of Philosophy
2008

Advisory Committee:

Professor Adel Shirmohammadi, Chair
Associate Professor Kaye L. Brubaker
Associate Professor Hubert J. Montas
Dr. Ali M. Sadeghi, Soil Physicist
Professor Fredrick W. Wheaton

© Copyright by
Chung-Yu Wu
2008

Acknowledgements

My deepest gratitude is to my major advisor, Dr. Adel Shirmohammadi. His patience, support, encouragement, and guidance helped me overcome many struggles and complete this dissertation. I would also like to express my gratefulness to my advisory committee, Dr. Kaye Brubaker, Dr. Hubert Montas, Dr. Ali Sadeghi, and Dr. Fredrick Wheaton for their greatly appreciated advice throughout the course of this study. I would like to express my heartfelt gratitude to my wife, Hsiu-Lan. Without her understanding, encouragement, and support, I wouldn't have a chance to complete this dissertation. I would also like to thank my children, Pei-Yun and Tung-Jim, for their understanding and support during this long period of study. Finally, I would like to thank all the people who have helped me throughout this study.

Table of Contents

Acknowledgements	ii
Table of Contents	iii
List of Tables	v
List of Figures	vii
Chapter 1: Introduction	1
Chapter 2: Background	4
2.1 Literature Review	4
2.2 Artificial Neural Network	11
2.3 Groundwater in Maryland	18
Chapter 3: Approach	23
3.1 Theory	23
3.2 ANN Model	31
3.3 Data Acquisition	38
3.3.1 Water Table Depth	38
3.3.2 Brightness Temperature Data	42
3.3.3 Soil Moisture Data	43
3.3.4 Soil Data	46
3.4 ANN Water Table Prediction Model	49
Chapter 4: Single Well ANN Water Table Prediction Modeling	51
4.1 Model Training and Results	53
Chapter 5: Regional Scale ANN Water Table Prediction Modeling	73
5.1 Model Training and Results	79
Chapter 6: Discussion	97
6.1 Single Well Modeling	97
6.2 Regional Scale Modeling	104
6.3 Determine Future Brightness Temperature and Soil Moisture	109
Chapter 7: Conclusions	113
Chapter 8: Suggestions for Further Study	115
Appendices	116
Appendix A: GrADS and FORTRAN Codes for Data Preparation	116
1. An example of GrADS format control filefor LADS data	116
2. An example of GrADS format control file for LDAS subsetted soil moisture data	117
3. An example of the GrADS script used to extract data from LDAS hourly soil moisture dataset at a well site	118
4. An example of the GrADS script used to extract data from LDAS hourly soil moisture dataset at a well site for each year	118
5. An example of the FORTRAN code used to generate monthly mean soil moisture dataset from LDAS hourly soil moisture dataset at a well site	121
6. An example of the Fortran code to generate water table on the first day of each month at selected well site	122
7. An example of the HDF script used to dump brightness temperature,	

latitude, and longitude from AMSR-E dataset	127
8. An example of satellite remote measuring time file for monthly brightness temperature data processing	128
9. An example of the FORTRAN code used to generate daily brightness temperature dataset	129
10. An example of the script to concatenate several files into one file	131
11. An example of the FORTRAN code used to generate daily brightness temperature data at a well site	132
12. An example of the FORTRAN code used to generate monthly mean brightness temperature data at a well site	135
Appendix B: Hydrologic Soil Group of Maryland	142
Appendix C: Comparison of Time Series of Water Table Change and Soil Moisture Variation at the 13 Well Sites in Piedmont Plateau, Maryland	143
Appendix D: Comparison of Training Outputs and Observations at 12 Available Wells in Piedmont Plateau, Maryland	150
Appendix E: Comparison of Validation Outputs and Observations at 12 Available Wells in Piedmont Plateau, Maryland	156
References	162

List of Tables

Table:	Page:
Table 1. Names, formations, longitudes, latitudes, and altitudes of Maryland water table wells.	40
Table 2a. Connection weights between input layer nodes and hidden layer nodes of Figure 17 for ANN model BA_BT_WT are shown here. The weight of bias input for each hidden layer node is also shown here.	58
Table 2b. Connection weights between hidden layer nodes and output layer node of Figure 17 for ANN model BA_BT_WT are shown here. The weight of bias input for the output layer node is also shown here.	58
Table 3a. Connection weights between input layer nodes and hidden layer nodes of Figure 17 for ANN model FR_BT_WT are shown here. The weight of bias input for each hidden layer node is also shown here.	63
Table 3b. Connection weights between hidden layer nodes and output layer node of Figure 17 for ANN model FR_BT_WT are shown here. The weight of bias input for the output layer node is also shown here.	63
Table 4a. Connection weights between input layer nodes and hidden layer nodes of Figure 27 for ANN model BA_SM_WT are shown here. The weight of bias input for each hidden layer node is also shown here.	70
Table 4b. Connection weights between hidden layer nodes and output layer node of Figure 27 for ANN model BA_SM_WT are shown here. The weight of bias input for the output layer node is also shown here.	70
Table 5. Names of the thirteen water table wells used in this regional scale study, the aquifers that these wells located, and their longitudes, latitudes, and surface elevations.	73
Table 6. Correlation coefficient of the water table depth changes of the first days of consecutive months and the monthly mean soil moisture	

variations for each individual water table well in the Piedmont Plateau, Maryland.	77
Table 7. Correlation coefficients between monthly soil moisture variations and water table changes of the first days of consecutive months at different soil layers.	77
Table 8. The RMS errors of training outputs and the correlations between training outputs and observations for ANN model training at different soil depths at 50,000 iterations.	82
Table 9. The RMS errors of training outputs and the correlation coefficients between training outputs and observations at the 13 well sites.	83
Table 10. The RMS errors of validation outputs at each individual well site (13 wells run).	84
Table 11a. Connection weights between input layer nodes and hidden layer nodes of Figure 35 for ANN model Regional_WTDP are shown here. The weight of bias input for each hidden layer node is also shown here.	86
Table 11b. Connection weights between hidden layer nodes and output layer node of Figure 35 for ANN model Regional_WTDP are shown here. The weight of bias input for the output layer node is also shown here.	87
Table 12. The RMS errors of training outputs and the correlation coefficients between training outputs and observations at the 12 well sites.	88
Table 13. The RMS errors of validation outputs at each individual well site (12 wells run).	91
Table 14. The monthly forecast results for the period from November 2001 to April 2002 at each individual well site. Month 1 is November 2001. Month 6 is April 2002.	92
Table 15. The monthly RMS errors of water table depth forecast at all 12 well sites.	96
Table 16. The percentage influence of input parameters on the model output.	104
Table 17. Maximum and minimum values of water table depth (WTD) data used in the model training, initial water table depth data used for the forecast, and the absolute difference between the first month's forecast and the observation at each well site.	108

List of Figures

Figure:	Page:
Figure 1. Schematic diagram of a biological neuron.	11
Figure 2. Schematic diagram of an artificial neuron.	13
Figure 3. Schematic diagram of a three-layer ANN.	15
Figure 4. Percentage of water supply from groundwater sources for various water sectors in the United States and Maryland in 2000.	20
Figure 5. Schematic water flow in the vadose zone. I represents infiltration. Ev represents evaporation. Et represents transpiration. R is the groundwater recharge. ΔS represents soil water change in vadose zone.	24
Figure 6. Schematic diagram showing the flow pathways of equations 7 and 8.	33
Figure 7. Schematic diagram showing the flow pathways of equations 9 and 10.	35
Figure 8. Locations of water table wells in the state of Maryland.	39
Figure 9. Comparison of the surface air temperature and the brightness temperature at Owings Mills (39.41N, 76.79W) in Baltimore County, Maryland for the period from September 2002 to September 2004.	43
Figure 10. Comparison of time series of LDAS soil moisture and SCAN soil moisture at 39.25N, 76.92W in Howard County, MD.	46
Figure 11. Soil map and the groundwater well locations in Baltimore County, Maryland.	48
Figure 12. Locations of the two water table wells for single well ANN modeling – BA EA 18 in Baltimore County, MD and FR DF 35 in Frederick County, MD.	51
Figure 13. Time series of the water table depth and brightness temperature at well site BA Ea 18 in Baltimore County, MD ($r = -0.17$).	54

Figure 14. Time series of the water table depth change and brightness temperature at well site BA Ea 18 in Baltimore County, MD (r = 0.53).	54
Figure 15. Time series of the water table depth and brightness temperature at well site FR Df 35 in Frederick County, MD (r = 0.05).	55
Figure 16. Time series of the water table depth change and brightness temperature at well site FR Df 35 in Frederick County, MD (r = 0.56).	55
Figure 17. Schematic diagram of a three layer ANN model which uses previous brightness temperature (BT1), current brightness temperature (BT2), water table depth change (WT2 – WT1), current water table depth (WT2), and subsequent brightness temperature (BT3) as input. The output is the prediction of the water table depth (WT3).	56
Figure 18. The ANN model training at well site BA Ea 18 reached a minimum root mean square error of 0.058m after 350,000 iterations.	57
Figure 19. Comparison of the model predicted water table depths during training with observations at well site BA Ea 18.	59
Figure 20. The scatter diagram of the model predicted water table depths during ANN training against the observed water table depths at well site BA Ea 18.	60
Figure 21. Comparison of the forecasted water table depths (by model BA_BT_WT) and the observed data at well site BA Ea 18. The forecast has a RMS error of 0.043m.	61
Figure 22. The ANN model training at well site FR Df 35 reached a minimum root mean square error of 0.04m after 350,000 iterations.	62
Figure 23. Comparison of the model predicted water table depths during ANN training with the observations at well site FR Df 35.	64
Figure 24. The scatter diagram of the model predicted water table depths during ANN training against the observed water table depths at well site FR Df 35.	65
Figure 25. Comparison of the forecasted water table depths (by model FR_BT_WT) and the observed data at well site FR Df 35. The forecast has a RMS error of 0.044m.	66

Figure 26. Time series of the water table depth and soil moisture content at well BA Ea 18 in Baltimore County, MD ($r = -0.65$).	67
Figure 27. Schematic diagram of a three layer ANN model using current soil moisture content, current water table depth, subsequent soil moisture content as input. The output is predicted water table depth.	68
Figure 28. The ANN model training at well site BA Ea 18 reached a minimum root mean square error of 0.059m after 400,000 iterations.	69
Figure 29. Comparison of the model predicted water table depths during ANN training with the observations at well site BA Ea 18.	71
Figure 30. The scatter diagram of the model predicted water table depths during ANN training against the observed water table depths at well site BA Ea 18.	71
Figure 31. Comparison of the forecasted water table depths (by model BA_SM_WT) and the observed data at well site BA Ea 18. The forecast has a RMS error of 0.047m.	72
Figure 32. Distribution of the water table wells in Piedmont Plateau, Maryland (between two green lines).	74
Figure 33. Time series of recorded and interpolated water tables at HO Bd 1 in Howard County, MD from 1994 to 2002.	75
Figure 34. Time series of the water table depth changes and soil moisture content variations for the months of November 1996 through October 2000 at water table well BA_CD_26 in Piedmont Plateau, Maryland.	76
Figure 35. Schematic diagram of a three layer ANN model using hydrologic soil type, monthly mean soil moisture content of the previous month, water table depth on the first day of the current month, and monthly mean soil moisture content of the current month as input. The output is the predicted water table depths on the first days of the subsequent months.	80
Figure 36. The RMS errors versus the number of iterations for the ANN training with soil moistures at four different layers.	81
Figure 37. The scatter diagram of the model predicted water table depths from ANN model training against the observed water table depths at all 12 wells.	86

Figure 38. Comparison of the model predicted water table depths during ANN training with the observations at well site BA Cd 26.	87
Figure 39. The scatter diagram of the model predicted water table depths from ANN model validation run against the observed water table depths at all 12 wells.	89
Figure 40. Comparison of the model predicted water table depths during the validation run with the observations at well site BA Cd 26.	90
Figure 41. Comparison of the predicted monthly water table depths generated by running ANN model BA_SM_WT with different errors on initial water table depths (WTD).	98
Figure 42. Comparison of the predicted monthly water table depths generated by running ANN model BA_BT_WT with different errors on initial water table depths (WTD).	99
Figure 43. Root mean square errors of 12 months' predicted water table depths generated by models BA_BT_WT and BA_SM_WT at different initial water table depth errors.	100
Figure 44. Comparison of the predicted monthly water table depths generated by running ANN model BA_BT_WT with different errors on initial brightness temperature (BT).	101
Figure 45. Comparison of the predicted monthly water table depths generated by running ANN model BA_SM_WT with different errors on initial soil moisture content (SM).	102
Figure 46. A scatter diagram of the model training output against the observation. Data from 13 well sites, including well MO Cc 14, were used in the input. A higher model outputs spread from 8m to 12m area are associated with the use of data at MO Cc 14.	105
Figure 47. Using the meteorological forecast data at the grid points, A, B, C, and D, around the well site, the needed data at the well site can be obtained by running the ANN model.	111

Chapter 1: Introduction

Groundwater contributes greatly to the amount of fresh water in the world. In many areas, groundwater is considered a major water source for both drinking and irrigation purposes. According to the UNDP (United Nations Development Programme) report, about 2 billion people, approximately one-third of the world's population, depend on groundwater supplies (UNDP et al., 2000). The United States uses more than 83.3 billion gallons of fresh groundwater each day for private and public water supplies, irrigation, livestock, manufacturing, mining, and other purposes (Hutson et al., 2004). In Maryland, the dependence on groundwater as a major fresh water resource is significant. Almost one-third of the state's 5.1 million citizens obtain their drinking water from underground sources (GWPC, 1999). In 1995, $0.931 \times 10^6 \text{ m}^3 / \text{d}$ (246 Mgal/d) of freshwater was withdrawn from groundwater sources in Maryland (Wheeler, 1995). Approximately 20% of statewide withdrawals were for agricultural uses (GWPC, 1999). The importance of groundwater for Marylanders' daily water needs is tremendous. However, the potential capability of groundwater for carrying and transporting polluted substances has raised serious concerns for the public. Groundwater quality has become an important issue for Maryland. High levels of nitrate and pesticides are discovered frequently in groundwater (Ator and Ferrari, 1997), and this causes serious problems for our environment and human health (Thorpe and Shirmohammadi, 2005). Groundwater storage and movement are mainly determined by relative water table variations at neighboring locations. Water table fluctuation also affects optimal crop production. Therefore, quick and accurate water

table prediction in areas under consideration can benefit water resource planners in developing better water resource planning, environmental engineers in designing better pollution control system, and farmers in developing earlier drainage and irrigation scheduling.

Physical models (Upadhyaya and Chauhan, 2001; and Song et al., 2007), water balance models (McCarthy and Skaggs, 1991; and Roulet 1991), and statistical regression models (Yakowitz, 1976; and Joginder et al, 1981) have been developed in the past to simulate water table variation in different areas. However, all of these models need extensive observations to perform the modeling. The physically based model also requires an explicit relationship between the input and output parameters. The presence of errors or uncertainties in the observations will result in errors or deviations in model output (Shirmohammadi et al., 2006). In addition to mathematical modeling, Artificial Neural Network (ANN) modeling provides another approach to predict water table fluctuation. ANN technology was developed around 65 years ago (McCulloch and Pitts, 1943). Since then, it has been widely used on pattern/speech recognition and image/signal processing in a variety of fields (Widrow and Lehr, 1992). The application of ANN in hydrology started in the early 1990s (ASCE, 2000). In the late nineties, ANN modeling began to be used in the simulation of water table fluctuations at different locations (Yang et al, 1997; Yang et al, 2000; Coulibaly et al. 2001; and Affandi et al., 2007). These studies indicate that ANN modeling is a convenient tool for predicting water table fluctuation, especially in areas where the aquifer system information is not available or where the available records are relatively short.

The purpose of this study was to develop a quick, easy, and convenient water table prediction model, that is based on ANN technology and uses remotely sensed satellite data as input to allow farmers, environmental engineers, and water resource planners to detect possible water table variations in a timely manner and to manage groundwater related issues more efficiently. Two experiments were conducted in this study. The first one was to build an ANN water table prediction model at a single well site. In this experiment, ANN models were developed to simulate the water table fluctuations at two locations in Maryland. Besides the water table records from water table wells at these two places, surface brightness temperature retrieved from the Advanced Microwave Scanning Radiometer – Earth Observing System (AMSR-E) satellite and soil moisture data produced by the Land Data Assimilation System (LDAS) over these two locations were used to train and validate the ANN models. The second experiment was to extend the ANN water table prediction model to a regional scale. An ANN model was developed to simulate the water table fluctuations at multiple locations in Piedmont Plateau of Maryland. In addition to water table records and LDAS soil moisture data over the selected well sites, the soil data obtained from Natural Resources Conservation Service were employed to train and validate the model. Forecast results of these two experiments were compared with the observations to evaluate the accuracy of their predictions. Statistical analysis was performed on the predictions to investigate the model's performance. In order to perform the water table fluctuation forecast, a method to produce future soil moisture and brightness temperature at a well site by using the forecast data of climate model is also suggested.

Chapter 2: Background

2.1 Literature Review

According to the report published in 2002 by the United Nations Environment Programme, about one-third of the world's population lives in countries suffering from moderate-to-high water stress and more than half the people in the world could be living in severely water-stressed areas by 2032 (UNEP GEO Team, 2002). Water shortage has become an urgent issue for the mankind. The total water on the earth is about 1,386,000,000 km³, of which 35,029,000 km³ is fresh water. Approximately 68.7% of the fresh water is locked up in glaciers and icecaps. The total fresh groundwater on the Earth is around 10,530,000 km³ which makes up 30.1% of total fresh water (USGS, 2008). Thus, groundwater is a vital water resource on the Earth. It plays an important role in the hydrological cycle and has great impact on the natural environment. According to a 1998 USGS report (Solley et al., 1998), about 22% of all the water used in the United States in 1995 came from groundwater sources. Also, 38% of water used for public supplies and 63% of water used for rural domestic and livestock depend on groundwater as the major source of water in the United States. In addition, 37% of agricultural water is also supplied by groundwater. Groundwater storage is a major source for both drinking and irrigation. However, the potential water-quality problems associated with the increasing use of agricultural chemicals in groundwater is a serious concern of the public. The capability of groundwater to carry and transport polluted substances becomes a major threat to our environment. Groundwater storage and movement are primarily affected by the water table changes

that have profound effects on agricultural productivity and profitability. The quantity of soil moisture and soil air in the root zone greatly depends on the depth of the water table. Ramirez and Finnerty (1996) showed that the inter-annual changes in water table elevations had a larger impact on root-zone soil moisture than potential precipitation change scenarios. The capillary rise from the water table could substitute directly for irrigation water use requirement.

The loss of nitrate from agricultural land into groundwater is one of the major pollution problems facing agriculture today. Sarwar and Kanwar (1996) indicated that nitrate concentration in the soil water is affected by water table depth. The nitrate transported with infiltrating water to zones conducive to denitrification is enhanced when the water table is elevated (Gambrell et al., 1975; Skaggs and Nassehzadeh-Tabrizi, 1982; and Kliever and Gilliam, 1995). Brunet et al. (2008) indicated that the variation of the water table modulated the concentrations of both ammonium ion and nitrate: low groundwater levels allowed aerobic oxidation but increased water levels reduced the production of nitrate. Hefting et al. (2004) pointed out that water table elevation turned out to be the prime determinant of the N dynamics and its end product. The water table fluctuation controls the movement of groundwater in the soil, which in turn affects the transport of pollutants underground. Groundwater fluctuation also affects oxidation-reduction processes in soils. When the groundwater level rises, air is driven out of the soil profile and naturally-occurring salts and other elements are brought to the upper zones in the soil profile. This process will affect the characteristics of surface soils (Nash et al., 1994), can bring high concentration of salinity and elements closer to the

surface, and reduce the available productive region in the soil profile (Schoneman et al., 1992). Gundogdu and Aslan (2007) pointed out in an irrigation system management study in northwestern Turkey that salinization could become a major hindrance to irrigation sustainability if the water table depth continued to decrease in that area. Wesseling (1974) reported that reduced oxygen supply to the roots resulting from shallow water table depths might hinder crop growth. Therefore, an understanding of local water table variation will provide farmers better knowledge to adequately maintain water and oxygen in the root zone for favorable crop growth.

Many studies have been performed to examine the effect of water table fluctuation on crop yield, water quality, and pollutant transport under different soil, hydrologic, and climatic conditions. (Kanwar, 1990; Thomas et al., 1992; Bengtson et al., 1993; Belcher and Merva, 1991; Fausey, 1991; Kalita and Kanwar, 1993; and Liaghat and Prasher, 1996). Stanley and Clark (1995) studied the influence of reduced water table and fertilizer levels on subirrigated tomato production. Guix-Hebrard et al. (2007) studied the influence of the spatial variation of water table fluctuations on vine water status. Munster et al. (1996) worked on the effect of water table management on the fate of the pesticide aldicarb. Controlled drainage and subirrigation used in the North Carolina coastal plains showed a higher yield and lower nutrient loss (Chescheir et al., 1995). The quantity of soil moisture and soil air in the root zone greatly depends on the depth of the water table and will affect plant growth. These investigations demonstrated that the water table needs to be maintained at a suitable level to provide enough water for optimal crop production while simultaneously minimizing water quality impacts.

Therefore, rapid capability to simulate the fluctuation of the water table is necessary for scheduling efficient drainage and irrigation regimes.

Fluctuation of water table depth also has profound impacts on hydrological, agricultural, and environmental related issues. Several different types of numerical models, governed by the Boussinesq equation, have been developed to simulate the water table variation at different climatic and hydrologic conditions (Lagace et al., 1982; Singh et al., 1991; Rai and Singh 1992; Teloglou and Zissis, 1997; Rai and Manglik, 1999; Manglik and Rai, 2000; Upadhyaya and Chauhan, 2001; and Song et al., 2007). Five numerical methodologies have been applied in groundwater modeling: finite differences, finite elements, integrated finite differences, the boundary integral equation method, and analytic elements (Anderson and Woessner, 1992). Among them, finite difference and finite element methods are more commonly used. However, the physically based models require an explicit understanding of the complicated input/output relationships and a great amount of meteorological, hydrological, and geological data of the study area as inputs (Yang et al., 1996; and Coulibaly, 2001). In addition to physically based models, water balance models (Skaggs, 1980, 1982; Hanks and Hill, 1980; McCarthy and Skaggs, 1991; and Roulet 1991) and statistical regression models (Yakowitz, 1976; and Joginder et al, 1981) have also been applied to predict water table fluctuations. However, they both need a large number of observations to fulfill the required calculations. In most field applications, the errors in model output to some extent are caused by the presence of errors or uncertainties in the input parameter

values (Shirmohammadi et al., 2006). Therefore, one has to be cautious about the simulation output.

Relative to mathematical modeling, Artificial Neural Network modeling provides an alternative method of forecasting the water table variations. The ANN modeling technology was first developed by McCulloch and Pitts (McCulloch and Pitts, 1943). Since its invention, it has been widely applied in solving problems in a variety of fields (Widrow and Lehr, 1992; Fausett, 1994; Haykin, 1999; Lingireddy and Brion, 2005; and Rabunal and Dorrado, 2006). The technique of ANN is to mathematically model neurons and their connections to simulate the work of the human brain to get a model to a level that is able to capture and represent complex input/output relationships. It has the ability to learn both linear and non-linear relationships directly from the data being modeled. ANN has the advantage of simplicity, flexibility, and accuracy. It does not need a thorough understanding of the relationship between the input and output parameters and requires only a small amount of data (ASCE, 2000). ANN modeling began to be applied to solving hydrological problems in the early nineties (ASCE, 2000) and has been successfully used in rainfall-runoff modeling (Hsu et al., 1995; Sajikumar and Thandavesware, 1999; Gautam, 2000; Rajukar et al., 2002; Jain and Srinivasulu, 2004; Rajukar et al., 2004; Jeong and Kim, 2005; Antar et al. 2006; and Ju et al., 2007) and stream flow forecasting (Karunanithi et al., 1994; Ranjan and Srinivasan, 1997; Zealand et al., 1999; Dibike and Solomatine, 2001; Kim and Barros, 2001; Wu et al., 2005; and Srivastava et al., 2006).

Shukla et al (1996) investigated the use of ANN as an alternative method to obtain solutions to the Boussinesq equation. The study showed that the simulation can be performed more rapidly with the application of ANN. It indicates the advantage of using ANN as a tool in real-time drainage control. Yang et al. (1996) used simulated water table data from DRAINMOD (Skaggs, 1980) to train an ANN model. Their results showed that the ANN model could make water table predictions similar to that of DRAINMOD. ANN models were also developed to simulate the fluctuations in midspan water table depths in agricultural fields in Ottawa, Ontario (Yang et al, 1997) and in Woodslee, Ontario (Yang et al, 2000). Daily rainfall and potential evapotranspiration were used as inputs in the Ottawa study, whereas rainfall, potential evapotranspiration, and irrigation were used as inputs for the Woodslee study. These studies indicated that ANN modeling could provide accurate results and require little time for training and execution. Coppola Jr. et al. (2004) demonstrated that ANNs could provide both excellent prediction capability and valuable sensitivity analyses. This could be used to make more appropriate groundwater management strategies. Affandi et al. (2007) used ANN to estimate the groundwater level fluctuation in Jakarta, Indonesia. Their work showed that an ANN could be used to estimate groundwater level fluctuation with relatively few data samples. Coulibaly et al. (2001) also showed that the ANN models were effective at predicting monthly groundwater level fluctuations in the Gondo aquifer located in the Sahel region. Their study indicated that ANN model provided a reliable tool for water table fluctuation modeling in areas where aquifer system information or the available records are relatively sparse. These studies point out that ANN modeling is an acceptable tool for performing the water table

fluctuation predictions, especially in areas where the observations are difficult to obtain or where the real-time simulation is needed. However, reliability on ANN simulations and their use heavily depends on the type and accuracy of input data in any region. With the advances in satellite technology, spatial and temporal data on the landscape are becoming more prevalent. Therefore, using remotely collected data such as brightness temperature, soil moisture, land use, and other physiographic features may be advantageous.

2.2 Artificial Neural Network

The Artificial neural network (ANN) is a system that mimics the function of the human brain and simulates its learning process. It performs computer-based simulations of a living nervous system and works quite differently from conventional computing. The human brain consists of about 10 billion neurons (Shepherd and Koch, 1990) that process incoming information and provide us with the ability to apply previous experiences to our every action. All natural neurons have four basic components, which are dendrites, soma, axon, and synapses (Figure 1). Each neuron is linked to a large number of its neighboring neurons with varying coefficients of connectivity that represent the strengths of these connections through synapses. The power of the brain comes from the number of these basic components and the multiple connections

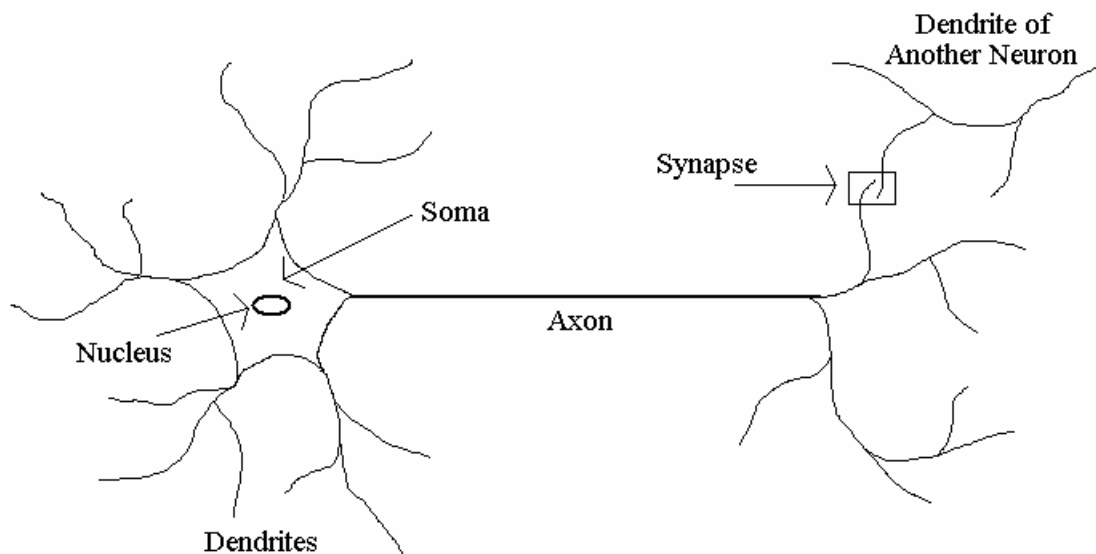


Figure 1. Schematic diagram of a biological neuron.

between them. Moreover, learning is a result of the modification of the strength of synaptic junctions between neurons (Freeman and Skapura, 1991). Basically, a biological neuron receives inputs from other sources, combines them in some way, performs a generally nonlinear operation on the result, and then outputs the final result. Incoming information that reaches the neuron's dendrites is added up and then delivered along the neuron's axon to the dendrites at its end, where the information is passed to other neurons if the stimulation has exceeded a certain threshold. If the incoming stimulation is too low, the information will not be transported any further (Nelson and Illingworth, 1991).

The idea of the ANN technique is to mathematically model the neurons and their connections to mimic the work of the human brain to get a model that is good at giving similar outputs from similar inputs. An ANN is an information-processing system that has certain performance characteristics in common with biological neural networks (Fausett, 1994). It has a natural inclination for storing experiential knowledge and making it available for use. The ANN resembles the brain in two respects: (1) knowledge is acquired by the network through a learning process and (2) inter-neuron connection strengths known as synaptic weights are used to store the knowledge (Haykin, 1999).

The main contribution of ANNs is that they allow very low level programming to solve complex problems, especially those that are non-analytical, and/or nonlinear, and/or nonstationary, and/or stochastic (Graupe, 1997). ANNs provide an analytical alternative

to conventional techniques that are limited by strict assumptions such as normality, linearity, and variable independence. Because ANNs can capture many kinds of relationships among participating parameters, it allows the user to model phenomena quickly and relatively easily which may have been very difficult or impossible to explore. Among the many interesting properties of an ANN, the property that is of primary significance is the ability of the network to learn from its environment and to improve its performance through learning.

The basic unit of ANN, the artificial neuron, simulates the four basic functions of natural neurons: input, summation, transfer, and output. However, an artificial neuron is much simpler than the biological neuron. Similar to a biological neuron, each input (X_i) to the artificial neuron is multiplied by a connection weight (W_i). All the inputs are summed together and fed through an activation function to generate a result. The result is then output to other artificial neurons if it is greater than the transmission threshold (Figure 2).

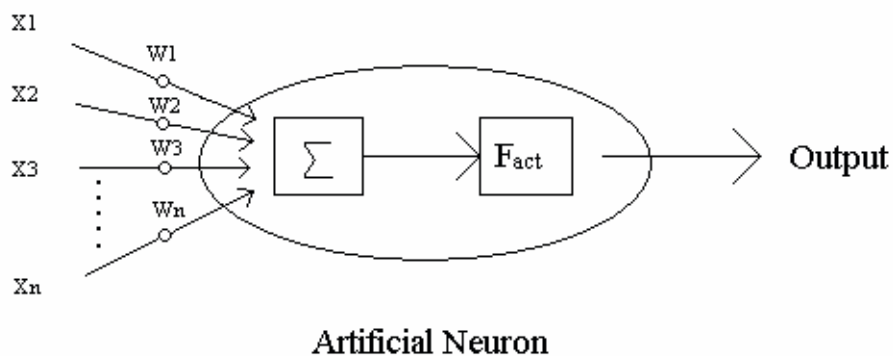


Figure 2. Schematic diagram of an artificial neuron.

The activation function is usually a nonlinear, bounded, and piece-wise differentiable function (Gallant, 1993). The most commonly used one is the sigmoid function which is represented by the mathematical relationship $1 / (1 + e^{-x})$. The sigmoid function acts as a gate for a node's output response. The Gaussian function, which is defined as e^{-x^2} , acts like a probabilistic output controller. The output response of both sigmoid and Gaussian functions is between 0 and 1. The hyperbolic tangent function, $(1 - e^{-2x}) / (1 + e^{-2x})$, is used when the desired range of output value is between -1 and 1. It is similar to the sigmoid function but can exhibit different learning dynamics during training.

An ANN usually has several layers. The first and last layers are the input and output layers, respectively. The rest of layers are the hidden layers. Each layer consists of a different number of nodes (artificial neurons). Generally, a neural network is characterized by its architecture that represents the pattern of the connection between nodes, its method of determining the connection weights, and the activation function (Fausett, 1994). Figure 3 is a schematic diagram of a three-layer ANN, which has an input layer, a hidden layer, and an output layer. The connections among neurons in an ANN have profound impact on its operation. A feedforward network can pass the outputs only to the next layer. A feedback network allows outputs to be input to preceding layers. A feedlateral connection would send some outputs to inputs of other nodes in the same layer. Recurrent networks are those with closed loops (Nelson and Illingworth, 1991).

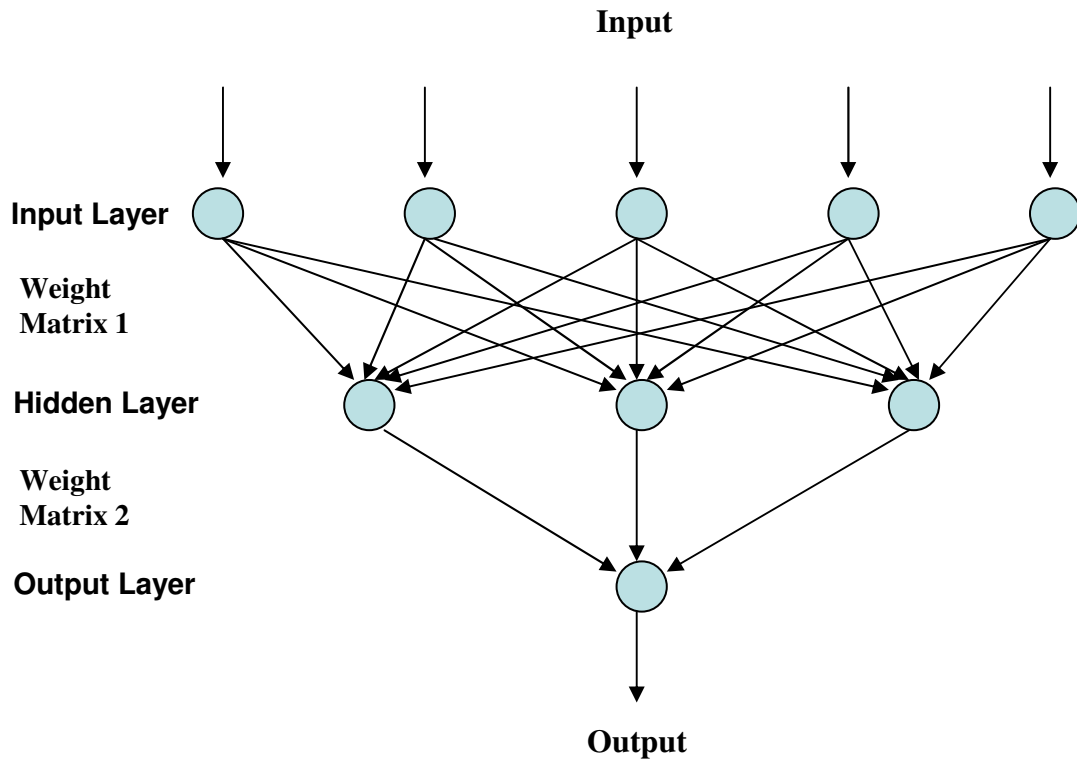


Figure 3. Schematic diagram of a three-layer ANN.

An important part of the ANN is its ability to learn. Learning is the process by which a neural system acquires ability to carry out certain task by adjusting its internal parameters according to some learning scheme (Karayiannis and Venetsanopoulos, 1993). A neural network learns about its environment through an iterative process of adjustments applied to the strength of synaptic junctions between neurons. Learning can be either supervised or unsupervised. Supervised learning requires the pairing of each input vector with a target vector representing the expected output. Once an input

is applied, the difference or error between the output of the network and the target value is calculated and fed back through the network. The connection weights are changed according to an algorithm that tends to minimize the error. The network parameters are adjusted under the combined influence of the training vector and the error signal. This procedure continues until the error for the entire training set meets the criterion. Unsupervised learning is performed in a self-organized manner. The training set consists solely of input vectors. The training algorithm modifies network weights to produce the same pattern of outputs for similar inputs. This type of training occurs without outside instruction.

Basically, learning rules dictate the efficiency of neural network training. Many learning rules have been developed since the invention of the ANN. Most of them are a variation of the Hebb's rule, which is the best-known and oldest learning rule (Nelson and Illingworth, 1991). The following are several learning rules commonly used: error-correction learning, Hebbian learning, competitive learning, Boltzmann learning, and back-propagation learning. Error-correction learning is used to train the network to obtain the optimized connection weights by minimizing the error between the actual output of a neuron in the network and the target response for that neuron. Hebbian learning was introduced by Donald Hebb (Hebb, 1949). When a neuron receives an input from another neuron, the weight between the neurons should be strengthened if the neurons on either side of the connection are highly active. If these two neurons are activated asynchronously, then the weight is weakened. In competitive learning the output neurons of a neural network compete among themselves for being the one to be

active. The neuron with the largest output is declared the winner. Only the winning neuron is active at any one time. Boltzmann learning is a stochastic learning algorithm. In a Boltzmann machine, the neurons constitute a recurrent structure, and they operate in a binary manner. A distinctive feature of Boltzmann learning is that it uses only locally available observations under two operating conditions: clamped and free-running.

Back-propagation learning (Werbos, 1974; Parker, 1985; and Rumelhart et al., 1986) is now the most widely used tool in the field of ANN (Werbos, 1990; Gallant, 1993). It is an effective systematic method for training multilayer ANNs (Wasserman, 1989). The mathematical basis for the back-propagation algorithm is the optimization technique known as gradient descent (Rumelhart et al., 1986). The training is to minimize the total squared error of the output computed by the network. The training of a network by the back-propagation method involves three stages: the feedforward of the input training pattern, the calculation and back-propagation of the associated error, and the adjustment of the weights (Fausett, 1994). The learning progresses by alternately propagating forward the activation and propagating backward the errors. Due to its competency in ANN applications, a multilayer feedforward backpropagation ANN will be developed and applied in this study.

2.3 Groundwater in Maryland

Maryland is located on the East Coast of the United States in the Mid-Atlantic region. It is between 75.07W and 79.55W longitude, 37.88N and 39.72N latitude. Maryland is approximately 402 km (250 miles) long and 145 km (90 miles) wide. It has 25,573.5 km² (9,874 square miles) of land, 1,820.8 km² (703 square miles) of rivers and streams, and 4,470.3 km² (1,726 square miles) of Chesapeake Bay (Walker, 1970). Based on the observations from 1971 to 2000, Maryland has an average annual rainfall of 103.53 cm (40.76 inches), with July and August normally being the months with the highest rainfall. The average annual snowfall is 52.32 cm (20.6 inches), and the average annual temperature is 12.83 °C (55.1 °F), with high and low temperatures normally occur in July and January, respectively (Maryland at a Glance, 2008).

Maryland has three distinct physiographic provinces. From west to east across the state, they are the Appalachian (Appalachian Plateau, Valley and Ridges, and Blue Ridge), Piedmont, and Coastal Plain. In the Appalachian Plateau, aquifer material is composed of fractured sedimentary rocks. The aquifers in Valley Ridges and Blue Ridge consist of fractured metamorphic, igneous, and sedimentary rocks. In the Piedmont region, an unconsolidated material, known as regolith, is on top of metamorphic and igneous rocks. The water-table aquifer is in the regolith and extends to the underlying bedrock. The aquifer in the Coastal Plain is a southeastwardly thickening sequence of sediments that consists of sand and gravel inter-layered with silt and clay confining units (USGS, 2000). In central and western Maryland, because most areas are underlain by crystalline

and consolidated layers of rocks, they do not yield large amounts of water to wells. In the eastern and southern regions of Maryland, the formation formed mainly by unconsolidated deposits consists mostly of sand and gravel; therefore, it is capable of providing large quantities of groundwater to the users. The area east of the Chesapeake Bay depends almost entirely on groundwater for freshwater supply (Wheeler, 1995).

Groundwater is an important source of fresh water in Maryland. In 1995, $0.931 \times 10^6 \text{ m}^3/\text{d}$ (246 Mgal/d) of freshwater was withdrawn from groundwater sources in Maryland. Among them, Anne Arundel County (Coastal Plain Province) had the largest groundwater withdrawals, $0.182 \times 10^6 \text{ m}^3/\text{d}$ (48 Mgal/d). Roughly, about 875,000 Marylanders (17 percent of the State's population) withdrew an estimated $0.276 \times 10^6 \text{ m}^3/\text{d}$ (73 Mgal/d) of water from individual house wells for water supply in 1995 (Wheeler, 1995). In highly developed Montgomery County (Piedmont Province), approximately 80,000 residents still rely on groundwater as their source of drinking water (Groundwater Indicators, 2001). Moreover, groundwater also plays an important role in agricultural, industrial, and commercial water usages. For example, during 1995, about $0.216 \times 10^6 \text{ m}^3/\text{d}$ (57 Mgal/d) of freshwater was used for irrigating farm crops, golf courses, and nursery stock. Of this amount, $0.136 \times 10^6 \text{ m}^3/\text{d}$ (36 Mgal/d), about 63%, was from groundwater sources (Wheeler, 1995). Data in figure 4 present a comparison of the percentages of water supply from groundwater sources in 2000 for various water sectors in the United States and in Maryland (Hutson et al., 2004). In most sectors, the percentages of the groundwater usages in Maryland are higher than

that in the United States. This indicates the important contribution of groundwater to the fresh water required in Maryland.

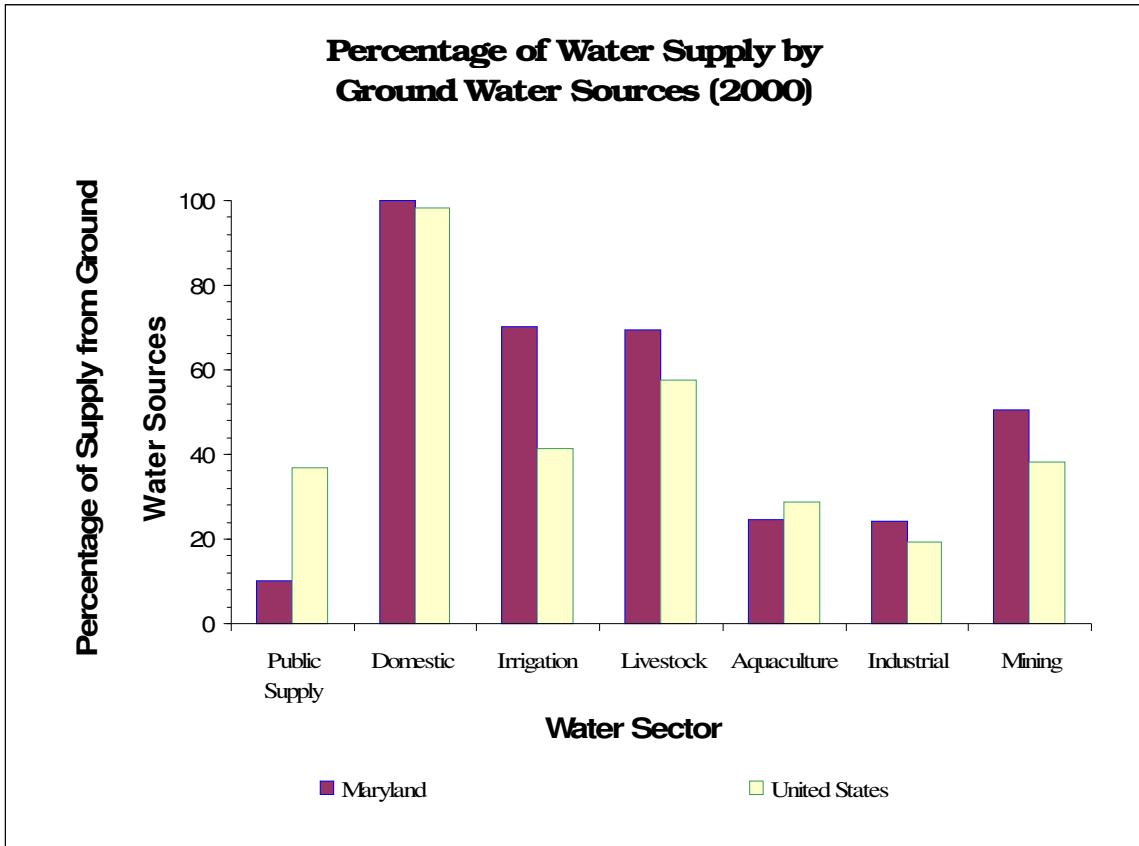


Figure 4. Percentage of water supply from groundwater sources for various water sectors in the United States and Maryland in 2000 (Courtesy Hanna, 2006).

Furthermore, pollutants carried by groundwater are considered as serious environmental problems in Maryland. Agricultural and urban land-use practices are possible sources of nitrate and pesticides to groundwater. High concentrations of nitrate

were found in groundwater in most parts of the surficial aquifer, and even in the deep part of the aquifer used for water supply. Pesticides used on common crops were found at trace concentrations in very shallow groundwater (USGS, 1999). According to the Maryland Department of Agriculture report (2001), the total area of farmland in Maryland in 2000 was 849,840 ha (2,100,000 acres), making up about 1/3 of the Maryland's land area. Therefore, agriculture is the largest single land use in Maryland. Since applied fertilizer and manure are normally potential sources of nitrate that can contaminate groundwater, groundwater coming out of cropland could have adverse health effects on humans, especially in the rural areas where groundwater is the major source of drinking water (Thorpe and Shirmohammadi, 2005). Other studies have also shown that nitrate concentrations are higher in groundwater in agricultural areas than in urban or forested areas (Ator and Ferrari, 1997). Phillips et al. (1999) have reported that groundwater contributed more than half (54 percent) of the total annual flow of streams in the Chesapeake Bay watershed, and groundwater nitrate loads contributed nearly half (48 percent) of the total nitrogen load to streams. Dillow and Greene (1999) have pointed out that the potential nitrate load to the coastal bays from direct discharge of groundwater is estimated to be 123,377 kg (272,000 pounds) per year. Nitrate from groundwater can also enter the coastal bays by way of base flow to streams that discharge to the bay. The potential nitrate load to the bays from the base flow of streams is estimated to be 390,997 kg (862,000 pounds) per year. Groundwater is certainly a major contributor to the pollution of coastal bays. How to reduce the pollutants carried by groundwater into the Chesapeake Bay still remains to be one of the major tasks required for the overall Bay clean-up effort.

Groundwater storage and water table depth can be greatly affected by climate changes. A study that analyzed 88 years (1917 to 2005) of monthly temperature data from the United States Historical Climatology Network showed that there is a $0.06^{\circ}\text{C}/10\text{yr}$ rise in Maryland (Collins, 2008). It was also reported that in many part of Maryland precipitation has increased by up to 10% over the last century (EPA, 1998). In its Third Assessment Report, the Intergovernmental Panel on Climate Change (IPCC) has suggested that North America could warm by $1\text{-}3^{\circ}\text{C}$ over the next century under low emission conditions. The warming could be as much as $3.5\text{-}7.5^{\circ}\text{C}$ for the higher emission condition (McCarthy et al., 2001). This warming trend could have a significant impact on our water resources. The drier summer conditions could reduce groundwater levels and jeopardize the water shortage situation in the areas that depend on groundwater as the major water supply. Therefore, early preparation for better groundwater monitoring and management is very important.

Chapter 3: Approach

3.1 Theory

Groundwater is recharged by percolation through the unsaturated zone. The fluctuation of the water table is determined by the relative rates of recharge versus outflow. The extent of vertical variation of the water table is primarily affected by the intensity and frequency of local precipitation. A net recharge of groundwater will result in water table rise. Inversely, the water table will descend if there is a net discharge of groundwater. This relation can be geometrically complex where the profile is heterogeneous or anisotropic or where sources and sinks of water are distributed unevenly (Hillel, 1982).

Based on the water balance concept, the groundwater recharge can be derived from the soil water budget in the vadose zone. The vadose zone refers to the geologic media that lie below the surface of the earth but above the water table of the shallowest year-round aquifer (Selker et al., 1999). Since the recharge affects the surface position of the saturated zone, the water table fluctuation and the soil moisture variation in the vadose zone are highly related. The vertical water movement between the vadose zone and the unconfined saturated zone in a geologic formation is the primary mechanism that results in the water table variation.

Considering the vadose zone as a water storage body, the infiltration across the upper boundary is the inflow to the vadose zone. The outflows from the vadose zone include

evaporation and transpiration from the upper boundary and groundwater recharge from the lower boundary (Figure 5). The one-dimensional water budget in the vadose zone may be expressed by equation (1) since the net inflow must equal the change in soil water stored in the vadose zone (Stephens, 1996).

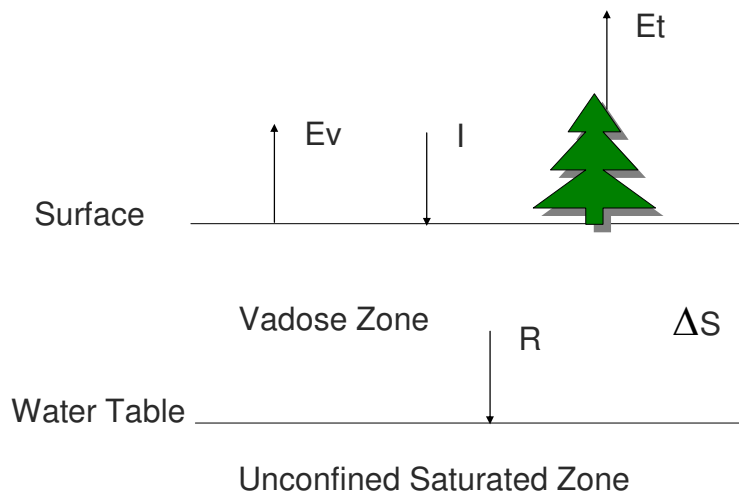


Figure 5. Schematic diagram of water flow in the vadose zone. I represents infiltration. Ev represents evaporation. Et represents transpiration. R is the groundwater recharge. ΔS represents soil water change in vadose zone.

$$I - E_v - E_t - R = \Delta S \quad (1)$$

where, I is the infiltration from the surface,

E_v is the evaporation,

E_t is the transpiration,

R is the groundwater recharge, and

ΔS is the soil water change in vadose zone.

The groundwater recharge can then be expressed as

$$R = I - E_v - E_t - \Delta S \quad (2)$$

The infiltration is mainly affected by the water application, antecedent soil moisture, soil hydraulic properties, and topography. An approximate solution for vertical infiltration into the vadose zone can be demonstrated by the following Philip's transient infiltration equation (Philip, 1957).

$$i(t) = \frac{1}{2} S t^{-1/2} + A \quad (3a)$$

Hence,

$$I = S t^{1/2} + A t \quad (3b)$$

where, i is an instantaneous infiltration rate,

I is total infiltration over a specified time interval,

S is the sorptivity of the soil,

t is time since infiltration began, and

A is a coefficient which is a function of hydraulic conductivity and hydraulic diffusivity of the soil.

Since S is only in relation to the initial state of the medium and the imposed boundary condition, S is a function of the soil's initial moisture content and the moisture content near saturation (Hillel, 1982). A is equal to saturated hydraulic conductivity if the surface water content is saturated after water is applied (Hanks, 1992). The hydraulic conductivity can be expressed as a function of soil moisture content in the vadose zone. Hence, A is also a function of soil moisture content, which implies that the infiltration is a function of the moisture content of the soil.

Generally, evaporation (E_v) and transpiration (E_t) are combined together as evapotranspiration (ET) which can be expressed as a fraction of the potential evapotranspiration. The potential evapotranspiration is the amount of evapotranspiration that would occur from a short green crop that fully shades the ground, exerts negligible resistance to the flow and is always well supplied with water (Stephens, 1996). The relation between evapotranspiration rate and potential evapotranspiration rate can be expressed by the following equation.

$$R_{ET} = Kc (R_{PET}) \quad (4a)$$

Therefore,

$$ET = t R_{ET} = t Kc (R_{PET}) \quad (4b)$$

where R_{ET} is evapotranspiration rate, R_{PET} is potential evapotranspiration rate, t is elapsed time, and Kc is a crop coefficient which can be represented by the following relation (Jensen et al., 1970).

$$Kc = Kco \left(\ln \left(\frac{100(AW)}{AW_{max}} + 1 \right) / \ln 101 \right) \quad (5)$$

where Kco is the crop coefficient for a field where water is not limiting, $AW = (\theta - \theta_{wp}) d$, and $AW_{max} = (\theta_{fc} - \theta_{wp}) d$. Here, AW is the available water, θ is the soil moisture content, θ_{fc} is the moisture content at the field capacity, θ_{wp} is the moisture content at the permanent wilting point, and d is the rooting depth. Kc is hence a function of moisture content in the soil, which implies that ET is a function of soil moisture content too.

The water change in the vadose zone (ΔS) can be simply expressed as the changes in moisture content at all depths in the vadose zone:

$$\Delta S = \int_0^{D_t} \theta_t(z) dz - \int_0^{D_0} \theta_0(z) dz \quad (6)$$

where $\theta_0(z)$ and $\theta_t(z)$ are the vertical soil moisture profiles at time 0 and time t, and D_0 and D_t are the thickness of vadose zone at time 0 and time t.

Based on the above discussion, the groundwater recharge, R, is a function of soil moisture content. Therefore, the water table fluctuation is directly related to the variation of soil moisture content in the vadose zone. This physical relationship provides a foundation to develop an ANN water table prediction model based mainly on the historical data of water table fluctuations and soil moisture status in the soil profile.

The thermal microwave radiation emitted from the soils strongly depends on the soil moisture content. The emission is a function of the radiometer wavelength and the distribution of the moisture in the soil (Schmugge et al., 1974). Because of the large dielectric contrast between dry soil and wet soil, the microwave brightness temperature can be estimated from the dielectric constant as a function of the amount of water in the soil. Schmugge (1978) has indicated that there is a correlation of up to 0.9 between the microwave brightness temperature and the moisture in the surface layer. Chen et al. (1989) pointed out that the emissivity of the ground surface also depends on the soil surface structure. They discovered that the increase was more apparent in compacted soils ($e = 0.915 + 0.052\theta$; where e is emissivity, θ is the volumetric water content) than in tilled soils ($e = 0.937 + 0.019\theta$).

Several algorithms have been developed and successfully retrieved soil moisture from surface brightness temperature at different spatial and temporal scales. Wang and Choudhury (1981) developed an algorithm to estimate moisture content of a bare soil from the observed brightness temperature. Their results compared favorably with the observations in the top 2 cm layer. Jackson (1993) presented his soil moisture estimation algorithms and a microwave simulation model to obtain surface soil moisture from a single wavelength (L band) microwave radiometer. Belisle et al. (1997) described an algorithm relating microwave brightness temperature and soil moisture status in the upper (10 cm) and lower (greater than 10 cm) soil depths. Schmugge (1998) indicated that the microwave emission at the 21 cm wavelength was a strong function of surface (0-5 cm) soil moisture and thus could be used to map spatial and temporal variations of the moisture content of this soil layer. Crow and Wood (2003) showed that the Ensemble Kalman filter was capable of extracting spatial and temporal trends in root-zone (40 cm) soil water content from surface brightness temperature measurements. Pellarin et al. (2003) developed a technique to retrieve surface soil moisture at global scale using a synthetic data set of L-band (1.4 GHz) brightness temperature. Narayan et al. (2004) examined existing algorithms for soil moisture retrieval from active and passive microwave remote sensors under high vegetation water content conditions. They indicated that the algorithms performed satisfactorily over the full range of vegetation conditions. All these studies showed a strong relationship between surface brightness temperature and soil moisture content. This relationship, accompanied by the relationship between soil moisture variation and

the water table fluctuation, provides another base to develop an ANN model for water table fluctuation prediction depending on the changes in brightness temperature.

3.2 ANN model

A multilayer feedforward ANN trained by the backpropagation method will be applied in this study. As described in the previous section, the backpropagation training algorithm includes feedforward of the input training data, the calculation and backpropagation of the associated error for each training pair, and the modification of the weights according to the errors. A supervised training is used in the learning process. Basically, the training is to build a system that can reach the desired mapping between the input data and the target data by applying the technique of artificial intelligence. This task is achieved by adjusting the connecting weight between each pair of nodes. At the beginning the initial weights will be randomly chosen. However, it is important to avoid choices of initial weights that would make it likely that either activations or derivatives of activations are zero. It was recommended that a better choice of the initial weights should be between -0.5 to 0.5 (Fausett, 1994).

Each input will be multiplied by the connection weight between the input node and the receiving node in the hidden layers or output layer. All the inputs pointing to the same receiving node will be summed together. Since the nodes in the hidden layer and the output layer may have biases, bias terms are connected to these nodes. These bias terms function as weights on connections between nodes and can be regarded as coming from units whose output are always one. Therefore, the signal that is received by the node in the hidden layer can be expressed as

$$h_i(j) = b_0(j) + \sum_{i=1}^n x(i) w(i,j) \quad (7a)$$

or

$$h_i(j) = \sum_{i=0}^n x(i) w(i,j) \quad (7b)$$

where, $h_i(j)$ is the signal received by the j th node in the hidden layer,

$x(i)$ is the input value pointing to each node in the hidden layer from the i th node in the input layer,

$w(i,j)$ is the connection weight between the i th node in the input layer and the j th node in the hidden layer,

$b_0(j)$ is a bias term to the j th node in the hidden layer and may be expressed as $x(0) w(0,j)$, where $x(0)=1$, and

n is the number of nodes in the input layer.

The selected activation function, f_a , such as a sigmoid function, will be applied on $h_i(j)$ to obtain the output value h_o from the j th node. h_o is therefore expressed as

$$h_o(j) = f_a(h_i(j)). \quad (8)$$

The flow diagram of equations 7 and 8 is shown in Figure 6.

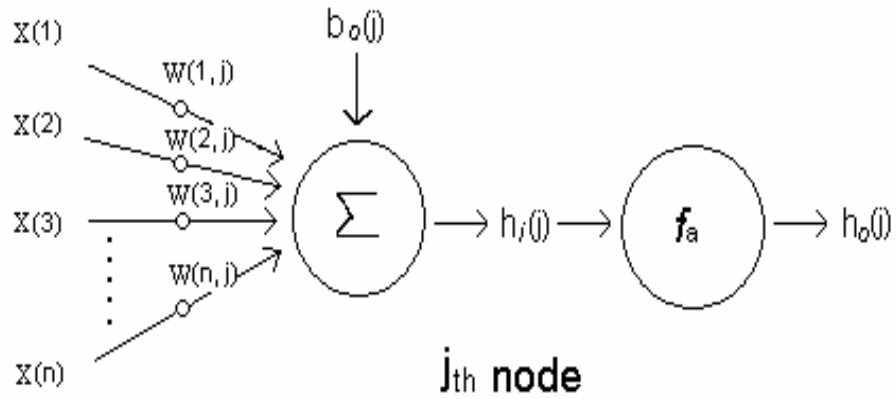


Figure 6. Schematic diagram showing the flow pathways of equations 7 and 8.

The output value will then be directed to either the nodes in the next hidden layer if there is more than one hidden layer in the model or the output nodes if there is only one hidden layer in the system. In case of having more than one hidden layer, the outputs from nodes in the current hidden layer will act as inputs to the nodes in the next hidden layer. The procedures described in equations (7) and (8) will be repeated until there is no more hidden layer left. The output from the nodes in the last hidden layer will go to the nodes in the output layer. The signal received by the output nodes may be expressed as

$$y_i(k) = b_h(k) + \sum_{j=1}^m h_o(j) w(j,k) \quad (9a)$$

or

$$y_i(k) = \sum_{j=0}^m h_o(j) w(j,k) \quad (9b)$$

where, $y_i(k)$ is the signal received by the k th node in the output layer,

$h_o(j)$ is the output value from the j th node in the last hidden layer,

$w(j,k)$ is the connection weight between the j th node in the last hidden layer and the k th node in the output layer,

$b_h(k)$ is a bias term to the k th node in the output layer and may be expressed

as $h_o(0) w(0,k)$, where $h_o(0) = 1$, and

m is the number of nodes in the hidden layer.

The $y_i(k)$ value will then be fed into a selected activation function, f_a , to get the output. The output value from each node in the output layer is expressed as

$$y_o(k) = f_a(y_i(k)). \quad (10)$$

The flow diagram of equations 9 and 10 is shown in Figure 7.

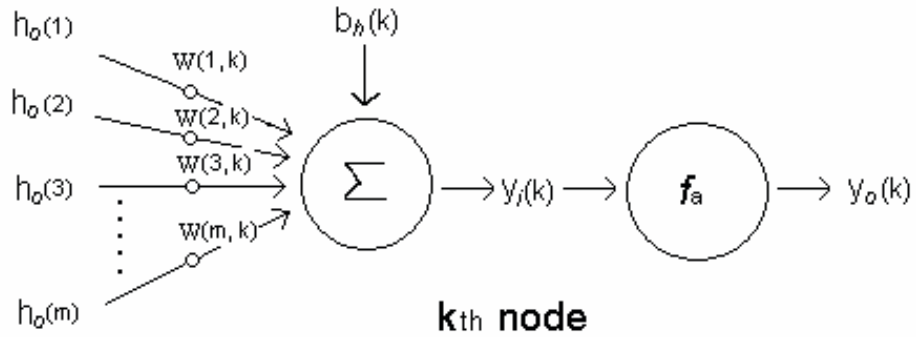


Figure 7. Schematic diagram showing the flow pathways of equations 9 and 10.

The error between this output value and the target value at each output node will then be calculated and propagated back to adjust the weights. The error at the k th output node is $e(k) = t(k) - y_o(k)$, where $t(k)$ is the target value (or observation) at the k th output node. Since gradient descent is the mathematical basis for the backpropagation algorithm (Rumelhart et al., 1986), this error correction training is hence to minimize the total squared error of the output computed by the network. An index of performance, $\frac{1}{2} e^2(k)$, can be defined to represent the squared error of the output (Haykin, 1999). The instantaneous value of the total error for the output layer may then be expressed as

$$\xi = \frac{1}{2} \sum_{k=1}^m e^2(k) \quad (11)$$

The weight correction terms, $\Delta w(j,k)$, are defined as

$$\begin{aligned}\Delta w(j,k) &= -\alpha \frac{\partial \xi}{\partial w(j,k)} \\ &= \alpha e(k) f_a'(y_i(k)) h_o(j)\end{aligned}\quad (12)$$

where, α is a predefined learning rate.

By letting

$$\delta(k) = e(k) f_a'(y_i(k)), \quad (13)$$

the weight correction terms, $\Delta w(j,k)$, for the weights between the last hidden layer and the output layer may be calculated from the following equation:

$$\Delta w(j,k) = \alpha \delta(k) h_o(j) \quad (14)$$

This procedure will be repeated until it reaches back to the first hidden layer. The correction term, $\Delta w(i,j)$, for weight can then be derived as shown in equation 15.

$$\Delta w(i,j) = \alpha \delta(j) x(i) \quad (15)$$

The correction of the bias terms follows the same procedure as that for the weight correction. These correction values will then be added to the previous weight and bias to start another cycle of training. The training is completed when the error in the output reaches the desired criterion.

3.3 Data Acquisition

Water table depth, brightness temperature, soil moisture content, and hydrologic soil type are the essential elements used as input data to train and execute the ANN water table prediction models. Except for the brightness temperature data which is only used in the single well ANN modeling study, the other parameters are used in both single well and regional scale ANN modeling studies. These data are obtained from different sources and processed with the use of different types of softwares, such as ArcView and GrADS (Grid Analysis and Display System), and Fortran codes (see Appendix A). The satellite and model generated data are then validated by recorded ground data for their correctness. These are explained in the following sections.

3.3.1 Water Table Depth

Water table depth is the vertical distance from ground surface to the water table. The relative variation of water table depths in an area determines the direction of ground water movement in that area. Water table depth is the primary parameter that is involved in this study. In order to carry out this research, several criteria are set to filter out the groundwater wells that do not qualify for this study. First, the groundwater level data must be from water table wells to account for the assumption of water balance in the vadose zone of an unconfined aquifer. Second, the selected groundwater wells need to have continuous records over the same time frame as that of the other input

parameters. Third, for regional scale multiple wells ANN modeling, the selected wells need to be spatially and geologically distributed.

There were 345 groundwater wells in Maryland that recorded the groundwater level in a variety of locations (USGS, 2001). The wells that provide groundwater level information for unconfined aquifers are shown in Figure 8. The names of these water table wells, the geological formations where these wells are located, and the longitude, latitude, and surface elevation of each well are shown in Table 1 (provided by Wendy McPherson of USGS). The water table data were downloaded from USGS NWISWeb (<http://waterdata.usgs.gov/nwis/gw>).

Maryland Water Table Wells

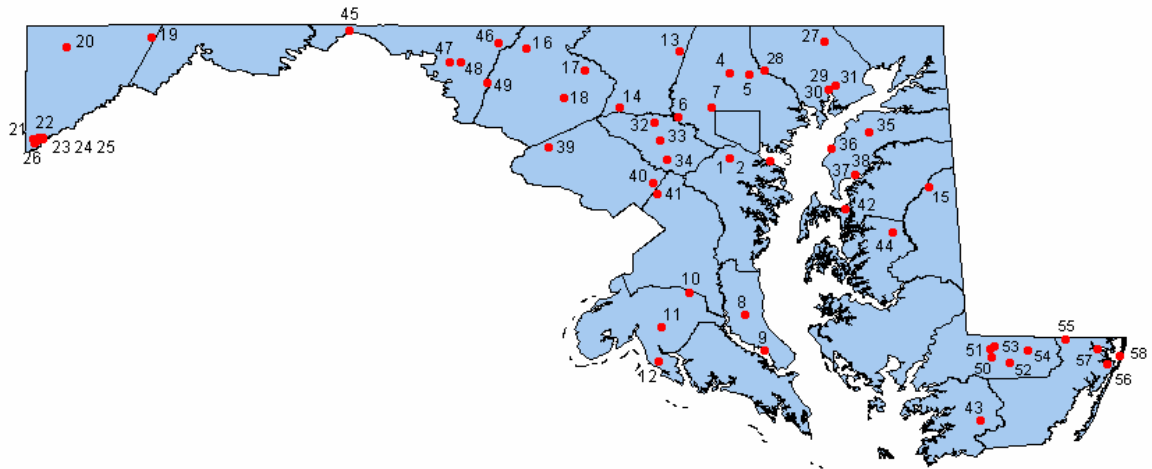


Figure 8. Locations of water table wells for unconfined aquifers in the state of Maryland.

Table 1. Names, formations, longitudes, latitudes, and altitudes of Maryland Water table wells.

	Well Name	Aquifer	Longitude	Latitude	Altitude
			(° W)	(° N)	(m)
1	AA Ad 108	Upper Patapsco aquifer in the Patapsco Formation	76.6497	39.1756	23.87
2	AA Ad 110	Upper Patapsco aquifer in the Patapsco Formation	76.6497	39.1756	23.6
3	AA Bf 3	Upper Patapsco aquifer in the Patapsco Formation	76.4822	39.1625	6.21
4	BA Cd 26	Baltimore Gneiss	76.645	39.5247	146.3
5	BA Ce 21	Loch Raven Formation	76.5717	39.5172	163.37
6	BA Ea 18	Woodstock Granite	76.8569	39.3458	149.66
7	BA Ec 43	Baltimore Gneiss	76.7222	39.3847	152.4
8	CA Db 65	Brandywine Formation	76.5872	38.5378	48.56
9	CA Fc 13	Choptank-St. Mary's undivided	76.5081	38.3947	14.46
10	CH Bg 12	Calvert Formation	76.8081	38.6294	45.63
11	CH De 45	Alluvium and Nanjemoy Formation	76.9231	38.4908	13.65
12	CH Ee 16	Ravens Crest Formation	76.9339	38.3508	12.19
13	CL Bf 1	Prettyboy Schist	76.85	39.6106	284.38
14	CL Ec 75	Prettyboy Schist	77.09	39.3831	167.64
15	CO Bc 1	Pensauken Formation	75.8458	39.0592	16.46
16	FR Bd 96	Catoctin Metabasalt	77.4633	39.6258	350.52
17	FR Cg 1	Ijamesville Formation	77.2325	39.5322	182.88
18	FR Df 35	Sama Creek Metbasalt	77.3178	39.4214	173.74
19	GA Ag 1	Pocono Formation	78.9714	39.6714	771.14
20	GA Bc 1	Hampshire Formation	79.3175	39.6303	736.09
21	GA Fa 29	Conemaugh Formation	79.4525	39.2533	880.87
22	GA Fa 34	Conemaugh Formation	79.4294	39.2608	797.97
23	GA Fa 38	Conemaugh Formation	79.4333	39.2503	816.86
24	GA Fb 25	Conemaugh Formation	79.4122	39.2583	771.14
25	GA Fb 30	Conemaugh Formation	79.41	39.2536	839.72
26	GA Ga 16	Conemaugh Formation	79.4469	39.2389	819.91
27	HA Bd 31	Baltimore Gabbro Complex	76.2667	39.6506	140.21
28	HA Ca 23	Loch Raven Formation	76.5072	39.5328	143.26
29	HA Dd 91	Talbot Formation(?)	76.2508	39.4558	6.01
30	HA Dd 92	Talbot Formation(?)	76.2508	39.4558	6.11
31	HA De 198	Talbot Formation(?)	76.2192	39.4719	5.77
32	HO Bd 1	Morgan Run Formation	76.9492	39.3194	192.02
33	HO Cd 79	Loch Raven Formation	76.9308	39.2458	137.88
34	HO Ce 38	Sykesville Formation	76.9	39.1669	131.06
35	KE Bc 185	Pensauken Formation in the Columbia aquifer	76.0844	39.2806	25.02
36	KE Cb 101	Kent Island Formation in the Columbia aquifer	76.2394	39.2133	9.49
37	KE Dc 89	Kent Island Formation in the Columbia aquifer	76.1425	39.1072	1.38
38	KE Dc 91	Aquia Formation	76.1425	39.1072	1.41
39	MO Cc 14	Ijamesville Formation	77.3783	39.2206	170.69
40	MO Eh 20	Loch Raven Formation	76.9583	39.0761	123.44
41	PG Bc 16	Patuxent Formation	76.9375	39.0308	57.91
42	QA Ec 1	Kent Island Formation in the Columbia aquifer	76.1814	38.9656	6.1

43	SO Cf 2	Kent Island Formation in the Columbia aquifer	75.6353	38.1044	6.1
44	TA Bf 74	Pensauken Formation in the Columbia aquifer	75.9919	38.8783	12.8
45	WA Ac 1	Romney Formation	78.1764	39.6983	134.11
46	WA Bk 25	Tomstown Dolomite	77.575	39.6475	240.79
47	WA Ch 106	Conococheague Limestone	77.7717	39.5706	158.5
48	WA Ci 82	Conococheague Limestone	77.7283	39.5672	152.4
49	WA Dj 2	Weaverton Formation	77.6208	39.4844	326.14
50	WI Ce 13	Pensauken Formation in the Columbia/ Salisbury aquifer	75.5892	38.3639	2.13
51	WI Ce 204	Pensauken Formation in the Columbia/ Salisbury aquifer	75.5983	38.4011	8.53
52	WI Cf 3	Pensauken Formation in the Columbia/ Salisbury aquifer	75.5189	38.3436	13.65
53	WI Cf 147	Pensauken Formation in the Columbia/ Salisbury aquifer	75.5792	38.4081	12.75
54	WI Cg 20	Parsonsborg Sand in the Columbia aquifer	75.4436	38.3914	20.73
55	WO Ae 25	Beaverdam Sand in the Columbia aquifer	75.295	38.4392	12.19
56	WO Bg 1	Sinepuxent Formation in the Columbia aquifer	75.1233	38.3394	3.05
57	WO Bg 45	Beaverdam Sand in the Columbia aquifer	75.1625	38.3994	3.05
58	WO Bh 84	Beaverdam Sand in the Columbia aquifer	75.0722	38.3708	1.52

Among these wells, two water table wells (BA Ea 18 and FR Df 35), both in the Piedmont region, have recorded daily water table depths for a time span of several years. Therefore, they were selected to be used in the single well ANN modeling study. For the regional scale study, thirteen available water table wells in the Piedmont region were chosen. Except for the two wells mentioned above, these water table wells do not provide regular daily water table depth measurements but only sporadic measurements each month. The data at each well were linearly interpolated to obtain the water table depth on the first day of each month at that well for the ANN modeling.

3.3.2 Brightness Temperature Data

The brightness temperature retrieved from the observation of the Advanced Microwave Scanning Radiometer – Earth Observing System (AMSR-E) is used in the single well ANN modeling study. AMSR-E was launched on board the NASA EOS Aqua satellite on May 4, 2002 (NSIDC, 2008). AMSR-E provides global passive microwave measurements of terrestrial, oceanic, and atmospheric variables. The AMSR-E Level 2A product (AE_L2A) contains brightness temperatures at six frequencies: 6.9 GHz, 10.7 GHz, 18.7 GHz, 23.8 GHz, 36.5 GHz, and 89.0 GHz. The footprint sizes of the observations are 56 km, 38 km, 24 km, 21 km, 12 km, and 5.4 km in diameter, respectively. The brightness temperature resampled at 89.0 GHz vertical (V) field with a footprint size of 5.4 km in diameter was selected to be used for this study. The monthly mean brightness temperature at the well site was computed by averaging the daily observations which fall inside a circle with a radius of 2.75km from the well site for each month. The surface air temperature obtained from the Maryland State Climatologist Office (MSCO, 2008) was compared with the brightness temperature at Owings Mills (39.41N, 76.79W) in Baltimore County, Maryland to check the usability of AMSR-E brightness temperature. Figure 9 shows their comparison for the period from September 2002 to September 2004. The trends of these two time series show a very good match with a correlation coefficient of 0.895. This supports the use of AMSR-E brightness temperature data obtained from the National Snow and Ice Data Center (Ashcroft and Wentz, 2006) in this study.

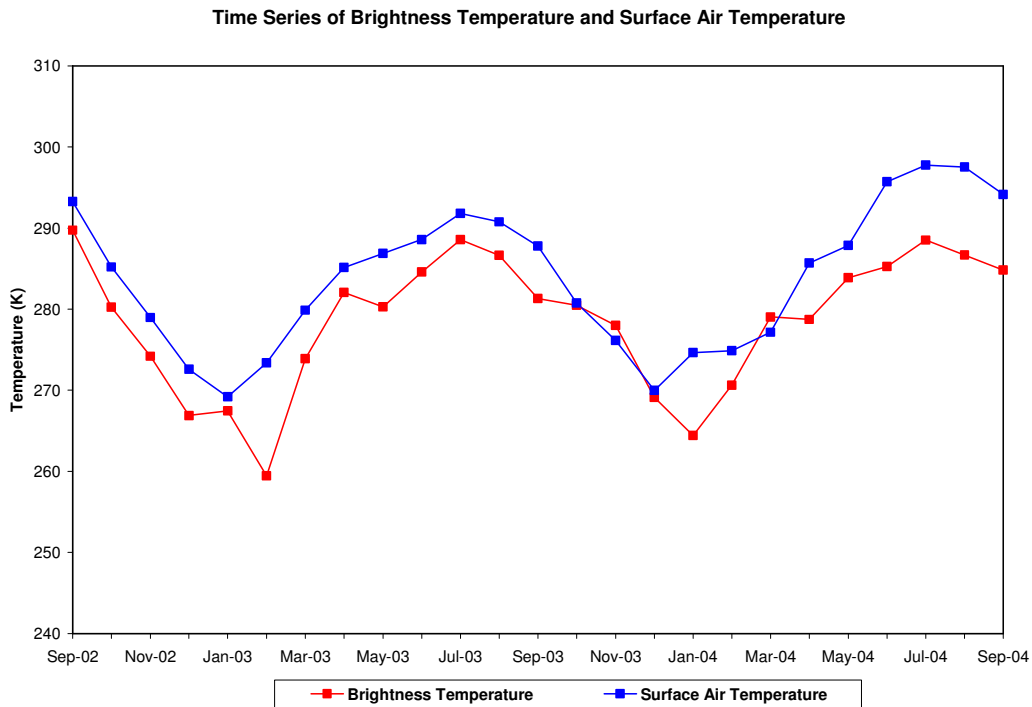


Figure 9. Comparison of the monthly surface air temperature and the brightness temperature at Owings Mills (39.41N, 76.79W) in Baltimore County, Maryland for the period from September 2002 to September 2004.

3.3.3 Soil Moisture Data

High-resolution satellite remotely sensed soil moisture data with several years of coverage would be optimal for this research. However, such information is not available for this study area. Therefore, the soil moisture data produced by the Land Data Assimilation System (LDAS) was used in this study.

The LDAS is a real-time, hourly, distributed, uncoupled, land surface simulation system. (Mitchell et al., 1999). This system is forced with real time output from numerical prediction models, satellite data, and terrestrial or space-based precipitation data. Model parameters are derived from the existing high-resolution vegetation and soil coverage. The forcing fields are observed hourly gage/radar precipitation and observed GOES-based satellite-derived surface solar insolation (Mitchell et al., 2000). The LDAS uses a 4-dimensional data assimilation modeling process to integrate past forecasts with observations to improve performance. The satellite-derived land-surface fields, such as soil moisture, skin temperature, snow, and vegetation density and greenness are included in the assimilation to produce accurate soil moisture data at different depths. The output of LDAS includes energy balance components, water balance components, evaporation components, surface water variables, and subsurface state variables. This LDAS produces its output at a higher spatial resolution and a longer temporal coverage which is essential in the training of ANN model. Soil moisture output from LDAS can be either hourly total soil column (0-200cm) moisture or hourly layered soil moisture at the layers of 0-10cm, 10-40cm, and 40-200cm. The data produced by North American Land Data Assimilation System (NLDAS), which is a subsystem of LDAS, was used here. The NLDAS runs in near real-time on an 1/8th degree grid. The spatial coverage is from 25 ° N to 53 ° N in latitude and from 125 ° W to 67 ° W in longitude. The temporal coverage ranges from October, 1996 through December, 2001 (Mitchell et al., 2000).

In order to examine the correctness of LDAS soil moisture, the LDAS soil moisture data was validated by the soil moisture measurements of Soil Climate Analysis Network (SCAN). SCAN is a nationwide network operated by the Natural Resources Conservation Service (NRCS, 2008). Its primary role is to provide soil and climate information at each SCAN site in a near real-time situation. The soil moisture is collected by a dielectric constant measuring device. Typical measurements are at 2, 4, 8, 20, and 40 inch of depth. SCAN sites generally reside on the agricultural areas of the United States. There are two SCAN sites in Maryland. One site is in Howard County, Maryland (39.25 ° N, 76.92 ° W), which operated from October 1, 1994 through December 19, 1998. The other site is in Prince George's County, Maryland (39.02 ° N, 76.85 ° W) and has been operating since October 30, 2001. The recorded soil moisture at the Howard County site is used to validate the LDAS soil moisture data. Figure 10 is a comparison of LDAS 0 – 10cm soil moisture and SCAN topsoil (at 5cm) soil moisture in Howard County, Maryland for the period of May 1997 through December 1998. These two time series show similar trends ($r = 0.68$) and both catch the high and low consistently. This suggests that the use of LDAS soil moisture data in this study is acceptable. The soil moisture data were downloaded from the LDAS website (LDAS, 2008). Then, they were processed using the Grid Analysis and Display System (GrADS). The soil moisture data at a grid location that was closest to the well site was used for model training at that well site.

Comparison of Soil Moisture at 39.25N, 76.92W (in Howard County, MD)

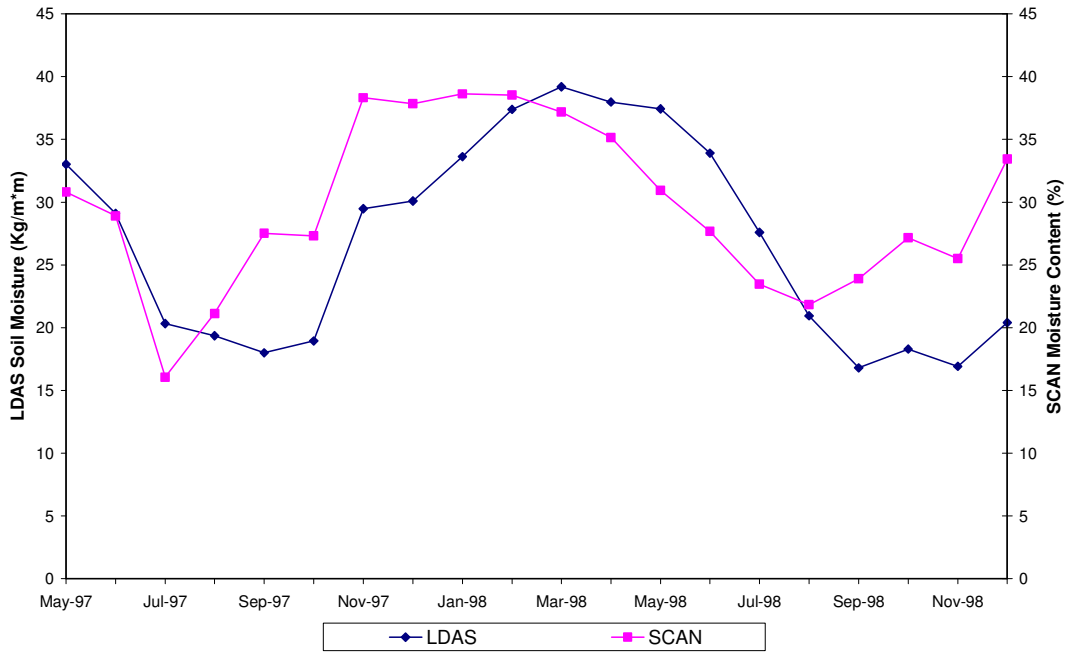


Figure 10. Comparison of time series of LDAS soil moisture and SCAN soil moisture at 39.25 ° N, 76.92 ° W in Howard County, MD.

3.3.4 Soil Data

For the single well ANN modeling, the soil data is not required. But, for the multiple wells ANN modeling at regional scale, the geological characteristics at different well sites need to be taken into consideration. Since the algorithm of this multiple ANN modeling is based on the variation of water storage in the vadose zone, the soil data need to be included in the modeling.

Coarse-textured soils such as sandy soils tend to have larger pores but smaller porosities. Fine-textured soils like clay soils have very small pores but larger porosities. These different types of soils, in terms of texture, respond to moisture holding capacity differently. A sandy soil will drain water quickly, but a clay soil will absorb more water and become waterlogged. The ANN water table prediction modeling at a regional scale is different from that at a single well site because several well sites which might have different soil types are involved. Different soil textural types could result in different water preserving capabilities at different locations, which would introduce different relationships between soil moisture change and water table fluctuation at different well sites. Therefore, the soil types at these different well sites need to be taken into account when doing a regional scale ANN water table prediction modeling.

Soil data were obtained from the Soil Data Mart of Natural Resources Conservation Services, Department of Agriculture. The soil information of each county in the Piedmont region was downloaded from the website. The well sites within each county were then located on the county soil map by using the Geographic Information System software ArcView. The soil information at the well location was then retrieved from the soil database with the help of ArcView. Figure 11 shows the soil map of Baltimore County, Maryland. The locations of four water table wells are pointed out on the map. The soil data at each water table well is assigned a hydrological soil type according to the Estimated Physical and Chemical Properties of Natural Soils Groups of Maryland

(Appendix C) provided by Maryland Department of Planning (1973). The hydrological soil type is then used as input for the ANN model.

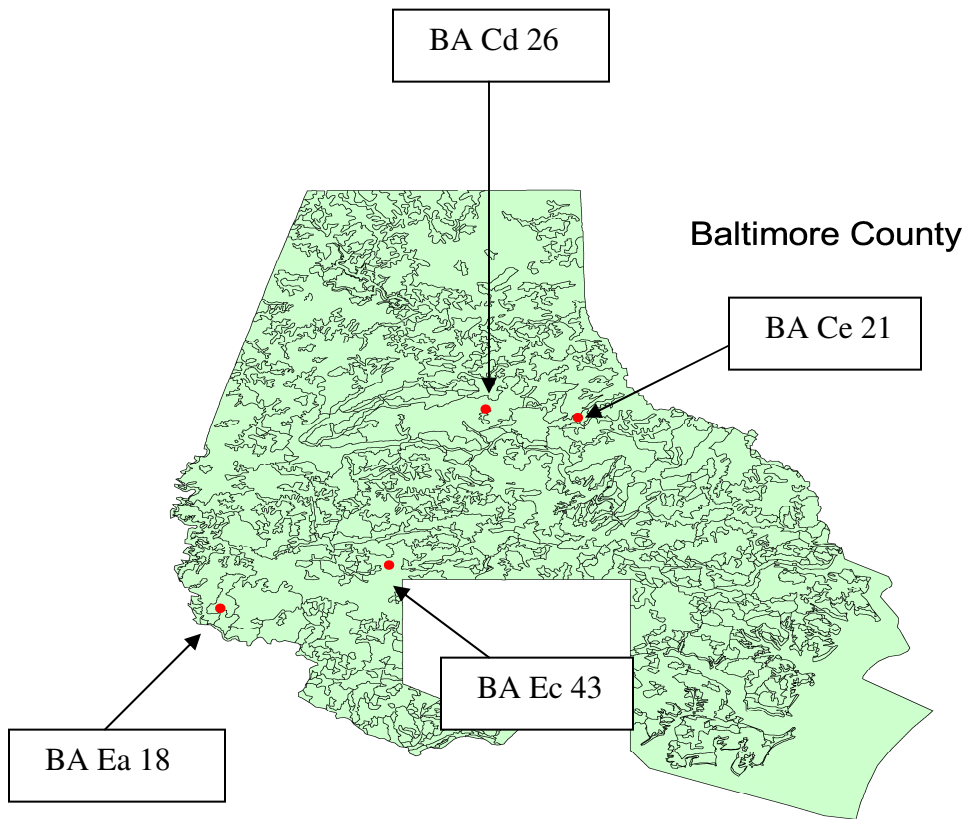


Figure 11. Soil map and the groundwater well locations in Baltimore County, Maryland.

3.4 ANN Water Table Prediction Model

Currently, there are many companies that produce artificial neural network software based on different ANN algorithms. The prices of ANN products range from several hundred dollars, such as the one produced by Logical Designs, to several thousand dollars, such as the one produced by Math Works. The ANN software that is based on a multilayer feedforward backpropagation algorithm, can be executed on a personal computer, and is priced around several hundred dollars is an ideal choice to perform this study.

The neural modeling system, Qnet 2000 (Qnet 2000), produced by Vesta Services Inc. was selected to build the ANN model in this study. Qnet 2000, which offers advanced network design features for creating complex networks, uses highly optimized backpropagation training algorithms, and is designed to run on a PC with a 32-bit operating system, fully satisfies the selection criteria. A feedforward three-layer backpropagation ANN with sigmoid function as the activation function is used to train the model.

First, single well ANN model will be trained to predict the water table fluctuation at selected locations. These ANN models are based on the relation between brightness temperature changes and water table variations or between soil moisture changes and water table variations at a well site. Only local brightness temperatures and water table measurements or local soil moisture contents and water table measurements are

involved in the training. The ANN model will be validated by data from a different time period at the same location. The forecasted water table fluctuation will then be compared with the groundwater level records to examine its accuracy. This portion of the study provides a site-dependent model to predict water table variation at the selected sites.

The second part of this study is an extension of the study in the first portion. An ANN model that is used to predict regional scale water table variation will be developed. At each time step, the training data includes hydrological soil type, current monthly mean column soil moisture content, subsequent monthly mean column soil moisture content, current water table measurement, and water table measurement of the next time step. The water table measurement of the next time step is used as the target, while the rest of the parameters are used as inputs in the training. These data are gathered from all selected wells in the Piedmont Plateau, Maryland. The ANN model will then be validated by data from a different time period. The forecasted results will be evaluated by comparing the predicted water table fluctuations with the groundwater level records at different sites in Maryland.

Chapter 4: Single Well ANN Water Table Prediction Modeling

Two water table wells (BA Ea 18 and FR Df 35, see Figure 12), both in the Piedmont Plateau, that record daily water table depths for a time span of several years are used in this single well ANN water table prediction modeling study. BA Ea 18 is located in Baltimore County, MD (39.35N, 76.86W) in the Woodstock Quartz Monzonite local aquifer. The land-surface elevation is 149.66 meters (491 feet) above mean sea level.

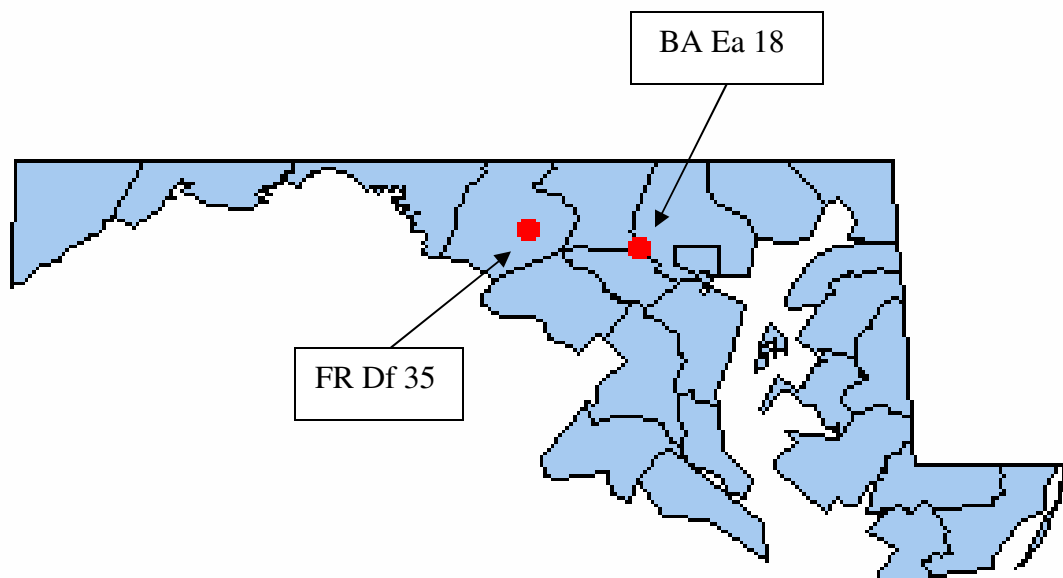


Figure 12. Locations of the two water table wells for single well ANN modeling – BA EA 18 in Baltimore County, MD and FR DF 35 in Frederick County, MD.

It has recorded monthly mean water table data from October 1999 through September 2007. FR Df 35 is located in Frederick County, MD (39.42N, 77.32W) in the Urbana Formation local aquifer. The land-surface elevation is 173.74 meters (570 feet) above mean sea level. It provides monthly mean water table measurements for the period from February 2004 to September 2006. Both wells have some months without monthly mean data.

4.1 Model Training and Results

The first attempt in the development of an ANN model for water table prediction utilized monthly mean brightness temperature and monthly mean water table depth as the primary input. The time series of water table depth and of brightness temperature at well BA Ea 18 from September 2002 through September 2004 indicates that there is no clear correlation ($r = -0.17$) between them (Figure 13). However, comparing the time series of water table depth change with that of brightness temperature for the same time period shows that they follow a similar trend ($r = 0.53$), as is depicted in Figure 14. A similar relationship was obtained for well site FR Df 35. The time series of water table depth and of brightness temperature (Figure 15) are not correlated well ($r = 0.05$), but the time series trends are very similar ($r = 0.56$) between water table depth change and brightness temperature (Figure 16). Therefore, using monthly mean water table change and monthly mean brightness temperatures as the input for the ANN model training at both well sites is a reasonable approach for this ANN water table prediction study.

A three-layer feedforward backpropagation ANN with five input nodes in the input layer and three hidden nodes in the hidden layer was selected for building the model. The number of hidden nodes selected here was based on results from several test runs. The model with three hidden nodes produced better results than that from other number of hidden nodes. The sigmoid function was used as the activation function. The monthly mean brightness temperature gathered by AMSR-E satellite and the monthly mean water table depth at BA Ea 18 were used as input data. Figure 17 shows the

Time Series of Water Table Depth and Brightness Temperature at BA Ea 18

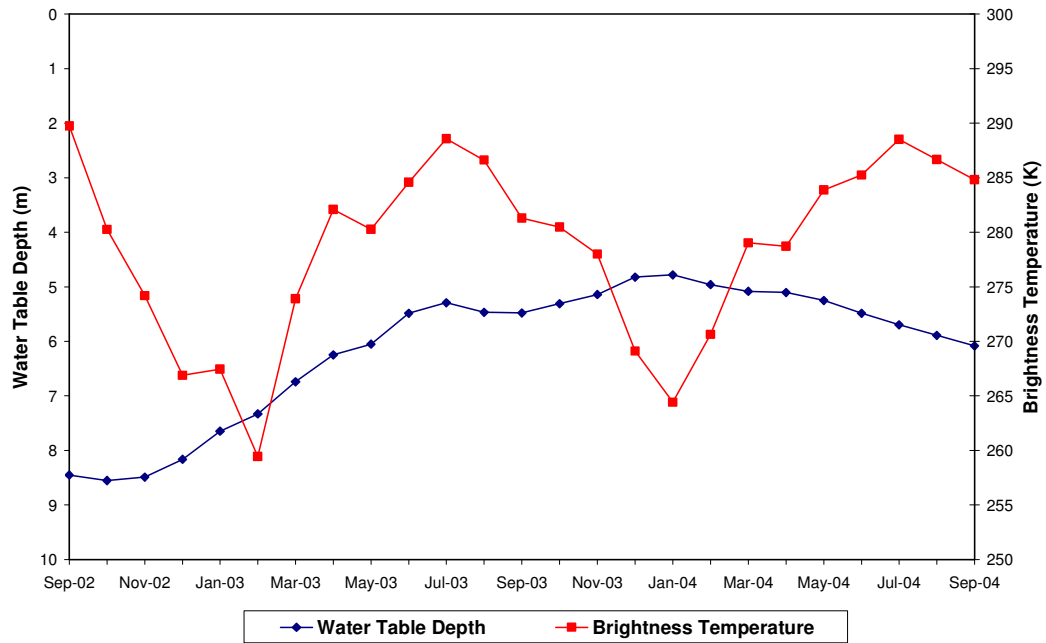


Figure 13. Time series of the water table depth and brightness temperature at well site BA Ea 18 in Baltimore County, MD ($r = -0.17$).

Time Series of Water Table Depth Change and Brightness Temperature at BA Ea 18

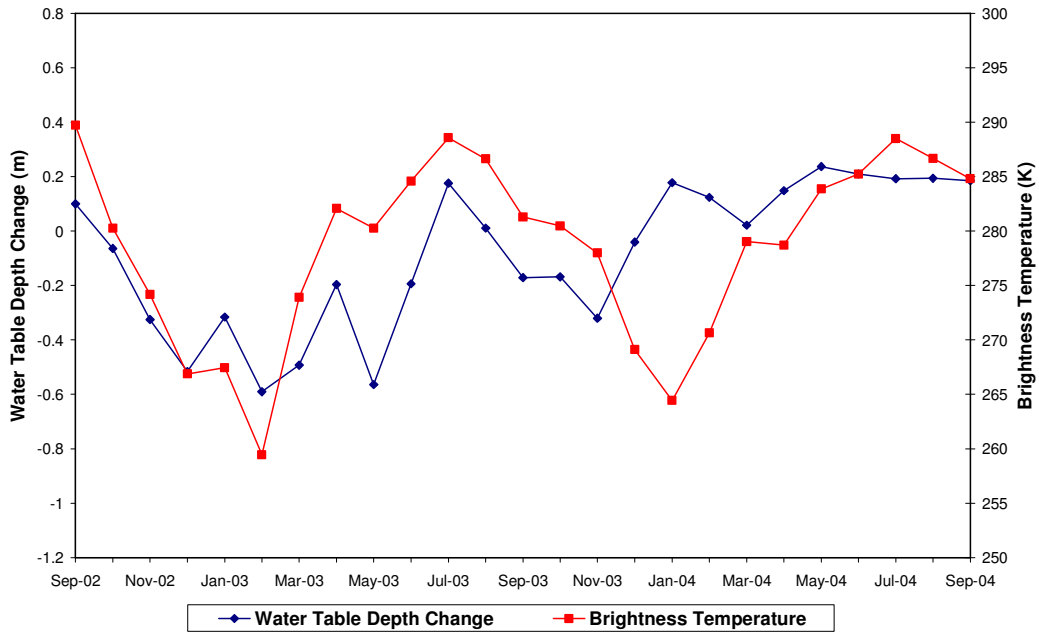


Figure 14. Time series of the water table depth change and brightness temperature at well site BA Ea 18 in Baltimore County, MD ($r = 0.53$).

Time Series of Water Table Depth and Brightness Temperature at FR Df 35

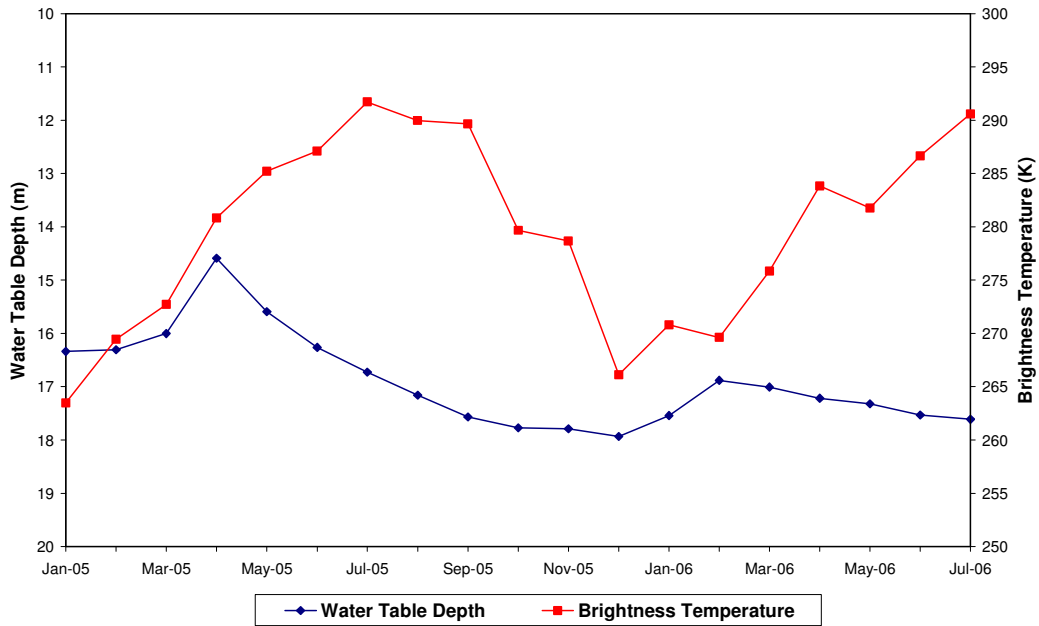


Figure 15. Time series of the water table depth and brightness temperature at well site FR Df 35 in Frederick County, MD ($r = 0.05$).

Time Series of Water Table Depth Change and Brightness Temperature at FR Df 35

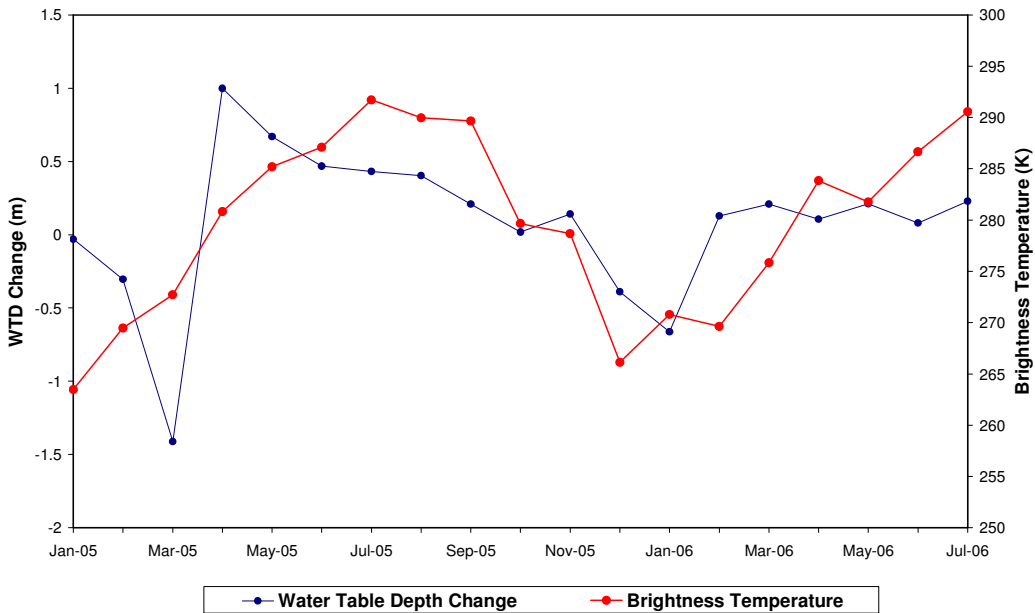


Figure 16. Time series of the water table depth change and brightness temperature at well site FR Df 35 in Frederick County, MD ($r = 0.56$).

structure of this three layer ANN model, which uses the previous month's brightness temperature, the current month's brightness temperature, the water table depth change in these two months, the current month's water table depth, and the subsequent month's brightness temperature as inputs. These parameters are all contained in the input file. The output is the predicted subsequent month's water table depth. Another file containing the measured water table depth for the subsequent month is used as the target file.

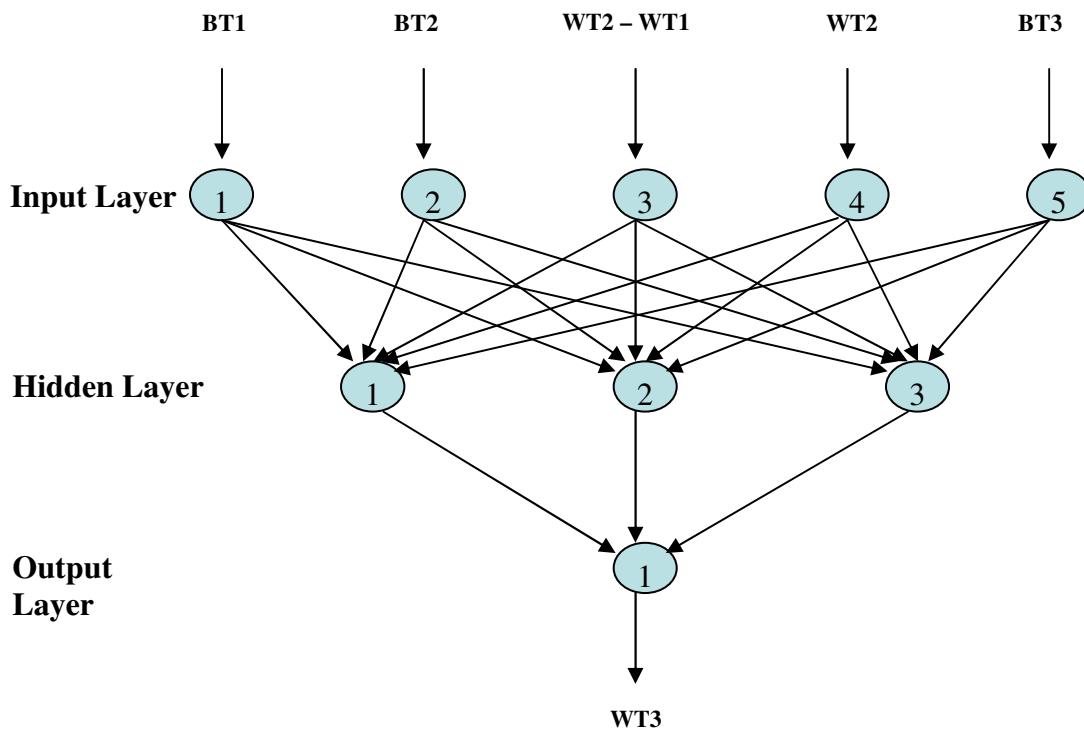


Figure 17. Schematic diagram of a three layer ANN model which uses previous brightness temperature (BT1), current brightness temperature (BT2), water table depth change (WT2 – WT1), current water table depth (WT2), and subsequent brightness temperature (BT3) as input. The output is the prediction of the water table depth (WT3).

The model was trained with the monthly mean data over the period of November 2002 through April 2004. The training outputs reached a minimum root mean square error of 0.058m after 350,000 iterations (Figure 18). This ANN model (BA_BT_WT) was selected as the water table prediction model at well site BA Ea 18. The connection weights between the input layer nodes and the hidden layer nodes and between the hidden layer nodes and the output layer node of the model are shown in Table 2a and Table 2b, respectively.

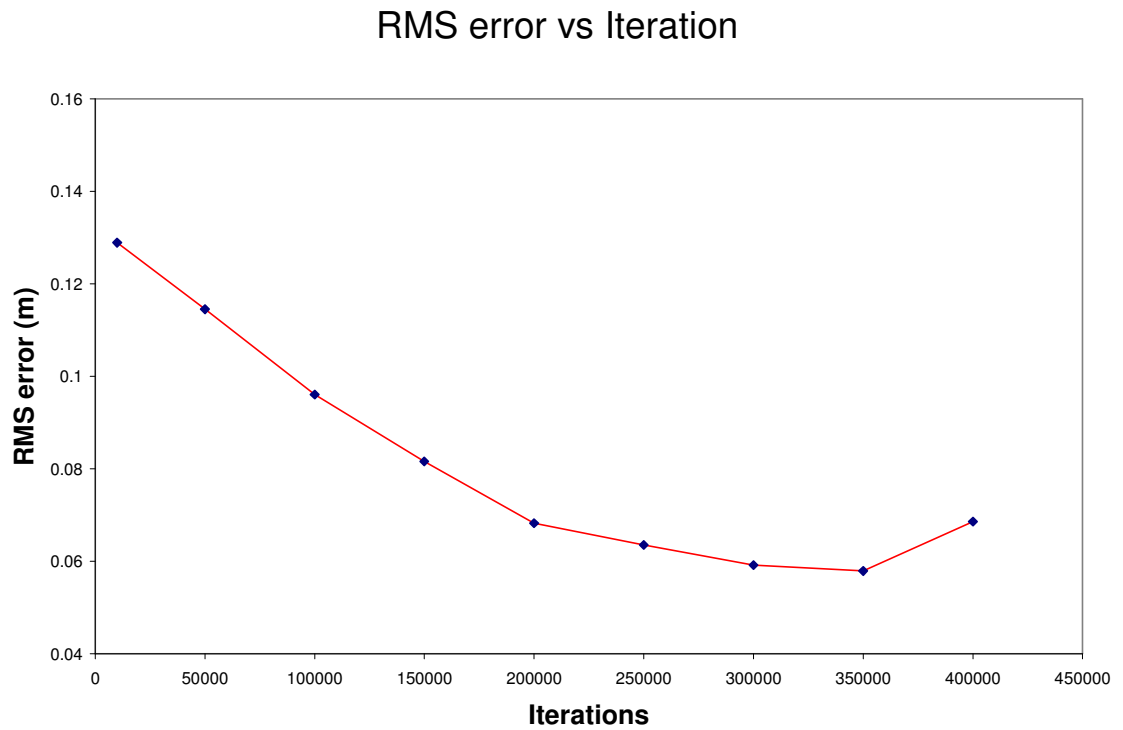


Figure 18. The ANN model training at well site BA Ea 18 reached a minimum root mean square error of 0.058m after 350,000 iterations.

Table 2a. Connection weights between input layer nodes and hidden layer nodes of Figure 17 for ANN model BA_BT_WT are shown in this table. The weight of bias input for each hidden layer node is also shown here.

Input Layer Node	Hidden Layer Node	Weight
1	1	-0.62529
2	1	3.97492
3	1	-0.33996
4	1	1.69158
5	1	0.32933
	1 (bias input)	-4.07365
1	2	0.42674
2	2	-0.9809
3	2	0.44079
4	2	-2.04207
5	2	0.01082
	2 (bias input)	2.22069
1	3	0.14678
2	3	2.22005
3	3	-1.39967
4	3	-3.62859
5	3	0.99287
	3 (bias input)	0.64362

Table 2b. Connection weights between hidden layer nodes and output layer node of Figure 17 for ANN model BA_BT_WT are shown in here. The weight of bias input for the output layer node is also shown in this table.

Hidden Layer Node	Output Layer Node	Weight
1	1	4.80523
2	1	-2.02508
3	1	-3.46757
	1 (bias input)	2.02535

The time series of the training output of the model matches the time series of the observation at this well site (Figure 19). A scatter diagram of model training output against the observed water table depths is also shown in Figure 20. This ANN model was validated by comparing the model's output with the observed data over the period of May 2004 through October 2004. The validation output resulted in a root mean square error of 0.107m. The validated water table prediction model's performance was examined for its forecast capability for the period of November 2002 to October 2003.

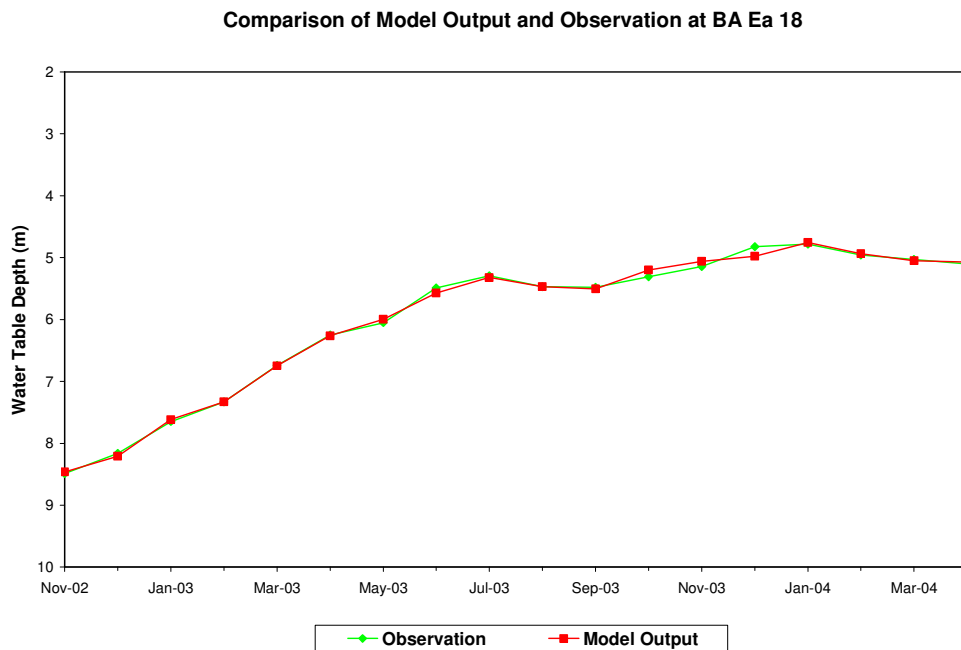


Figure 19. Comparison of the model predicted water table depths during ANN training with the observations at well site BA Ea 18.

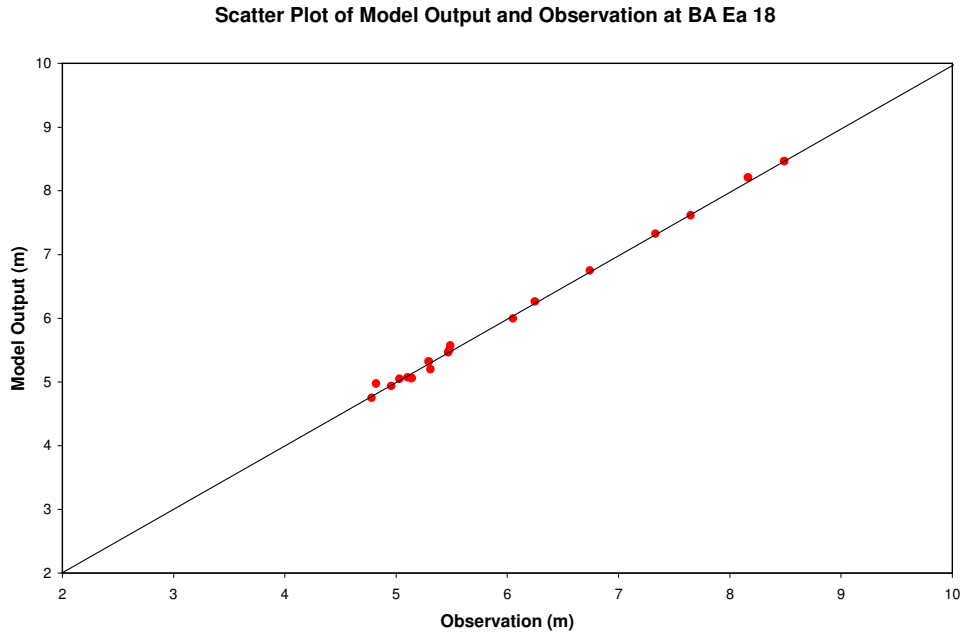


Figure 20. The scatter diagram of the model predicted water table depths during ANN training against the observed water table depths at well site BA Ea 18.

Except using the predicted water table depth as the input for the subsequent month, the rest of the inputs remained unchanged in the forecast simulations. The comparison between the forecasted and the observed water table depths is shown in Figure 21. The absolute difference between the forecasted and the observed water table depths changes from 0.025m for the first month to 0.116m for the 12th month. The root mean square error of the forecast for 12 months was found to be 0.043m.

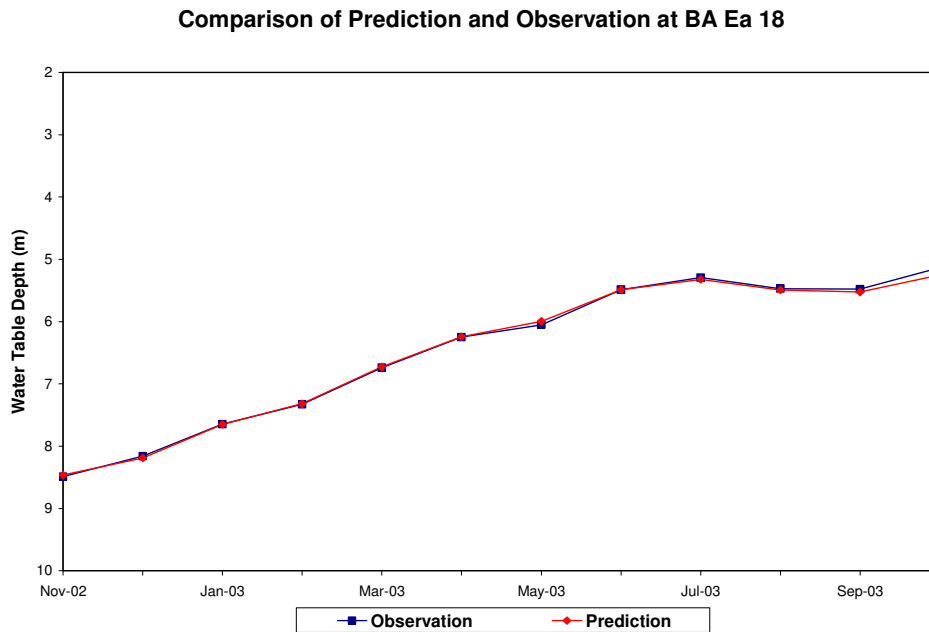


Figure 21. Comparison of the forecasted water table depths (using model BA_BT_WT) and the observed data at well site BA Ea 18. The forecast has a RMS error of 0.043m.

For the purpose of comparison, the same type of model training was conducted in Frederick County, MD at well site FR Df 35. The ANN model structure was the same as that used for BA Ea 18 site. The model (FR_BT_WT) was trained with the monthly mean brightness temperature and water table depth over the period from March 2005 to August 2006. The training output came to a minimum root mean square error of 0.04m after 350,000 iterations (Figure 22). Table 3a and Table 3b are the connection weights between the input layer nodes and the hidden layer nodes and between the hidden layer nodes and the output layer node used for this model. The comparison of the time series

of water table depth resulting from the training phase of the ANN model and the observed

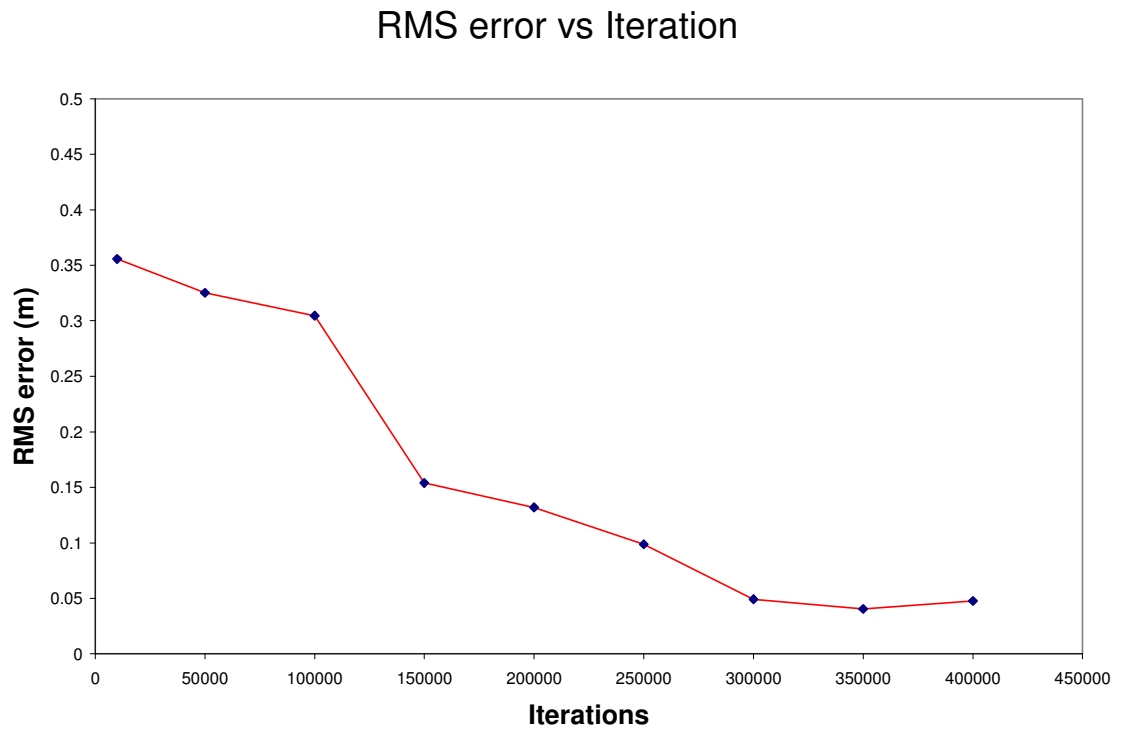


Figure 22. The ANN model training at well site FR Df 35 reached a minimum root Mean square error of 0.04m after 350,000 iterations.

Table 3a. Connection weights between input layer nodes and hidden layer nodes of Figure 17 for ANN model FR_BT_WT are shown in this table. The weight of bias input for each hidden layer node is also shown in this table.

Input Layer Node	Hidden Layer Node	Weight
1	1	-1.41744
2	1	-4.15786
3	1	0.91901
4	1	11.88938
5	1	-2.23375
	1 (bias input)	-2.78621
1	2	-2.66123
2	2	-4.82916
3	2	-0.27544
4	2	6.56021
5	2	-3.10731
	2 (bias input)	4.6746
1	3	4.21234
2	3	3.84454
3	3	1.03323
4	3	-0.97458
5	3	1.02484
	3 (bias input)	-1.12654

Table 3b. Connection weights between hidden layer nodes and output layer node of Figure 17 for ANN model FR_BT_WT are shown in this table. The weight of bias input for the output layer node is also shown here.

Hidden Layer Node	Output Layer Node	Weight
1	1	6.34815
2	1	-7.56729
3	1	4.01383
	1 (bias input)	-0.97243

water table depth is shown in Figure 23. It demonstrates a good match between these two time series. Figure 24 is the scatter diagram of the model's output during training against the observed data. Results indicate almost perfect correlation between these two data sets, thus indicating the ANN model's ability in predicting water table depth for the conditions of this study. This ANN model is thus used as the water table prediction model for this well site. Validation using available data from September 2006 through November 2006 has a root mean square error of 0.089m, indicating a very reasonable performance by the model. Using the validated model, the forecast run was performed over the period from March 2005 to February 2006.

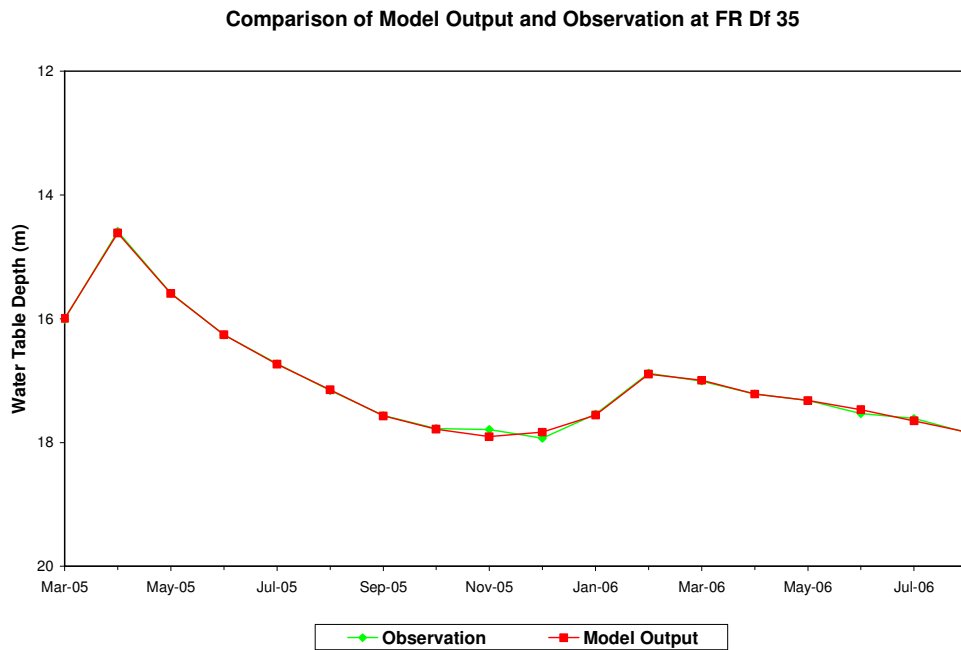


Figure 23. Comparison of the model predicted water table depths during ANN training with the observations at well site FR Df 35.

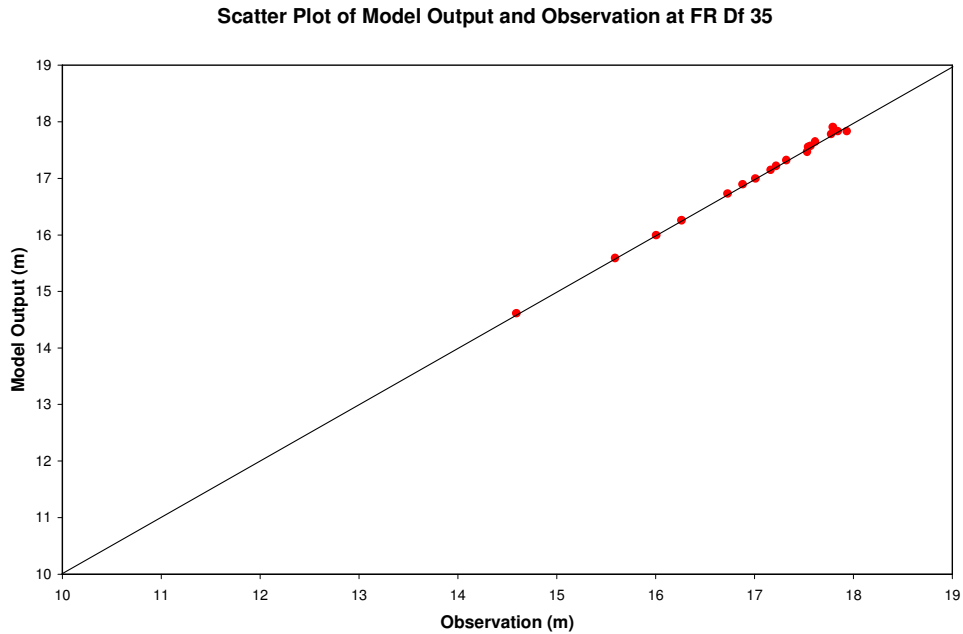


Figure 24. The scatter diagram of the model predicted water table depths during ANN training against the observed water table depths at well site FR Df 35.

The absolute error was found to be 0.009m and 0.039m for the first month and 12th month, respectively. The root mean square error over the 12 months' forecast was determined to be 0.044m, indicating a highly accurate forecasting. Figure 25 shows the time series comparison of the forecasted and the observed water table depth for the same well site, FR Df 35. Again, this relationship indicates the accuracy of the ANN model's predictions.

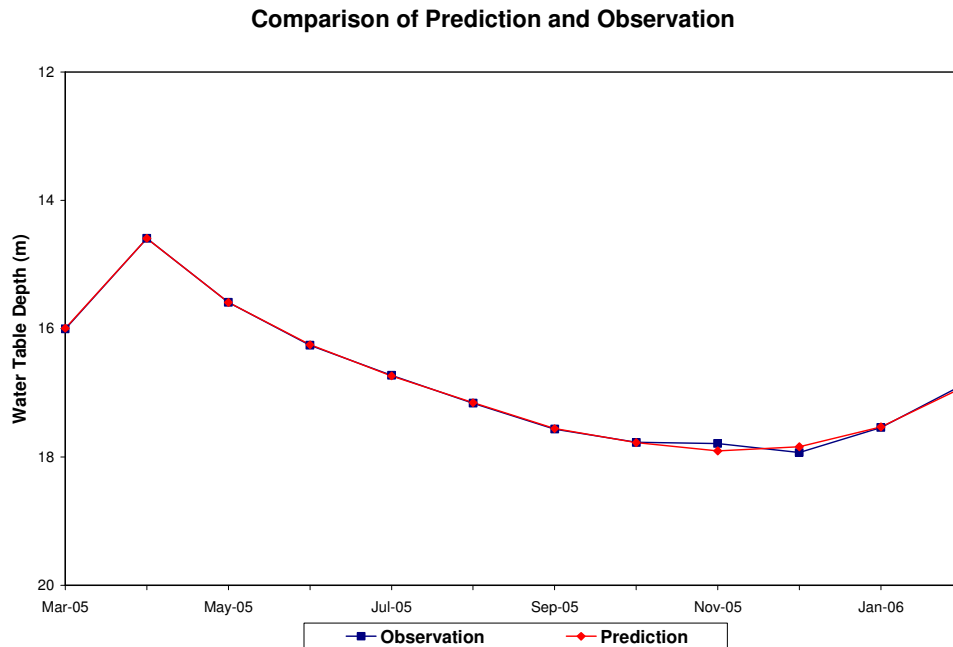


Figure 25. Comparison of the forecasted water table depths (using model FR_BT_WT) and the observed data at well site FR Df 35. The forecast has a RMS error of 0.044m.

The second attempt in the development of an ANN model for water table prediction utilized monthly mean soil moisture content and monthly mean water table depth as input. Figure 26 shows time series of the monthly mean water table depth and LDAS monthly mean column (0-200cm) soil moisture content at well site BA Ea 18 in Baltimore County, MD from October 1999 to December 2002. Basically, a water table rise comes with a wet period when soil is moist. A dry period in which soil moisture is low is always associated with a drop in the water table. There is a good correlation ($r = -0.65$) between these two parameters.

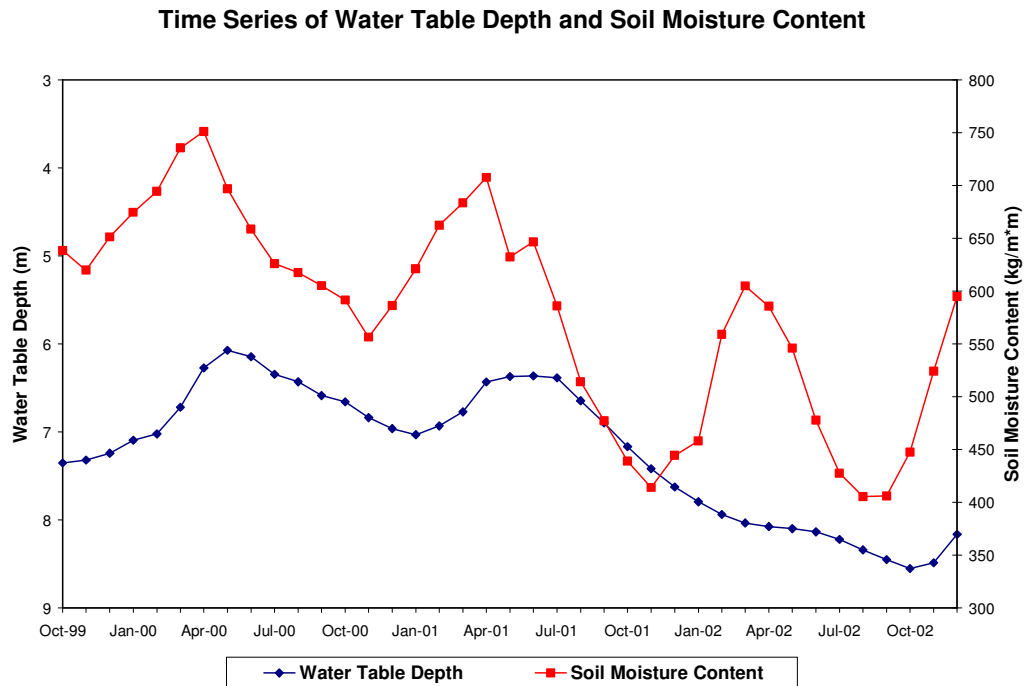


Figure 26. Time series of the water table depth and soil moisture content at well BA Ea 18 in Baltimore County, MD ($r = -0.65$).

After trial and error test, a three-layer feedforward backpropagation ANN with three nodes in the input layer, two nodes in the hidden layer, and one node in the output layer was used to build the model. The sigmoid function was selected as the activation function. The structure of this ANN model is depicted in Figure 27. The three input nodes are current monthly mean soil moisture, current monthly mean water table depth, and subsequent monthly mean soil moisture. The output node is the predicted water table depth. LDAS monthly mean column (0-200cm) soil moisture and measured water table depth were used in the input.

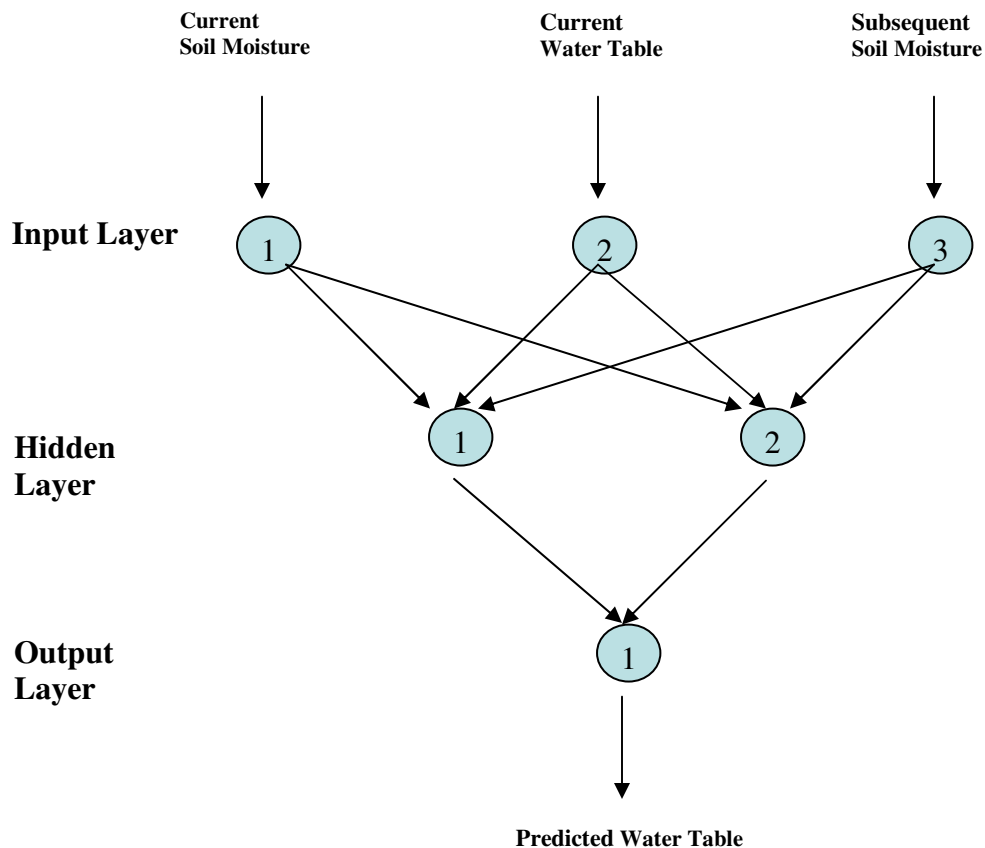


Figure 27. Schematic diagram of a three layer ANN model using current soil moisture content, current water table depth, subsequent soil moisture content as input. The output is predicted water table depth.

The model was trained with the monthly mean data over the period of November 2000 through December 2002. After 400,000 iterations, the training output reached a minimum root mean square error of 0.059m (Figure 28). This ANN model (BA_SM_WT) was hence selected as the water table prediction model. The connection weights between the input layer nodes and the hidden layer nodes and between the hidden layer nodes and the output layer node of the model are shown in Table 4a and

Table 4b, respectively. The comparison of the model predicted water table depth during ANN training with the

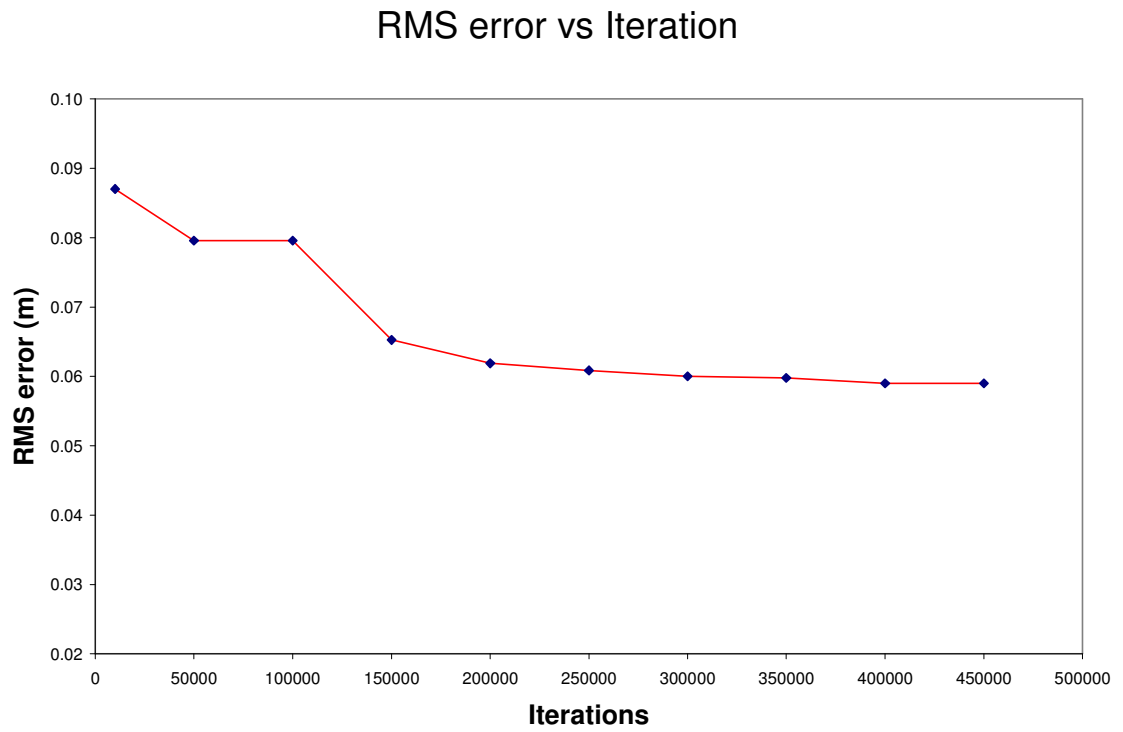


Figure 28. The ANN model training at well site BA Ea 18 reached a minimum root mean square error of 0.059m after 400,000 iterations.

Table 4a. Connection weights between input layer nodes and hidden layer nodes of Figure 27 for ANN model BA_SM_WT are shown in this table. The weight of bias input for each hidden layer node is also shown here.

Input Layer Node	Hidden Layer Node	Weight
1	1	0.16162
2	1	-2.49647
3	1	0.19332
	1 (bias input)	1.44859
1	2	-2.46467
2	2	5.66167
3	2	-3.16399
	2 (bias input)	4.42196

Table 4b. Connection weights between hidden layer nodes and output layer node of Figure 27 for ANN model BA_SM_WT are shown in this table. The weight of bias input for the output layer node is also shown here.

Hidden Layer Node	Output Layer Node	Weight
1	1	-5.99023
2	1	3.67721
	1 (bias input)	0.04375

observation is shown in Figure 29. They match very well except in the last three months when the water table is low. The scatter plot of the training output against the observation is shown in Figure 30. This ANN model was then validated by comparing the model's output with the observed data over the period from November 1999 through October 2000. The root mean square error of the validation output was 0.069m.

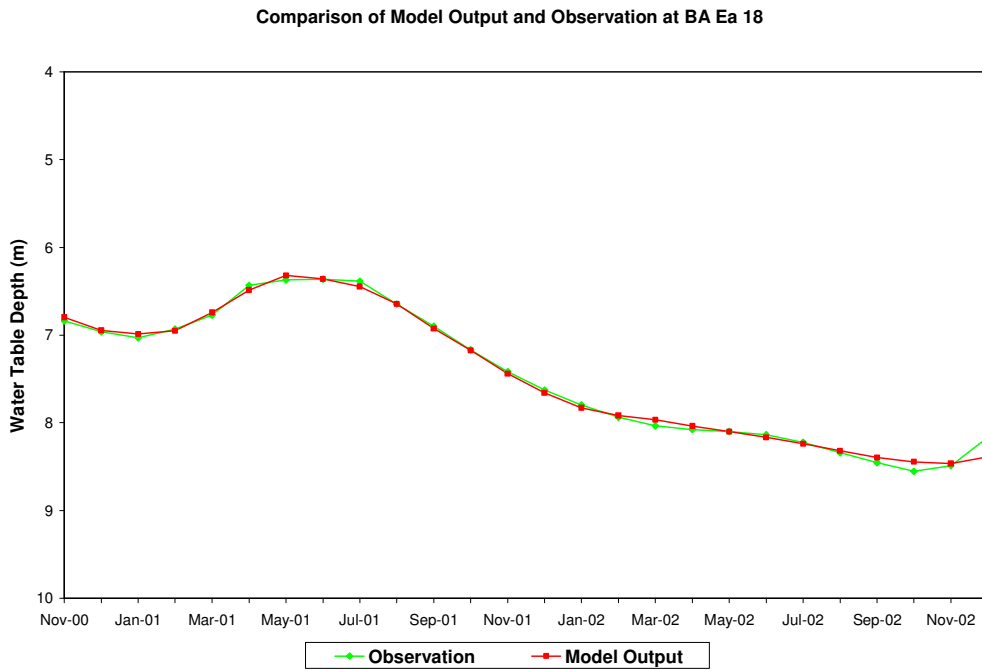


Figure 29. Comparison of the model predicted water table depths during ANN training with the observations at well site BA Ea 18.

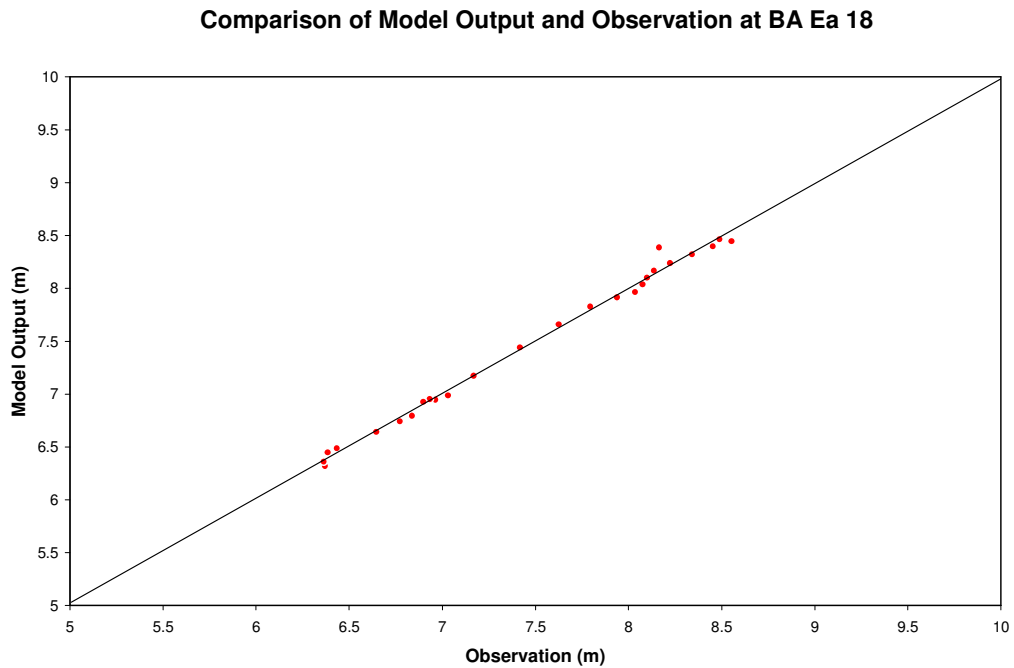


Figure 30. The scatter diagram of the model predicted water table depths during ANN training against the observed water table depths at well site BA Ea 18.

A forecast simulation was conducted for the period from January 2001 to December 2001 to investigate its forecast strength. A comparison of the forecast with the observation is shown in Figure 31. The absolute difference between the forecasted and the observed water table depths changes from 0.044m for the first month to 0.089m for the 12th month. The root mean square error of the forecast over 12 months is 0.047m.

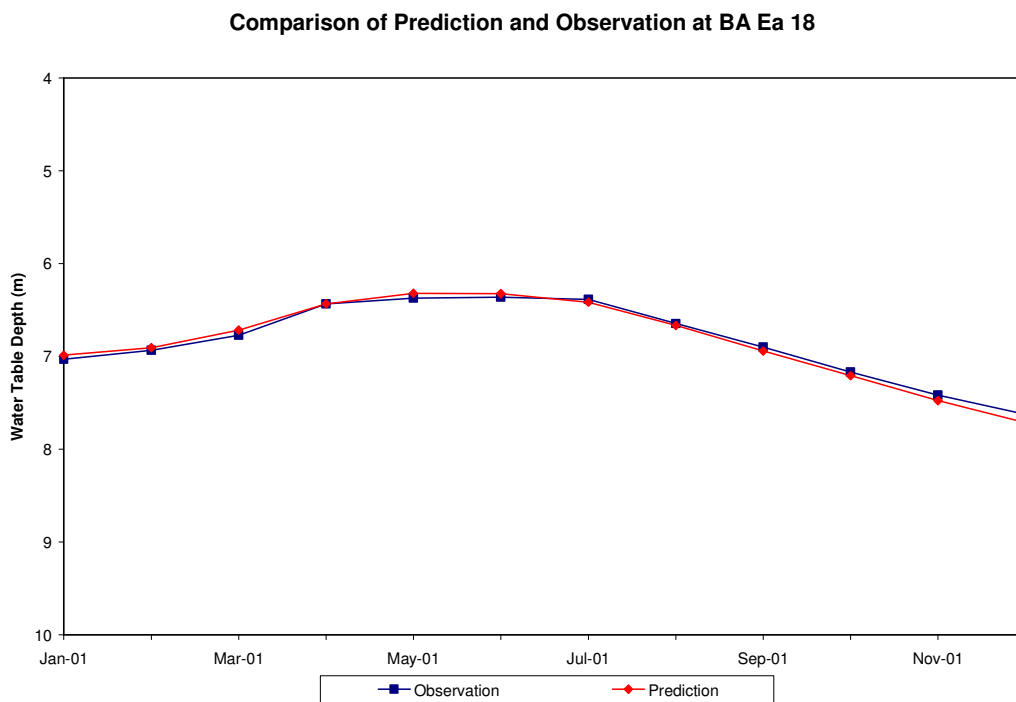


Figure 31. Comparison of the forecasted water table depths (using model BA_SM_WT) and the observed data at well site BA Ea 18. The forecast has a RMS error of 0.047m.

Chapter 5: Regional Scale ANN Water Table Prediction Modeling

Thirteen water table wells (Table 5) located in Piedmont Plateau, Maryland (Figure 32) were selected for the regional scale water table prediction modeling study. Most of them only provide sporadic measurements at different days in each month. In order to consistently model the water table fluctuations using the relationship between soil moisture content and water table depth, the water table depths at each well were linearly interpolated to obtain the water table depth on the first day of each month at that well for the ANN modeling. Figure 33 is an example of the comparison of the time series of the recorded and interpolated water tables for the period from 1994 through 2002 at the well site HO Bd 1 in Howard County, Maryland.

Table 5. Names of the thirteen water table wells used in this regional scale study, the aquifers that these wells located, and their longitudes, latitudes, and surface elevations.

Number	Well Name	Aquifer	Longitude (W)	Latitude (N)	Altitude (m)
4	BA Cd 26	Baltimore Gneiss	76.645	39.5247	146.3
6	BA Ea 18	Woodstock Granite	76.8569	39.3458	149.66
7	BA Ec 43	Baltimore Gneiss	76.7222	39.3847	152.4
17	FR Cg 1	Ijamesville Formation	77.2325	39.5322	182.88
18	FR Df 35	Sama Creek Metbasalt	77.3178	39.4214	173.74
27	HA Bd 31	Baltimore Gabbro Complex	76.2667	39.6506	140.21
28	HA Ca 23	Loch Raven Formation	76.5072	39.5328	143.26
32	HO Bd 1	Morgan Run Formation	76.9492	39.3194	192.02
33	HO Cd 79	Loch Raven Formation	76.9308	39.2458	137.88
34	HO Ce 38	Sykesville Formation	76.9	39.1669	131.06
39	MO Cc 14	Ijamesville Formation	77.3783	39.2206	170.69
40	MO Eh 20	Loch Raven Formation	76.9583	39.0761	123.44
41	PG Bc 16	Patuxent Formation	76.9375	39.0308	57.91

Maryland Water Table Wells

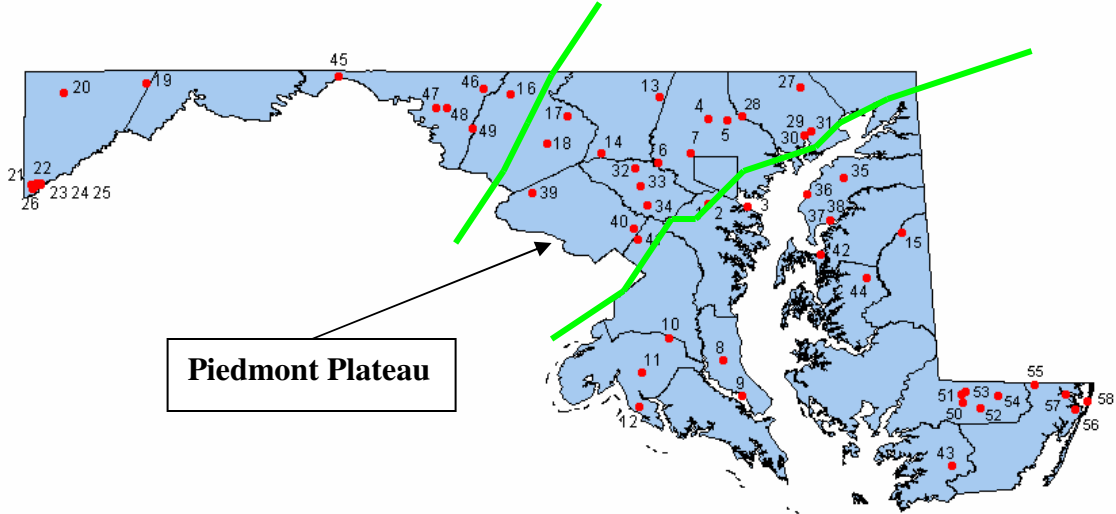


Figure 32. Distribution of the water table wells in Piedmont Plateau, Maryland (between two green lines).

Recorded and Interpolated Water Table at Howard County, MD (HO Bd 1)

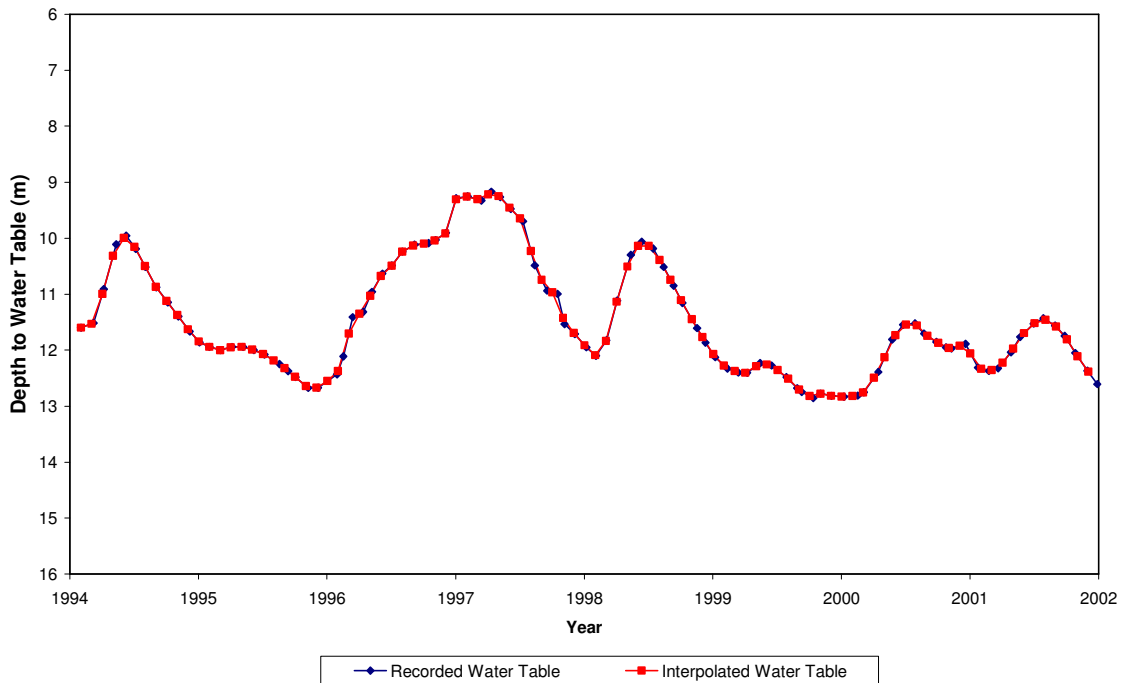


Figure 33. Time series of recorded and interpolated water tables at HO Bd 1 in Howard County, MD from 1994 to 2002.

The time series of water table depth changes between the first day of consecutive months and the time series of monthly mean soil moisture variations at 0 – 200cm of soil layer were compared at these thirteen available water table well sites. Figure 34 is the time series of water table depth changes and soil moisture content variations for the months of November 1996 through October 2000 at water table well BA_CD_26 in the Piedmont Plateau. The time series of water table depth changes and soil moisture content variations at the other 12 water table well sites are placed in Appendix C. Basically, there is an inverse correspondence between the changes in

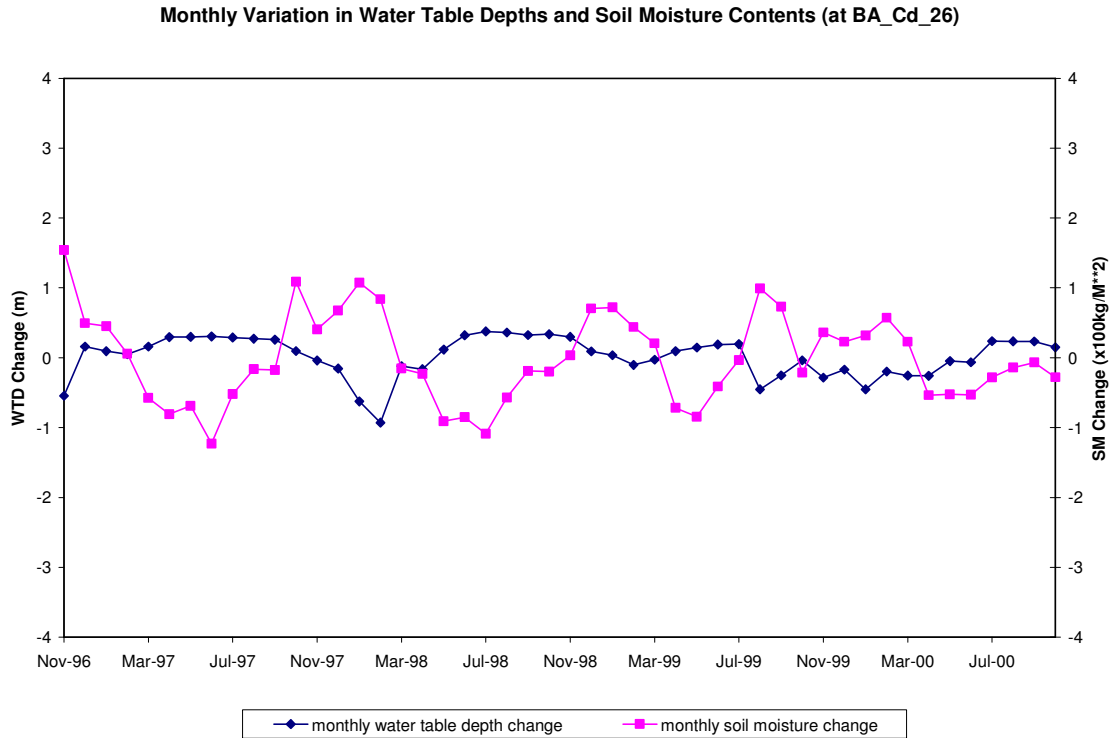


Figure 34. Time series of the water table depth changes and soil moisture content variations for the months of November 1996 through October 2000 at water table well BA_CD_26 in Piedmont Plateau, Maryland.

water table depths and the changes in soil moisture contents. The correlation coefficient of the water table depth change of the first days of consecutive months and the monthly mean soil moisture variations at 0 – 200cm of the soil layer at each of the thirteen individual water table wells for the same period of time are shown in Table 6. Except wells HO Bd 1 and HO Ce 38, the absolute correlation coefficients are above 0.5. The highest correlation coefficient is -0.789 at well HA Ca 23.

Table 6. Correlation coefficient of the water table depth changes of the first days of consecutive months and the monthly mean soil moisture variations for each individual water table well in the Piedmont Plateau, Maryland.

Well Name	Correlation Coefficient
BA Cd 26	-0.655
BA Ea 18	-0.620
BA Ec 43	-0.666
FR Cg 1	-0.541
FR Df 35	-0.657
HA Bd 31	-0.696
HA Ca 23	-0.789
HO Bd 1	-0.338
HO Cd 79	-0.524
HO Ce 38	-0.494
MO Cc 14	-0.726
MO Eh 20	-0.725
PG Bc 16	-0.651

The correlation coefficients between monthly mean soil moisture variations and water table depth changes of the first days of consecutive months at different soil layers for all available thirteen water table wells in Piedmont Plateau are shown in Table 7. In

Table 7. Correlation coefficients between monthly soil moisture variations and water table changes of the first days of consecutive months at different soil layers.

Soil Moisture Layer (cm)	Correlation Coefficient
0 - 10	-0.446
0 - 40	-0.455
0 - 100	-0.522
0 - 200	-0.530

general, there exists a negative correlation between these two parameters for all the layers involved. This demonstrates that a decrease in the water table depth, which means a rise of the water table, is associated with the increase in soil moisture content in each of the four soil layers, and vice versa.

The absolute correlation coefficient between the water table changes and the soil moisture variations increases with the soil layer thickness. It reaches an absolute maximum of 0.53 when the soil moisture change in the layer of 0 - 200cm is compared with the water table depth variation. This higher correlation suggests that using the soil moisture content of 0 – 200cm soil column is better for this study. Besides soil moisture content, there exist some other factors such as soil type, land use, and land cover at the water table well sites that might affect the water table depth variations. Since the soil moisture is measured beneath the ground surface, the land use and land cover on the surface at each well site are not considered at this stage. Hydrologic soil type which directly affects the storage of water in the soil is the parameter (in addition to soil moisture content and water table depth) taken into the ANN model to represent the geological characteristics at each well site.

5.1 Model Training and Results

A three-layer feedforward backpropagation ANN with four nodes in the input layer, two nodes in the hidden layer, and one node in the output layer was used to build the regional scale ANN model. Basically, there was no significant difference in the results that caused by the use of other number of hidden nodes in the test runs. The sigmoid function was used as the activation function. The structure of this ANN model is depicted in Figure 35. The three input nodes are monthly mean soil moisture content of the previous month, water table depth on the first day of the current month, and monthly mean soil moisture content of the current month. The output is the predicted water table depth on the first day of the subsequent month. The monthly mean soil moistures produced by NLDAS and the recorded water table depths obtained from USGS were used in the modeling.

The model was trained for the period of November 1996 through October 2000 using data from all thirteen available well sites with soil moisture contents from four different soil layers, 0 – 10cm, 0 – 40cm, 0 – 100cm, and 0 – 200cm. Figure 36 shows the RMS errors of the training outputs at different iterations for the model training at four different soil layers. Results indicated that the model trained with soil moistures from 0 – 200cm soil layer had the smallest RMS errors at different iterations relative to that from the other layers. The associated RMS errors decreased as the number of iterations increased. After 50,000 iterations, the training output reached a root mean square error of 0.351m, where not much change observed after that point. Table 8 shows the RMS

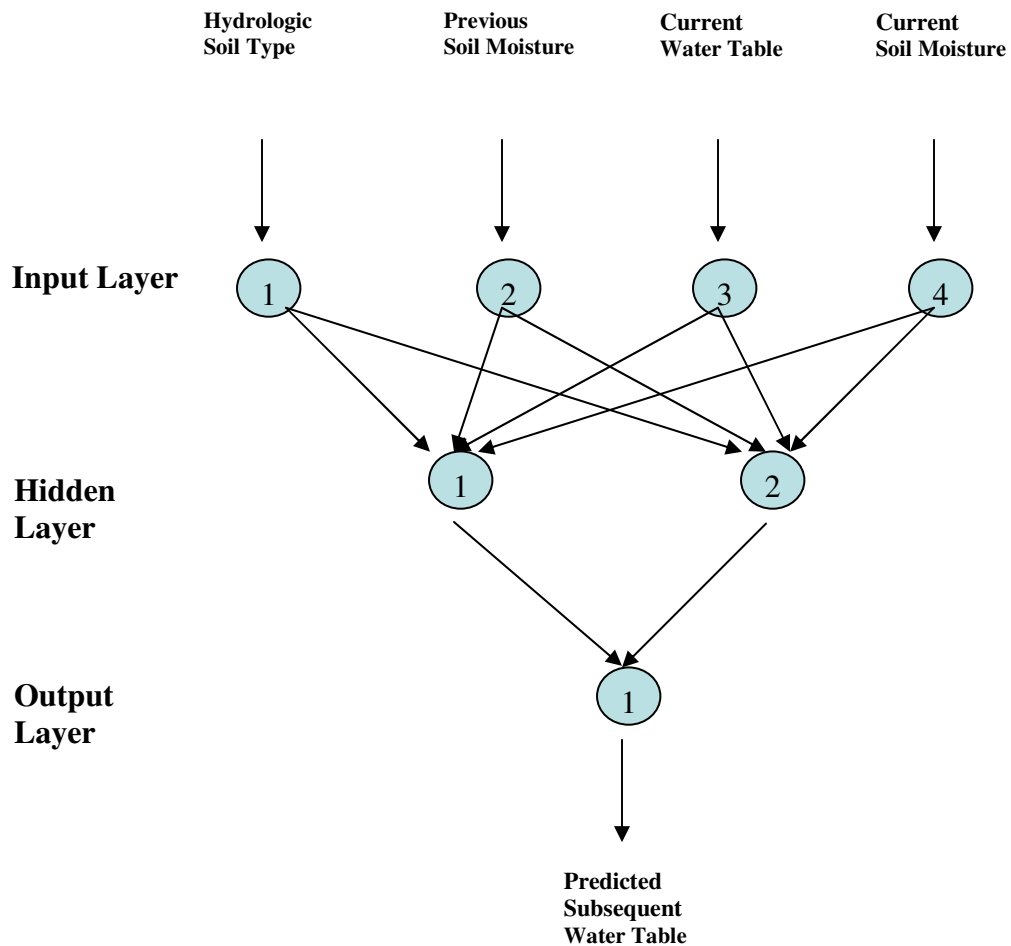


Figure 35. Schematic diagram of a three layer ANN model using hydrologic soil type, monthly mean soil moisture content of the previous month, water table depth on the first day of the current month, and monthly mean soil moisture content of the current month as input. The output is the predicted water table depths on the first days of the subsequent month.

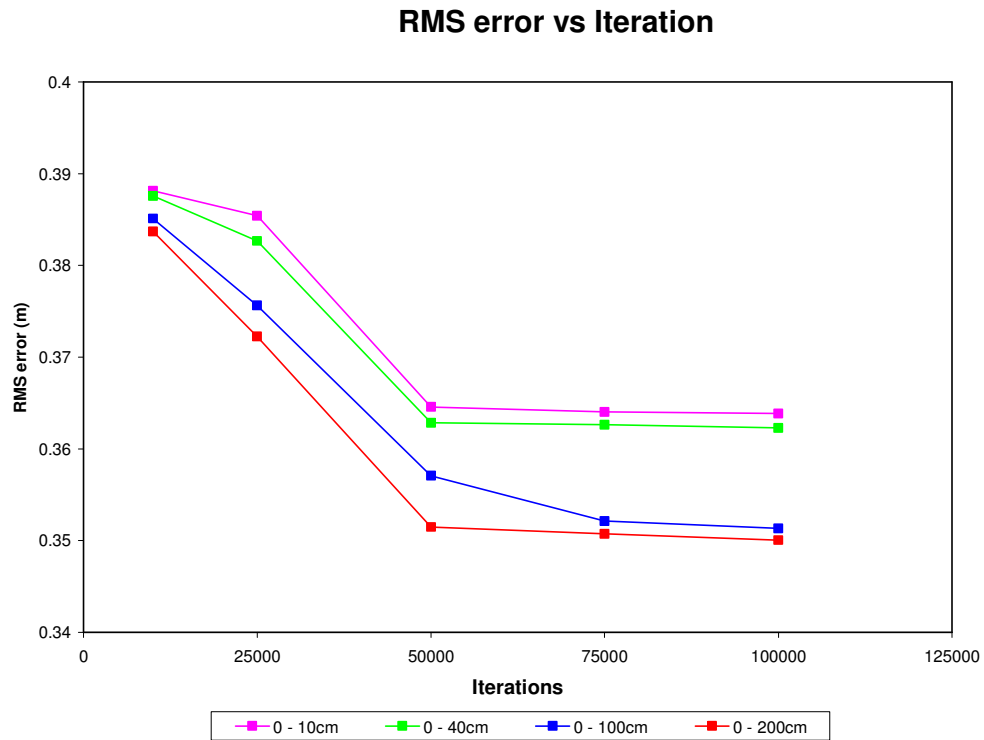


Figure 36. The RMS errors versus the number of iterations for the ANN training with soil moistures at four different layers.

errors of training outputs and the correlations between training outputs and observations for training at different soil depths at 50,000 iterations. Overall, that the model which trained with soil moisture content of 0 – 200cm soil stratum has a RMS error of 0.351m and a correlation coefficient of 0.997 is the best choice for this study.

Table 8. The RMS errors of training outputs and the correlations between training outputs and observations for ANN model training at different soil depths at 50,000 iterations.

Soil Layer (cm)	RMS Error (m)	Correlation Coefficient
0 - 10	0.384	0.996
0 - 40	0.382	0.996
0 - 100	0.370	0.997
0 - 200	0.351	0.997

The RMS error of the training outputs, as well as the correlation coefficient between training outputs and observations at each well site, are listed in Table 9. While at most of the well sites the training outputs have RMS errors less than 0.22m, three well sites have RMS errors around 0.4m, and one well site, MO Cc 14, had a RMS error of 0.865m. The exceptionally high RMS error at MO Cc 14 attracted attention for a further investigation. Most of the correlation coefficients between the training outputs and the observations at the well sites are above 0.9. Only at three well locations, the correlation coefficients are a little less than 0.9.

Table 9. The RMS errors of training outputs and the correlation coefficients between training outputs and observations at the 13 well sites.

Well Name	RMS error (m)	Correlation Coefficient
BA Cd 26	0.203	0.971
BA Ea 18	0.223	0.967
BA Ec 43	0.120	0.874
FR Cg 1	0.397	0.891
FR Df 35	0.399	0.953
HA Bd 31	0.430	0.925
HA Ca 23	0.117	0.961
HO Bd 1	0.285	0.969
HO Cd 79	0.208	0.977
HO Ce 38	0.209	0.933
MO Cc 14	0.865	0.895
MO Eh 20	0.215	0.938
PG Ec 16	0.154	0.971

A validation run was performed on the model with the data from all thirteen well sites for the period from November 2000 to October 2001. The overall RMS error of the validation outputs was 0.282m. The RMS error at each individual well site is listed in

Table 10. The RMS errors are less than or around 0.3m at most of the well sites except at MO Cc 14, which has a RMS error of 0.66m.

Table 10. The RMS errors of validation outputs at each individual well site (13 wells run).

Well Name	RMS error (m)
BA Cd 26	0.203
BA Ea 18	0.142
BA Ec 43	0.110
FR Cg 1	0.277
FR Df 35	0.337
HA Bd 31	0.258
HA Ca 23	0.099
HO Bd 1	0.277
HO Cd 79	0.242
HO Ce 38	0.195
MO Cc 14	0.660
MO Eh 20	0.243
PG Ec 16	0.162

The high RMS errors of the model training and validation outputs at well MO Cc 14 pointed out that the accuracy of the model outputs at this well site was questionable. This may have caused by the inaccurate input data at MO Cc 14 or by other factors that might have strong influence on the water table fluctuation at this particular site. An ANN model with the same structure, but trained by excluding the data at MO Cc 14, was therefore constructed. This ANN model, a Regional Water Table Depth Prediction Model (Regional_WTDP), was trained by using the recorded water table depths and the NLDAS generated soil moisture at 0 – 200cm layer at the twelve available well sites. Fifty thousand iterations were performed during the training. The RMS error of model training outputs improved from 0.351m to 0.26m. The correlation coefficient between the training outputs and the observation also showed a small improvement, from 0.997 to 0.998. The scatter plot of the model outputs against the observations at the 12 wells is showed in Figure 37, which suggests a good correlation between the model output and the observation. Table 11a and Table 11b are the connection weights between the input layer nodes and the hidden layer nodes and between the hidden layer nodes and the output layer node used for this model.

The model outputs during ANN training were compared with the observations at each individual well site. Figure 38 is an example of the comparison at well BA Cd 26. The comparisons at the rest of well locations are displayed at Appendix D. In general, the match between the training outputs and the observations are very good for all the locations. The RMS error of the training outputs and the correlation coefficient between

Scatter Diagram of Model Training Output Against Observation

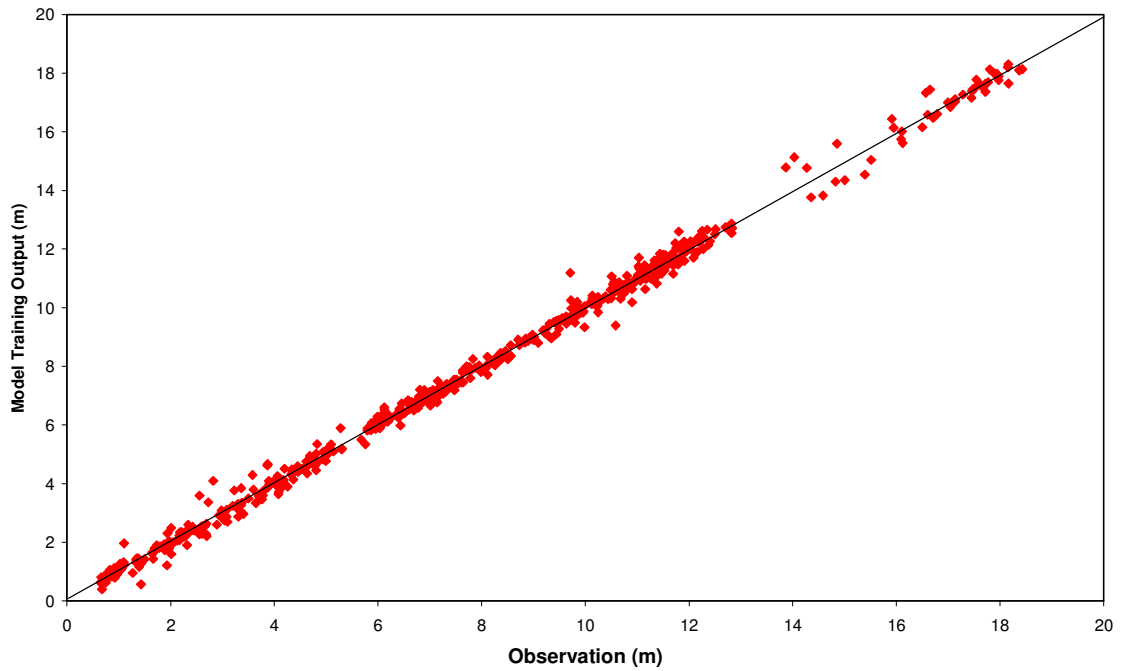


Figure 37. The scatter diagram of the model predicted water table depths from ANN model training against the observed water table depths at all 12 wells.

Table 11a. Connection weights between input layer nodes and hidden layer nodes of Figure 35 for ANN model Regional_WTDP are shown here. The weight of bias input for each hidden layer node is also shown here.

Input Layer Node	Hidden Layer Node	Weight
1	1	0.02005
2	1	0.45966
3	1	5.44681
4	1	-0.42208
	1 (bias input)	0.07445
1	2	-0.01734
2	2	-0.27782
3	2	-4.06683
4	2	0.42545
	2 (bias input)	4.12543

Table 11b. Connection weights between hidden layer nodes and output layer node of Figure 35 for ANN model Regional_WTDP are shown in this table. The weight of bias input for the output layer node is also shown here.

Hidden Layer Node	Output Layer Node	Weight
1	1	5.2695
2	1	-6.45252
	1 (bias input)	0.81234

Comparison of Model Output and Observation at BA Cd 26

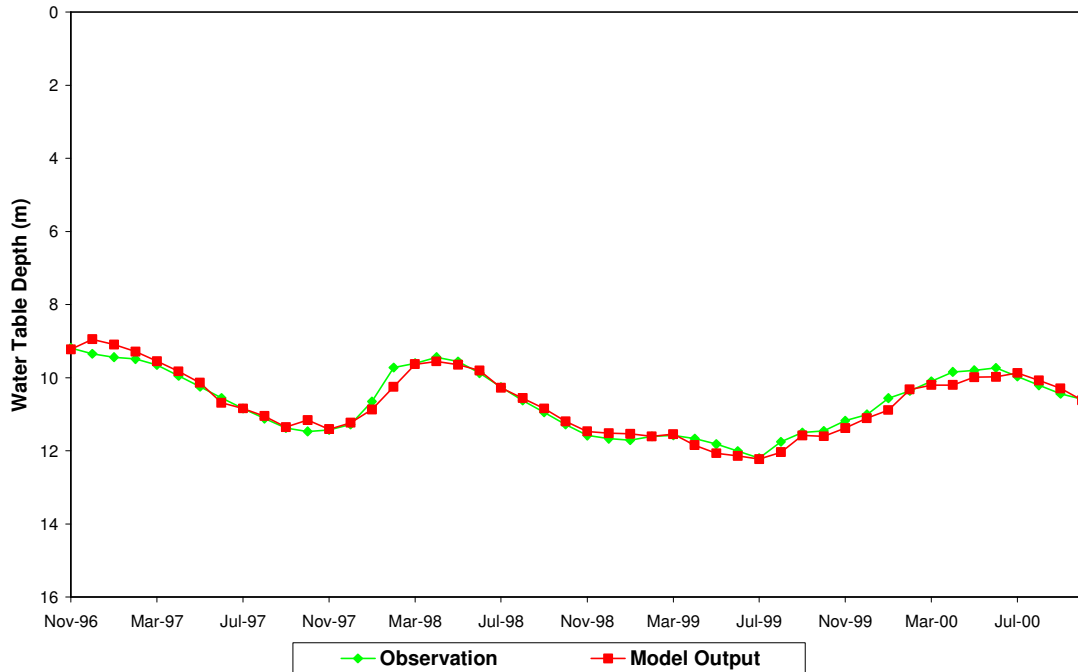


Figure 38. Comparison of the model predicted water table depths during ANN training with the observations at well site BA Cd 26.

training outputs and observations at each well site are listed in Table 12. Except at three well sites, FR Cg 1, FR Df 35, and HA Bd 31, the RMS errors are a little more than 0.4m, and the values at the rest of the well locations are around or below 0.22m. At most well sites the correlation coefficients are above 0.9, except at BA Ec 43 and FR Cg 1 where the correlation coefficients are around 0.88.

Table 12. The RMS errors of training outputs and the correlation coefficients between training outputs and observations at the 12 well sites.

Well Name	RMS error (m)	Correlation Coefficient
BA Cd 26	0.182	0.979
BA Ea 18	0.210	0.970
BA Ec 43	0.126	0.878
FR Cg 1	0.421	0.876
FR Df 35	0.424	0.946
HA Bd 31	0.432	0.924
HA Ca 23	0.116	0.962
HO Bd 1	0.221	0.981
HO Cd 79	0.173	0.984
HO Ce 38	0.143	0.970
MO Eh 20	0.217	0.937
PG Ec 16	0.125	0.979

The model was validated by running the model on the data from all twelve well sites for the period from November 2000 to October 2001. The scatter diagram of the validation outputs against the observations at the 12 wells is displayed in Figure 39. The RMS error of the validation outputs is 0.206m. The validation outputs were compared with the observations at each individual well site. Figure 40 shows the comparison at well BA Cd 26. The comparisons at the rest of the well sites are

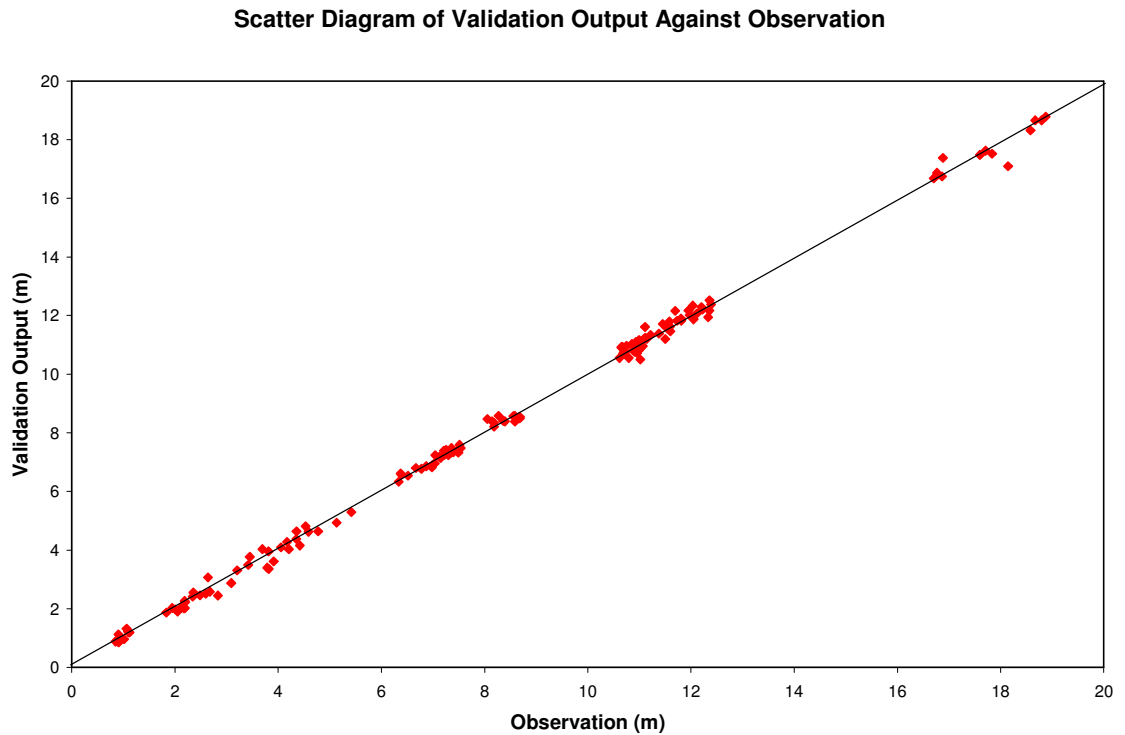


Figure 39. The scatter diagram of the model predicted water table depths from ANN model validation run against the observed water table depths at all 12 wells.

Comparison of Validation Output and Observation at BA Cd 26

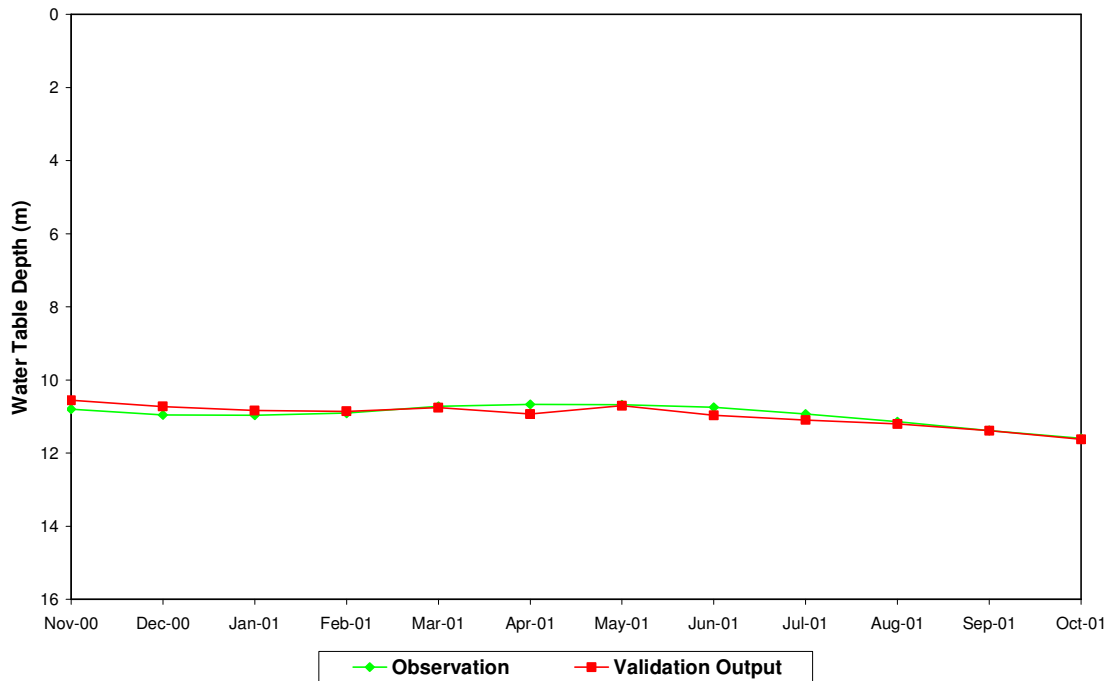


Figure 40. Comparison of the model predicted water table depths during the validation run with the observations at well site BA Cd 26.

displayed in Appendix E. The RMS error at each individual well site is listed in Table 13. At most of the well sites the RMS errors are less than or around 0.25m except at FR Df 35, which has a RMS error of 0.366m. By excluding the data at MO Cc 14 for the model training, the overall RMS error of model validation outputs improved from 0.282m to 0.206m. The correlation coefficient between the training outputs and the observation also improved slightly, from 0.998 to 0.999.

Table 13. The RMS errors of validation outputs at each individual well site (12 wells run)

Well Name	RMS error (m)
BA Cd 26	0.154
BA Ea 18	0.115
BA Ec 43	0.118
FR Cg 1	0.274
FR Df 35	0.366
HA Bd 31	0.258
HA Ca 23	0.095
HO Bd 1	0.216
HO Cd 79	0.194
HO Ce 38	0.146
MO Eh 20	0.238
PG Ec 16	0.116

A forecast simulation was conducted for the period from November 2001 to April 2002 at each individual well site using this ANN model to investigate its forecast capability. The forecast results at each of these 12 well locations are shown in Table 14. The differences between forecasted and observed water table depths are displayed in the last

column of Table 14. In general, the absolute difference increases with the increase of forecast time. Except at FR_Df_35 and HA_Ca_23, the absolute differences for the first month of other sites are equal to or less than 0.18m. Table 15 shows the monthly RMS errors of the six forecast months for all the well sites. The RMS error increases from 0.142m of the first month to 0.614m of the sixth month. It clearly shows that the forecast error in the previous month has a huge influence on the accuracy of the forecast of water table depth for the subsequent month.

Table 14. The monthly forecast results for the period from November 2001 to April 2002 at each individual well site. Month 1 is November 2001. Month 6 is April 2002.

Well Name	Month	Observed WTD (m)	Predicted WTD (m)	Difference (m)
BA_Cd_26	1	11.80	11.70	-0.10
	2	12.02	11.83	-0.18
	3	12.19	11.77	-0.42
	4	12.31	11.74	-0.57
	5	12.39	11.88	-0.51
	6	12.45	12.10	-0.35
BA_Ea_18	1	7.72	7.55	-0.18
	2	7.88	7.59	-0.29
	3	7.99	7.37	-0.61
	4	8.06	7.23	-0.83

Table 14. (continued)

	5	8.11	7.32	-0.79
	6	8.13	7.48	-0.65
BA_Ec_43	1	1.11	1.04	-0.06
	2	1.09	1.03	-0.05
	3	1.10	0.85	-0.25
	4	1.01	0.78	-0.23
	5	1.06	0.91	-0.15
	6	1.09	1.05	-0.04
FR_Cg_1	1	12.43	12.46	0.03
	2	12.45	12.59	0.14
	3	12.39	12.51	0.12
	4	12.03	12.47	0.44
	5	11.97	12.52	0.55
	6	12.03	12.64	0.61
FR_Df_35	1	18.97	18.67	-0.30
	2	19.09	18.53	-0.56
	3	19.26	18.24	-1.02
	4	19.17	18.01	-1.15
	5	19.17	17.93	-1.24
	6	19.32	17.92	-1.40

Table 14. (continued)

HA_Bd_31	1	5.53	5.48	-0.04
	2	5.47	5.54	0.07
	3	5.55	5.40	-0.15
	4	5.08	5.36	0.28
	5	4.95	5.52	0.57
	6	4.89	5.74	0.86
HA_Ca_23	1	2.76	2.54	-0.21
	2	2.80	2.45	-0.35
	3	2.85	2.21	-0.65
	4	2.78	2.05	-0.73
	5	2.83	2.07	-0.76
	6	2.84	2.12	-0.72
HO_Bd_1	1	12.64	12.50	-0.14
	2	12.85	12.63	-0.22
	3	12.92	12.56	-0.37
	4	13.12	12.50	-0.62
	5	13.20	12.63	-0.57
	6	13.28	12.86	-0.42
HO_Cd_79	1	8.77	8.61	-0.16
	2	8.95	8.67	-0.28
	3	9.08	8.55	-0.53

Table 14. (continued)

	4	9.18	8.47	-0.71
	5	9.22	8.59	-0.63
	6	9.22	8.78	-0.44
HO_Ce_38	1	11.31	11.29	-0.02
	2	11.40	11.38	-0.02
	3	11.46	11.28	-0.18
	4	11.50	11.20	-0.30
	5	11.51	11.33	-0.18
	6	11.48	11.53	0.06
MO_Eh_20	1	4.50	4.56	0.06
	2	4.52	4.60	0.09
	3	4.60	4.51	-0.09
	4	4.34	4.47	0.13
	5	4.33	4.61	0.28
	6	4.60	4.77	0.17
PG_Bc_16	1	7.63	7.56	-0.07
	2	7.71	7.62	-0.09
	3	7.77	7.54	-0.23
	4	7.81	7.50	-0.31
	5	7.83	7.62	-0.20
	6	7.85	7.78	-0.07

Table 15. The monthly RMS errors of water table depth forecast at all 12 well sites.

Month	1	2	3	4	5	6
RMS error(m)	0.142	0.246	0.467	0.599	0.615	0.614

Chapter 6: Discussion

6.1 Single Well Modeling

Two ANN water table prediction models, BA_BT_WT and FR_BT_WT, using brightness temperature and water table depth change as input were created. Generally, both models performed very well in predicting water table variation. The root mean square errors of the model predicted water table depths during ANN training ranged from 0.04m for FR_BT_WT to 0.058m for BA_BT_WT at different well sites. An experiment that used brightness temperature and water table depth only for model training was performed, but the results were not acceptable. It indicates that the relationship between input parameters, as mentioned previously, plays a key factor for the success of this type of modeling. The third ANN model (BA_SM_WT) that utilized soil moisture content and water table depth as input had a root mean square error of 0.059m for the model training output. It is compatible with that of BA_BT_WT. The root mean square errors of the twelve month's water table depth forecasts were determined as 0.043m, 0.044m, and 0.047m for BA_BT_WT, FR_BT_WT, and BA_SM_WT, respectively. Compared with the study of Coulibaly et al. (2001) who used a recurrent neural network to simulate the water table fluctuations and whose 1st month's prediction had a root mean square error ranging from 0.39m to 0.54m at four well sites, these results are very encouraging.

Sensitivity tests were performed for models BA_SM_WT and BA_BT_WT at the Baltimore County well site. BA_SM_WT was tested for the period of January 2001 through December 2001. The monthly mean soil moisture contents remained the same for all cases. But, the initial water table depth was inputted with -5%, -2.5%, 2.5%, or 5% of error for each case of this experiment. After 12 months of model run, the root mean square errors for the monthly predicted output for these four cases were found to be 0.201m, 0.125m, 0.12m, and 0.281m respectively. They are higher than the 0.047m of root mean square error for the 12 months long forecast, which started without initial error, for the same time period. The results showed that the predictions started to converge after 6 months of run for all cases (Figure 41). Although they

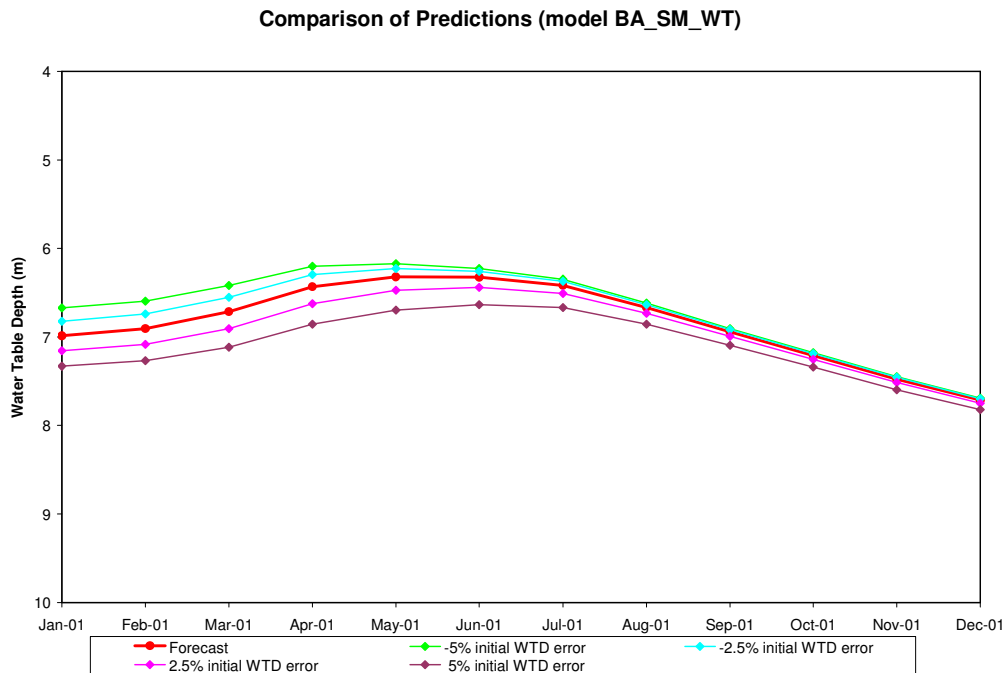


Figure 41. Comparison of the predicted monthly water table depths generated by running ANN model BA_SM_WT with different errors on initial water table depths (WTD).

did not fully converge within 12 months, results indicate that the influence of the initial error on the input water table depth dissipated after several months of forecasting. A similar test was conducted at the same well site for the period of November 2002 through October 2003 for model BA_BT_WT. The monthly mean brightness temperature remained the same for all cases. The initial water table depth was fed into the model with -5%, -2.5%, 2.5%, or 5% of error for each of these four testing cases. The root mean square errors of the 12 months' prediction for these four cases are 0.121m, 0.068m, 0.061m, and 0.085m respectively. They are higher than 0.043m of the 12 months long forecast. The convergence of the predictions occurred at the beginning of the forecast (Figure 42), and they completely converged after 5

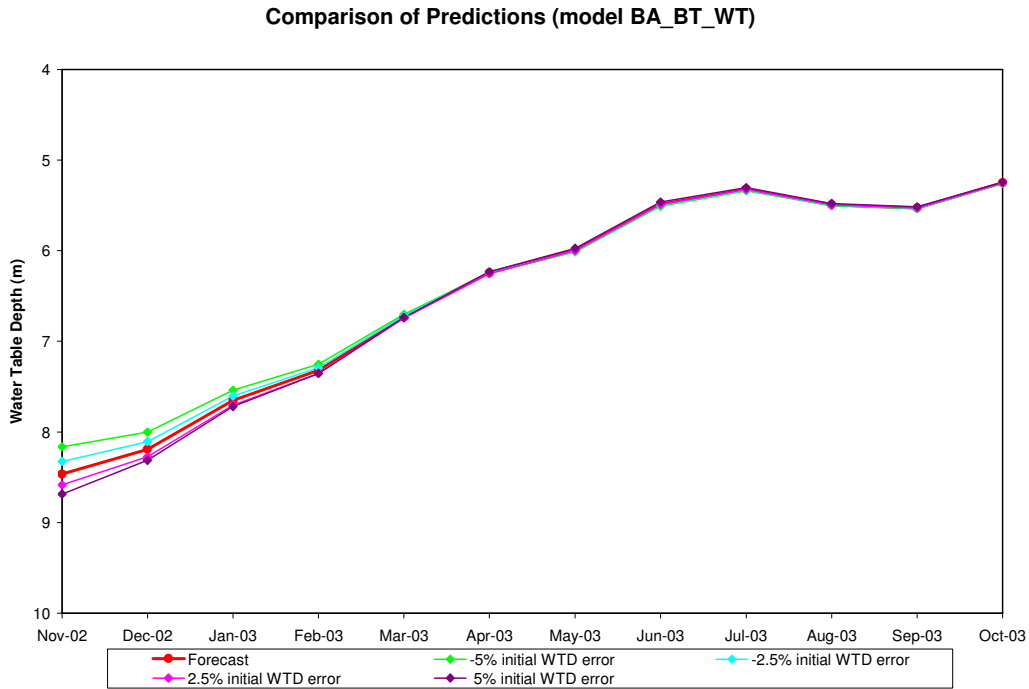


Figure 42. Comparison of the predicted monthly water table depths generated by running ANN model BA_BT_WT with different errors on initial water table depths (WTD).

months of forecast. This again shows the advantage of applying the ANN model on the long term water table fluctuation forecast. The root mean square errors of models BA_BT_WT and BA_SM_WT are shown in Figure 43. The RMS error of BA_SM_WT is larger than that of BA_BT_WT at every test. This might be due to the higher correlation between the soil moisture content and the water table depth, which makes the model more sensitive to the change in soil moisture content.

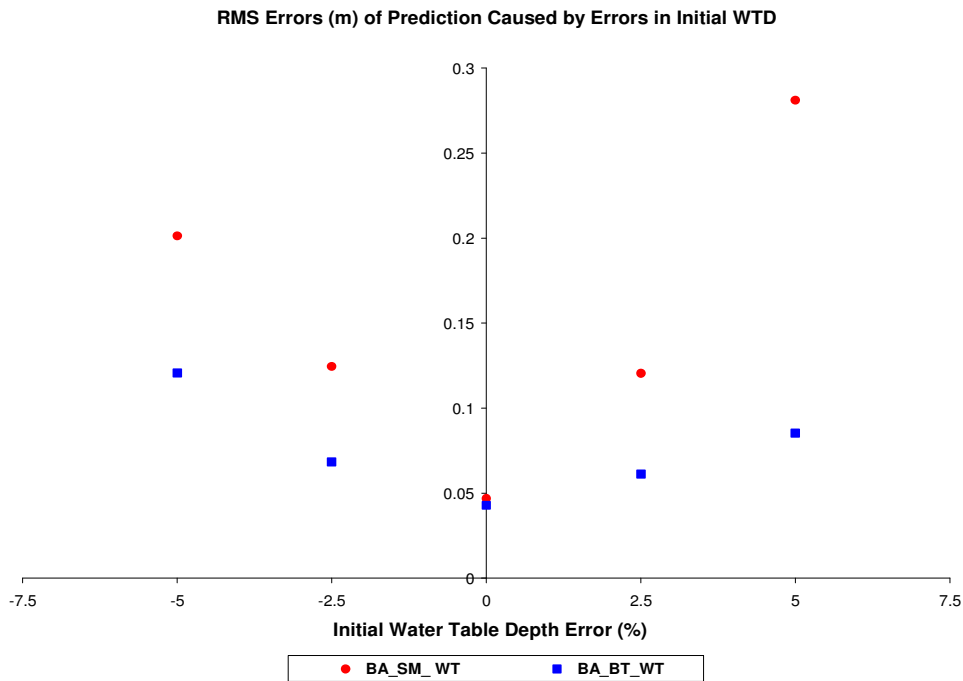


Figure 43. Root mean square errors of 12 months' predicted water table depths generated by models BA_BT_WT and BA_SM_WT at different initial water table depth errors.

The sensitivity test on brightness temperature was also conducted for model BA_BT_WT. The test was performed over the period from November 2002 through October 2003. Four cases, each with -10K, -5K, 5K, or 10K of initial brightness temperature error, were tested. The monthly mean water table depth remained the same for each month. The results showed that there is no significant difference among these four predictions (Figure 44), suggesting that this model is much more sensitive to the water table depth error than to the brightness temperature error.

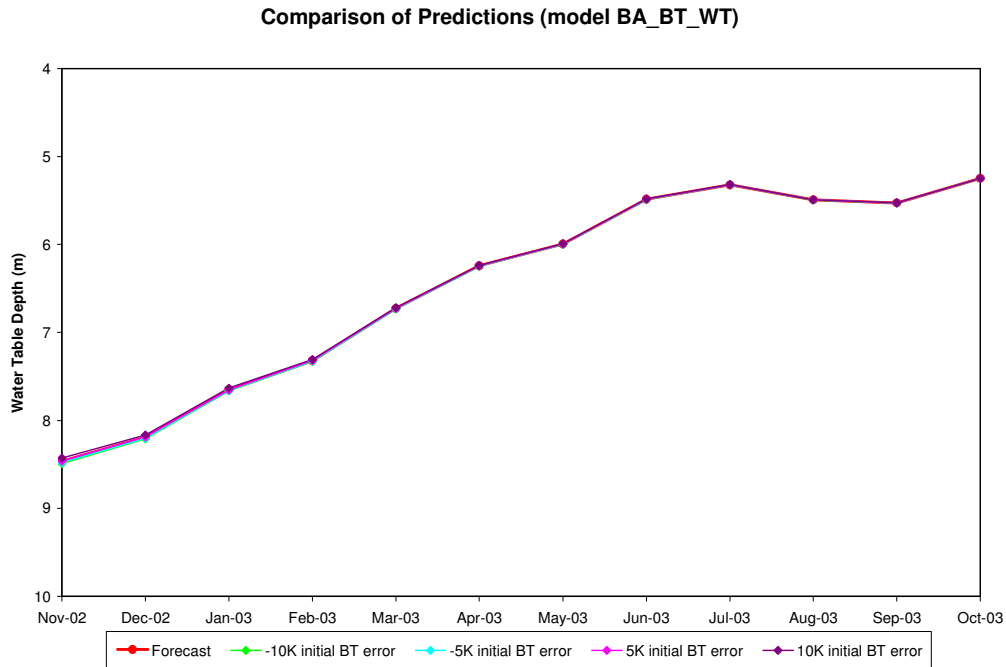


Figure 44. Comparison of the predicted monthly water table depths generated by running ANN model BA_BT_WT with different errors on initial brightness temperature (BT).

Another sensitivity test was performed for model BA_SM_WT for the period from January 2001 through December 2001 by only changing the initial soil moisture content. For each case, -10%, -5%, 5%, or 10% of error was added onto the initial soil moisture content. The comparison of the predicted water table depth of these four tests and the forecast is shown in Figure 45. It shows that the convergence of these predictions occurs at the very beginning and there exists no significant difference among these predictions after 6 months of run. The root mean square errors of the monthly predicted water table depth are 0.05m, 0.044m, 0.058m, and 0.076m for

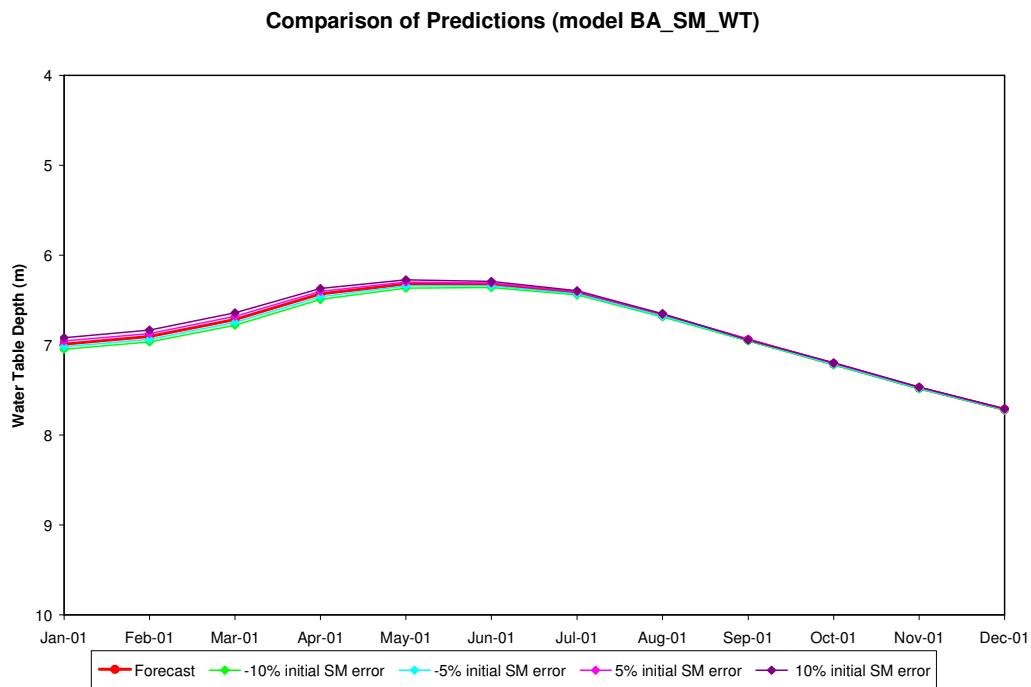


Figure 45. Comparison of the predicted monthly water table depths generated by running ANN model BA_SM_WT with different errors on initial soil moisture content (SM).

each of these four cases, respectively. Except for the second case, they all have higher root mean square errors than that of the forecast. Results of the above four experiments clearly indicate that the water table depth error, if it exists, is the major factor that would affect the prediction. The influence of the initial brightness temperature error is the least important.

6.2 Regional Scale Modeling

An ANN water table prediction model, Regional_WTDP, using hydrologic soil type, NLDAS soil moisture content in 0 – 200cm, and water table depth at 12 selected well locations as input was created. The root mean square error of the predicted water table depths during ANN model training was 0.26m. The RMS error for each individual well site range from 0.116m at HA Ca 23 to 0.432m at HA Bd 31, with most well sites around or below 0.22m. Clearly, the accuracy of the regional scale water table prediction is not as good as that of the single well water table prediction. The percentage influence of input parameters on the model output (Table 16) indicated that the predicted water table depth was very sensitive to the current water table depth (85.44%). The antecedent soil moisture and subsequent soil moisture play similar roles on the prediction, whereas the hydrologic soil type is the least important in affecting the model output. Comparing the water table depth (see Table 14) and the well site elevation (see Table 5) with the RMS error of model training output (Table 12) at each well site, there appears to be no clear effect from either parameter on the prediction.

Table 16. The percentage influence of input parameters on the model output.

Hydrologic Soil Type	Antecedent Soil Moisture	Current Water Table Depth	Subsequent Soil Moisture
0.34%	6.53%	85.44%	7.69%

The model was built based on the available data at 12 well sites in Piedmont Plateau, Maryland. The data of well MO Cc 14 was available but not included in the input for the model training because of its higher RMS error of the model training output. Comparing with Figure 37 which came from the model training output of 12 wells run, a higher model outputs spread from 8m to 12m area are associated with the use of the data at MO Cc 14 (Figure 46). Not counting data at well MO Cc 14 makes a significant

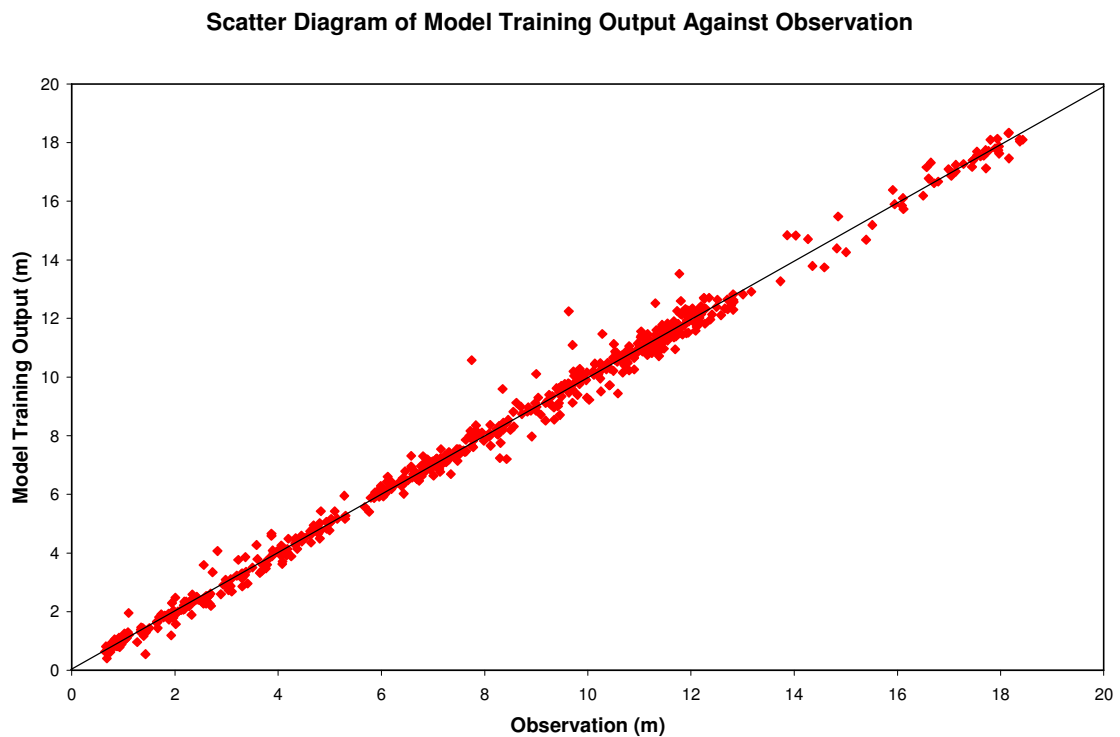


Figure 46. A scatter diagram of the model training output against the observation. Data from 13 well sites, including well MO Cc 14, were used in the input. A higher model outputs spread from 8m to 12m area are associated with the use of data at MO Cc 14.

improvement in the modeling results, which improves the overall RMS error of model training outputs from 0.351m to 0.26m. The error in the measured data or other factors that are not included in the model, such as lateral flow, might be possible reasons that cause the high root mean square error at MO Cc 14.

Except for wells FR Cg 1, FR Df 35, and HA Bd 31, which have RMS errors of training output around 0.4m, at the rest of the well sites the RMS errors of the training output are less than 0.22m. Wells FR Cg 1 and FR Df 35 are in Frederick County, MD and are very close to the other geologic region. Well HA Bd 31 is in Harford County, MD and is very close to the northern end of the Piedmont geologic region of Maryland. More data are needed to investigate the causes that result in the high RMS error at these three well sites.

Seven wells, BA Cd 26, BA Ec 43, FR Cg 1, HA Bd 31, HO Ce 38, MO Eh 20, and PG Bc 16 have the difference between forecast and observation less than 0.1m for the first month. Four wells, BA Ea 18, HA Ca 23, HO Bd 1, and HO Cd 79 have the difference around or less than 0.2m. FR Df 35 has a difference up to 0.3m. The RMS error of the forecast of the first month for these 12 well sites was 0.142m. Compared with the results of the single site study of Coulibaly et al. (2001), this model performed well on predicting one month's water table variation at a regional scale. The RMS error, however, increased as the forecast time became longer. The error in the predicted water table depth of the current month was carried over to the next month's prediction. This dramatically increased the inaccuracy of the prediction in the following month. The

uncertainty in the measured data is another concern. The satellite remotely sensed data still has some limitation in the accuracy of its measurements. The continuous long term daily recorded water table is only available for a few well sites. A much accurate high resolution satellite remotely sensed data and more well sites with daily water table depth recording capability definitely would improve the modeling results.

The effect of the range of input data in the model training on the prediction was investigated. Table 17 shows the maximum and minimum values of water table depth data used in the model training, the initial water table depth data used for the forecast, and the absolute difference between the first month's forecast and the observation at each well site. Among these 12 well sites, at five well sites the initial water table depth for the forecast run at each single well site is larger than the maximum water table depth used in the model training at that well site. Among these five well sites, the absolute difference between the first month's forecast and the observation at BA Ea 18, FR Df 35 and HA Ca 23 are around or above 0.18m and that at FR Cg 1 and HA Bd 31 are smaller than 0.04m. For the other seven well sites, the initial water table depth for the forecast run at each well site is in the range of minimum and maximum input water table depths, and the absolute difference between the first month's forecast and the observation is less than 0.16m. This indicates that a better forecast would be achieved if the value of initial water table depth in the forecast run is in the range of the input water table depths used in the training of the model. On the other hand, if the initial water table depth in the forecast is out of the range of the input water table depths used in the model training, the occurrence of a larger error in the forecast is possible.

Table 17. Maximum and minimum values of water table depth (WTD) data used in the model training, initial water table depth data used for the forecast, and the absolute difference between the first month's forecast and the observation at each well site.

Well Name	Maximum WTD (m)	Minimum WTD (m)	Initial WTD for Forecast (m)	Absolute Difference (m)
BA Cd 26	12.20	9.18	11.8	0.1
BA Ea 18	7.54	4.63	7.72	0.18
BA Ec 43	1.11	0.65	1.11	0.06
FR Cg 1	12.27	9.57	12.43	0.03
FR Df 35	18.43	13.87	18.97	0.3
HA Bd 31	5.30	0.81	5.53	0.04
HA Ca 23	2.69	1.27	2.76	0.21
HO Bd 1	12.83	9.22	12.64	0.14
HO Cd 79	9.09	5.87	8.77	0.16
HO Ce 38	11.43	9.39	11.31	0.02
MO Eh 20	4.94	2.94	4.5	0.06
PG Ec 16	7.76	5.79	7.63	0.07

6.3 Determine Future Brightness Temperature and Soil Moisture

In order to apply the ANN water table prediction model on water table forecast, future monthly brightness temperature and soil moisture at the study site are needed. A method to produce future brightness temperature and soil moisture is hence proposed here. The idea is to derive the two future parameters based on the output of the climate forecast model. Currently, there exist several climate models that can forecast meteorological parameters at different temporal and spatial resolutions. One of them is the Climate Forecast System (CFS) (Saha et al., 2006) developed by the Environmental Modeling Center at the National Centers for Environmental Prediction (NCEP). The Climate Forecast System is a fully coupled ocean–land–atmosphere dynamical seasonal prediction system. The atmospheric component of the CFS is a lower-resolution version of the Global Forecast System based upon the meteorological primitive equations. It was the operational global weather prediction model at NCEP during 2003. The oceanic component is the GFDL (Geophysical Fluid Dynamics Laboratory) Modular Ocean Model version 3 (MOM3) (Pacanowski and Griffies 1998), which is a finite difference version of the ocean primitive equations under the assumptions of Boussinesq and hydrostatic approximations. The land component is the NOAA (NCEP, Oregon State University, Air Force, and Hydrologic Research Lab – National Weather Service) Land Surface Model, which applies finite-difference spatial discretization methods to numerically integrate the governing equations of the physical processes of the soil-vegetation-snowpack medium (NASA, 2008). The CFS became operational at NCEP in August 2004. Recently, four CMIP (Coupled Model Intercomparison Project) T126L64

runs (Thiaw and Saha, 2007), CMIP1, CMIP2, CMIP3, and CMIP4, were completed. These four runs cover the time period from January 1, 1984 to December 31, 2101. The data can be obtained at <http://cfs.ncep.noaa.gov/cmip126/monthly> (NCEP CFS, 2008). The outputs of these forecast runs contain atmospheric pressure level data, surface flux data, and ocean data. Among them, monthly surface temperature, monthly soil temperatures at 0 – 10cm and 10 – 200cm, and monthly soil moistures at 0 – 10cm and 10 – 200cm are produced at 384 x 190 grid points.

Although a higher resolution data is not available at this time, the required data at the study well site still can be obtained with the help of ANN modeling. Based on the historical data, an ANN model can be built to correlate the data, such as monthly soil moisture, at the four grid points around a well site with that at the well site (Figure 47). Once the ANN model is constructed, the future data, such as monthly soil moisture, at the well site can be produced from this ANN model using the forecasted data from the climate model. Utilizing this method, the monthly surface temperature, monthly soil temperatures at 0 – 10cm and 10 – 200cm, and monthly soil moistures at 0 – 10cm and 10 – 200cm at a specific well site can be obtained.

Ogawa et al. (2006) showed that the thermal infrared emissivity increase was found to be qualitatively correlated with an increase in AMSR derived soil moisture in some of their study regions. In the study of Chen et al. (1989), they indicated that the

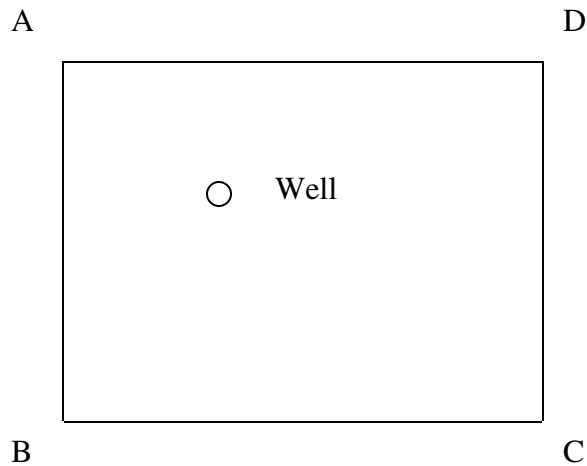


Figure 47. Using the meteorological forecast data at the grid points, A, B, C, and D, around the well site, the needed data at the well site can be obtained by running the ANN model.

emissivity could be expressed as a function of surface moisture. Pan et al. (2000) indicated that different types of land covers have their own characteristic emissivity. Vegetation, surface roughness and water content are the main factors affecting land emissivity. Assuming that the soil type does not change with time at a well site, soil moisture and surface vegetation are the only two time-dependent parameters that have great influence on the emissivity. Although surface vegetation varies with time, it may approximately be assumed to be constant for each month. This means that for each month in a year the emissivity at a specific well site can be expressed as a function of soil moisture only. A regression equation based on the historical data at that well site may be developed to calculate the emissivity for each month in a year. Once the soil

moisture content of a future month at a well site is determined by the ANN model using the forecasted data, the emissivity can then be determined as well.

Finally, the microwave brightness temperature at a well site can be related to the soil temperature through the emissivity as:

$$T_B = e T_{soil} \quad (\text{Schmugge, 1990}),$$

where, T_B is the brightness temperature, T_{soil} is the soil temperature, and e is the emissivity. The brightness temperature at the well site may then be calculated by the derived emissivity and the forecasted soil temperature.

Chapter 7: Conclusions

Three single well water table depth prediction models which are based on ANN technology were constructed for two locations in Maryland. The successful application of satellite data on building these models for water table fluctuations prediction is very encouraging. The forecast capability of these three models at a single well site is reliable. An extension of the study to a regional scale was also performed in the area of Piedmont Plateau, Maryland. The results of one month long prediction are acceptable. A network of groundwater distribution can therefore be formed a month ahead, which can be used to determine the groundwater movement earlier. However, the accuracy of the monthly prediction decreases with the increase of time. More data are needed for a further study to improve the accuracy of water table fluctuations prediction in a longer time frame.

ANN technique does provide a very good way to quickly and accurately construct a water table prediction model, when even if there is only a small amount of available data. However, the performance of these ANN models, in general, benefits from better correlations among the input parameters and the target parameter. A use of suitable parameters in the model is a key to the success of ANN modeling. In addition, the range of the values of the training data, such as water table depth, is crucial on the water table prediction. The forecast might lose its accuracy if the value of the input data is out of the range of the data that trained the model.

The results of sensitivity test showed that the models were more sensitive to the uncertainty in water table depth than to that in brightness temperature or in soil moisture content. This implies that an ANN water table prediction model still can be built once the trend of the time series of the observed data, such as brightness temperature or soil moisture, at a place that is the closest to the study site correlates well with the measurements at the study site, even if high resolution remotely sensed data is not available. However, in order to improve the accuracy of prediction, observed data with higher spatial and temporal resolution are still highly required.

The capability of being able to correctly predict water table fluctuations at a well site is the advantage of using these ANN water table prediction models. These ANN models can be applied to run past data at a well site to fill up the missing period of the water table depth measurements. This can provide a much more complete data sets for water resource research. Moreover, with the help of a climate forecast model, the future soil moisture and brightness temperature over a study site can be derived. These data can be used for the ANN water table prediction model to conduct the water table fluctuation forecast. This can provide farmers, water resource planners, and environmental engineers a better way to foresee the possible water table variation and groundwater movement in order to take necessary action in a more efficient way.

Chapter 8: Suggestions for Further Study

Being able to apply satellite data in the ANN water table prediction modeling is the advantage of this study. However, limited by the availability of higher resolution satellite remotely sensed soil moisture data, the assimilated soil moisture data was used, in stead, to perform the ANN water table prediction modeling. Once the data is available, a further study that uses satellite observed soil moisture data in the modeling is recommended.

This study was conducted in the Piedmont Plateau, Maryland. It was indicated that the impact on the forecast from the different soil types in this area was not significant in the regional scale modeling. It is suggested to extend this study to include other physiographic provinces of Maryland in the model to evaluate the model's prediction capability in a region with larger geological diversity. It is showed that the model is more sensitive to the water table depth than to other parameters. An extension of the model to include Maryland Eastern Shore could provide an opportunity to examine how the model would respond in the shallow water table area.

Single well model showed excellent prediction capability in this study. It is recommended to include more well sites in the study when it becomes available. The forecasted water table depths at these well sites can be used to construct a groundwater flow system. Based on this system, the moving direction and the total amount of pollutants transported in the groundwater can then be estimated. This could provide us a better chance to protect the environment.

Appendices

Appendix A. GrADS and Fortran Codes for Data Preparation

1. An example of GrADS format control file for LDAS data

```
dset ./%y4%m2%d2/%y4%m2%d2%h2.mosaic.grb
index ./199610.idx
undef 9.999E+20
options template
title mosaicexplicit.grb
* produced by grib2ctl v0.9.12.5p26
dtype grib 0
ydef 224 linear 25.063000 0.125
xdef 464 linear -124.938000 0.125000
tdef 744 linear 00Z01oct1996 1hr
zdef 6 levels
20099 16003 10099 4099 3002 1001
vars 43
ACONDSfc 0 174,1,0 ** Aerodynamic conductance [m/s]
ACPCPsfc 0 63,1,0 ** Convective precipitation [kg/m^2]
ALBDOsfc 0 84,1,0 ** Albedo [%]
ARAINsfc 0 132,1,0 ** Rainfall (unfrozen precipitation) [kg/m^2]
ASNOWsfc 0 131,1,0 ** Snowfall (frozen precipitation) [kg/m^2]
AVSFTsfc 0 138,1,0 ** Average surface temperature [K]
BGRUNsfc 0 234,1,0 ** Baseflow-groundwater runoff [kg/m^2]
CCONDSfc 0 181,1,0 ** Canopy Conductance [m/s]
CNWATsfc 0 223,1,0 ** Plant canopy surface water [kg/m^2]
DLWRFsfc 0 205,1,0 ** Downward long wave flux [W/m^2]
DSWRFsfc 0 204,1,0 ** Downward short wave flux [W/m^2]
EVBSsfc 0 199,1,0 ** Direct evaporation from bare soil [W/m^2]
EVCWsfc 0 200,1,0 ** Canopy water evaporation [W/m^2]
EVPsfc 0 57,1,0 ** Evaporation [kg/m^2]
GFLUXsfc 0 155,1,0 ** Ground heat flux [W/m^2]
LAIsfc 0 182,1,0 ** Leaf area index [1]
LHTFLsfc 0 121,1,0 ** Latent heat flux [W/m^2]
MSTAVtot 0 207,112,20099,0 ** Moisture availability [%] 200cm Total Column
MSTAVroot 0 207,112,4099,0 ** Moisture availability [%] Root Zone, 0-40cm
NLWRSsfc 0 112,1,0 ** Net long wave (surface) [W/m^2]
NSWRSsfc 0 111,1,0 ** Net short wave (surface) [W/m^2]
PRESsfc 0 1,1,0 ** Pressure [Pa]
SBSNOsfc 0 173,1,0 ** Snow sublimation [W/m^2]
```

SHTFLsfc 0 122,1,0 ** Sensible heat flux [W/m²]
 SNODsfc 0 66,1,0 ** Snow depth [m]
 SNOHFsfsc 0 229,1,0 ** Snow phase-change heat flux [W/m²]
 SNOMsfsc 0 99,1,0 ** Snow melt [kg/m²]
 SNOWCsfc 0 238,1,0 ** Snow cover [%]
 SOILM1 0 86,112,1001,0 ** Soil moisture content [kg/m²] Layer 1, 0-10cm
 SOILM2 0 86,112,3002,0 ** Soil moisture content [kg/m²] Layer 2, 10-40cm
 SOILM3 0 86,112,16003,0 ** Soil moisture content [kg/m²] Layer 3, 40-200cm
 SOILMtot 0 86,112,20099,0 ** Soil moisture content [kg/m²] Total Column, 200cm
 SOILMroot 0 86,112,4099,0 ** Soil moisture content [kg/m²] Root Zone, 0-40cm
 SOILMtop1m 0 86,112,10099,0 ** Soil moisture content [kg/m²] Top 1 Meter, 0-100cm
 SPFHsfsc 0 51,1,0 ** Specific humidity [kg/kg]
 SSRUNsfsc 0 235,1,0 ** Surface runoff [kg/m²]
 TMPsfsc 0 11,1,0 ** 2 Meter Temp. [K]
 TRANSsfsc 0 210,1,0 ** Transpiration [W/m²]
 TSOILdlr 0 85,112,1001 ** Deep Soil temp. [K]
 UGRDsfc 0 33,1,0 ** u wind [m/s]
 VEGsfsc 0 87,1,0 ** Vegetation greenness [%]
 VGRDsfc 0 34,1,0 ** v wind [m/s]
 WEASDsfc 0 65,1,0 ** Liq Equivalent Accum. snow [kg/m²]
 ENDVARS

2. An example of GrADS format control file for LDAS subsetted soil moisture data

```

dset LDAS_9602_MD.grd
undef 9.999E+20
title mosaicexplicit.grb
* produced by grib2ctl v0.9.12.5p26
ydef 17 linear 37.813 0.125
xdef 37 linear -79.563 0.125
tdef 54792 linear 00Z01oct1996 1hr
zdef 1 levels 62099
vars 6
SOILM1 0 86,112,1001,0 ** Soil moisture content [kg/m2] Layer 1, 0-10cm
SOILM2 0 86,112,3002,0 ** Soil moisture content [kg/m2] Layer 2, 10-40cm
SOILM3 0 86,112,16003,0 ** Soil moisture content [kg/m2] Layer 3, 40-200cm
SOILMtot 0 86,112,20099,0 ** Soil moisture content [kg/m2] Total Column, 200cm
SOILMroot 0 86,112,4099,0 ** Soil moisture content [kg/m2] Root Zone, 0-40cm
  
```

```
SOILMtop1m 0 86,112,10099,0 ** Soil moisture content [kg/m^2] Top 1 Meter, 0-100cm  
ENDVARS
```

3. An example of the GrADS script used to extract data from LDAS hourly soil moisture dataset at a well site

```
'open LDAS_9602_MD.ctl'  
'set fwrite AA_Ad_108.dat'  
'set gxout fwrite'  
'set grads off'  
'set x 24'  
'set y 12'  
'set z 1'  
i=1  
while (i<54793)  
'set t 'i  
'd SOILMtot'  
i=i+1  
endwhile  
return
```

4. An example of the GrADS script used to extract data from LDAS hourly soil moisture dataset at a well site for each year

```
'open LDAS_1996_MD.ctl'  
'set fwrite AA_Bf_3_1996.dat'  
'set gxout fwrite'  
'set grads off'  
'set x 26'  
'set y 12'  
'set z 1'  
i=1  
while (i<2209)  
'set t 'i  
'd SOILMtot'
```

```

i=i+1
endwhile
return
'open LDAS_1997_MD.ctf'
'set fwrite AA_Bf_3_1997.dat'
'set gxout fwrite'
'set grads off'
'set x 26'
'set y 12'
'set z 1'
i=1
while (i<8761)
'set t 'i
'd SOILMtot'
i=i+1
endwhile
return
'open LDAS_1998_MD.ctf'
'set fwrite AA_Bf_3_1998.dat'
'set gxout fwrite'
'set grads off'
'set x 26'
'set y 12'
'set z 1'
i=1
while (i<8761)
'set t 'i
'd SOILMtot'
i=i+1
endwhile
return
'open LDAS_1999_MD.ctf'
'set fwrite AA_Bf_3_1999.dat'
'set gxout fwrite'
'set grads off'
'set x 26'
'set y 12'
'set z 1'
i=1
while (i<8761)
'set t 'i
'd SOILMtot'
i=i+1
endwhile
return
'open LDAS_2000_MD.ctf'

```

```
'set fwrite AA_Bf_3_2000.dat'  
'set gxout fwrite'  
'set grads off'  
'set x 26'  
'set y 12'  
'set z 1'  
i=1  
while (i<8785)  
'set t 'i  
'd SOILMtot'  
i=i+1  
endwhile  
return  
'open LDAS_2001_MD.ctl'  
'set fwrite AA_Bf_3_2001.dat'  
'set gxout fwrite'  
'set grads off'  
'set x 26'  
'set y 12'  
'set z 1'  
i=1  
while (i<8761)  
'set t 'i  
'd SOILMtot'  
i=i+1  
endwhile  
return  
'open LDAS_2002_MD.ctl'  
'set fwrite AA_Bf_3_2002.dat'  
'set gxout fwrite'  
'set grads off'  
'set x 26'  
'set y 12'  
'set z 1'  
i=1  
while (i<8761)  
'set t 'i  
'd SOILMtot'  
i=i+1  
endwhile  
return
```

5. An example of the Fortran code used to generate monthly mean soil moisture dataset from LDAS hourly soil moisture dataset at a well site

```
program readSM

integer irec
real*4 TSoilMoisture, SoilMoisture

iu = 10
iv = 20

open(iu,file='PG_Bc_16.dat',form='unformatted', &
     access='direct',recl=4)

open(iv,file='PG_Bc_16_mean.txt')

irec = 0

do iy = 1996, 2002

im = 1

if (iy .eq. 1996) im = 10

do m= im, 12

TSoilMoisture = 0.0

if(m .eq. 1) nday=31
if(m .eq. 2) nday=28
if(m .eq. 2 .and. iy .eq. 2000) nday=29
if(m .eq. 3) nday=31
if(m .eq. 4) nday=30
if(m .eq. 5) nday=31
if(m .eq. 6) nday=30
if(m .eq. 7) nday=31
if(m .eq. 8) nday=31
if(m .eq. 9) nday=30
if(m .eq. 10) nday=31
if(m .eq. 11) nday=30
if(m .eq. 12) nday=31

ntime = 24 * nday

ltime = 0
```

```

do n=1,ntime

irec = irec + 1

read (iu,rec=irec) SoilMoisture

if (SoilMoisture .gt. 9.0E+20) ltime = ltime + 1
if (SoilMoisture .gt. 9.0E+20) go to 121

TSoilMoisture = TSoilMoisture + SoilMoisture

121  continue

end do

print*, 'ltime = ',ltime

TSoilMoisture = TSoilMoisture / (24.0 * nday - ltime)

write(iv,*) TSoilMoisture

end do

end do

stop
end

```

6. An example of the Fortran code to generate water table on the first day of each month at selected well site

```

program readWT

integer iday(80)
integer id1(12),id2(12),jday(12)
real rw(80),rd(80),wt(80)

iu = 10
iv = 20

open(iu,file='57_WO_Bg_45.txt')
open(iv,file='57_WO_Bg_45_use.txt')

```

```
id1(1)=1
id1(2)=32
id1(3)=60
id1(4)=91
id1(5)=121
id1(6)=152
id1(7)=182
id1(8)=213
id1(9)=244
id1(10)=274
id1(11)=305
id1(12)=335
```

```
id2(1)=1
id2(2)=32
id2(3)=61
id2(4)=92
id2(5)=122
id2(6)=153
id2(7)=183
id2(8)=214
id2(9)=245
id2(10)=275
id2(11)=306
id2(12)=336
```

```
nn = 1
```

```
111 continue
```

```
read(iu,*,end=222) a,b,iday(nn),wt(nn)
```

```
nn = nn + 1
```

```
go to 111
```

```
222 continue
```

```
do iy = 1, 8
```

```
if(iy .eq. 1) im1=1
```

```
if(iy .eq. 1) im2=4
```

```
if(iy .eq. 2) im1=4
```

```
if(iy .eq. 2) im2=16
```

```

if(iy .eq. 3) im1=16
if(iy .eq. 3) im2=28

if(iy .eq. 4) im1=28
if(iy .eq. 4) im2=40

if(iy .eq. 5) im1=40
if(iy .eq. 5) im2=52

if(iy .eq. 6) im1=52
if(iy .eq. 6) im2=64

if(iy .eq. 7) im1=64
if(iy .eq. 7) im2=76

if(iy .eq. 8) im1=76
if(iy .eq. 8) im2=77

it = 0

do kk=1,77
rw(kk)=0.0
rd(kk)=0.0
end do

do im = im1, im2

it = it + 1

rw(it) = wt(im)
rd(it) = iday(im)

end do
if(iy .eq. 1) then
rd(1) = 244 + rd(1)
rd(2) = 274 + rd(2)
rd(3) = 305 + rd(3)
rd(4) = 335 + rd(4)
end if

if(iy .eq. 1) go to 888

if(iy .eq. 5) then
rd(1) = rd(1) - 31
rd(2) = rd(2)
rd(3) = 31 + rd(3)

```

```
rd(4) = 60 + rd(4)
rd(5) = 91 + rd(5)
rd(6) = 121 + rd(6)
rd(7) = 152 + rd(7)
rd(8) = 182 + rd(8)
rd(9) = 213 + rd(9)
rd(10) = 244 + rd(10)
rd(11) = 274 + rd(11)
rd(12) = 305 + rd(12)
rd(13) = 335 + rd(13)
end if
```

```
if(iy .eq. 5) go to 888
```

```
rd(1) = rd(1) - 31
rd(2) = rd(2)
rd(3) = 31 + rd(3)
rd(4) = 59 + rd(4)
rd(5) = 90 + rd(5)
rd(6) = 120 + rd(6)
rd(7) = 151 + rd(7)
rd(8) = 181 + rd(8)
rd(9) = 212 + rd(9)
rd(10) = 243 + rd(10)
rd(11) = 273 + rd(11)
rd(12) = 304 + rd(12)
rd(13) = 334 + rd(13)
```

```
888 continue
```

```
if(iy .eq. 1 .or. iy .eq. 5) go to 333
```

```
do ii = 1, 12
```

```
  jday(ii) = id1(ii)
```

```
end do
```

```
go to 555
```

```
333 continue
```

```
do ii = 1, 12
```

```
  jday(ii) = id2(ii)
```

```
end do
```

555 continue

jm = 1
km = 12

if(iy .eq. 1) jm = 10

if(iy .eq. 8) km = 1

do jj = jm, km

ll = 1

660 continue

if(jday(jj) .ge. rd(ll) .and. jday(jj) .le. rd(ll+1)) go to 666

ll = ll + 1

go to 660

666 continue

if(jday(jj) .eq. rd(ll)) go to 771

if(jday(jj) .eq. rd(ll+1)) go to 772

x1 = 1.0*jday(jj) - rd(ll)

x2 = rw(ll+1) - rw(ll)

x3 = rd(ll+1) - rd(ll)

watertable = rw(ll) + (x1 * x2) / x3

go to 775

771 continue

watertable = rw(ll)

go to 775

772 continue

```

    watertable = rw(11+1)

775  continue

    write(iv,30) watertable
30   format(f8.2)

    end do
    end do
    stop
end

```

7. An example of the HDF script used to dump brightness temperature, latitude, and longitude from AMSR-E data set

dump data from July 1 through July 31 2004

```

hdp dumpsds -i 7 -d -o temp.01.dat -b
06459_01302_AMSR_E_L2A_BrightnessTemperatures_V08_200407011804_A.hdf
cat temp.01.dat > AMSR_E_L2A_Latitude_200407011804_A_index.grd
rm temp.01.dat
hdp dumpsds -i 8 -d -o temp.02.dat -b
06459_01302_AMSR_E_L2A_BrightnessTemperatures_V08_200407011804_A.hdf
cat temp.02.dat > AMSR_E_L2A_Longitude_200407011804_A_index.grd
rm temp.02.dat
hdp dumpsds -n "89.0V_Res.5A_TB_(not-resampled)" -d -o temp.01.dat -b
06459_01302_AMSR_E_L2A_BrightnessTemperatures_V08_200407011804_A.hdf
cat temp.???.dat > AMSR_E_L2A_89.0V_Res.5_200407011804_A_index.grd
rm temp.???.dat

.
.
.
.
.

hdp dumpsds -i 7 -d -o temp.01.dat -b
06459_01302_AMSR_E_L2A_BrightnessTemperatures_V08_200407311804_A.hdf
cat temp.01.dat > AMSR_E_L2A_Latitude_200407311804_A_index.grd
rm temp.01.dat

```

```
hdp dumpsds -i 8 -d -o temp.02.dat -b
06459_01302_AMSR_E_L2A_BrightnessTemperatures_V08_200407311804_A.hdf
cat temp.02.dat > AMSR_E_L2A_Longitude_200407311804_A_index.grd
rm temp.02.dat
hdp dumpsds -n "89.0V_Res.5A_TB_(not-resampled)" -d -o temp.01.dat -b
06459_01302_AMSR_E_L2A_BrightnessTemperatures_V08_200407311804_A.hdf
cat temp.??.dat > AMSR_E_L2A_89.0V_Res.5_200407311804_A_index.grd
rm temp.??.dat
```

8. An example of a satellite remote measuring time file for monthly brightness temperature data processing

Jul2004.txt

200407011752
200407021657
200407031740
200407041823
200407051727
200407061811
200407071715
200407081758
200407091703
200407101746
200407111650
200407111829
200407121734
200407131817
200407141721
200407151805
200407161709
200407171752
200407181657
200407191740
200407201823
200407211727
200407221811
200407231715
200407241758
200407251703

200407261746
200407271650
200407271829
200407281734
200407291817
200407301721
200407311804

9. An example of the Fortran code used to generate daily brightness temperature data set

```
program write_BT_data

real*4  bt,xlon,xlat
integer*2  ibt
character*12  cday(60)
character*60  Lon_file, Lat_file, BT_file

open (8, file='Jul2004.txt')

iday = 0

do nday=1,60

  read(8,*,end=222) cday(nday)

  iday = iday + 1

end do

222  continue

close(8)

open(50,file='AMSR_E_L2A_V_BA_Ea_Jul2004_day.txt')

111  format(a12,3f8.2)

lrecl = 4
```

```

lrecm = 2

do nnn = 1, iday

Lon_file = 'AMSR_E_L2A_Longitude_//cday(nnn)//_A_index.grd'

Lat_file = 'AMSR_E_L2A_Latitude_//cday(nnn)//_A_index.grd'

BT_file = 'AMSR_E_L2A_89.0V_Res.5_//cday(nnn)//_A_index.grd'

open(10, file= Lon_file,ACCESS='DIRECT', RECL=lrecl, &
      FORM='UNFORMATTED', status='old')

open(20, file= Lat_file,ACCESS='DIRECT', RECL=lrecl, &
      FORM='UNFORMATTED', status='old')

open(30, file= BT_file,ACCESS='DIRECT', RECL=lrecm, &
      FORM='UNFORMATTED', status='old')

irec = 1

nt = 486*300

do i=1, nt
  read(10,rec=irec,iostat=ios) xlon

  if(ios .ne. 0) then

    go to 333

  end if

  read(20,rec=irec) xlat

  read(30,rec=irec) ibt

  bt = ibt * 0.01 + 327.68

  if (bt .eq. 0.0) go to 888

  dlat2 = abs(abs(xlat) - abs(39.3458))

  dlon2 = abs(abs(xlon) - abs(76.8569))

  if (dlat2 .le. 0.025 .and. dlon2 .le. 0.0325) write(50,111) cday(nnn), xlon, xlat, bt

```

```
888  continue

      irec = irec + 1

    end do

333  continue

      close(10)

      close(20)

      close(30)

    end do

    stop

  end
```

10. An example of script to concatenate files together

```
cat_Jul2004
```

```
cp AMSR_E_L2A_Latitude_200407011752_A_index.grd AMSR_E_L2A_Latitude_Jul2004.grd
cat AMSR_E_L2A_Latitude_200407021657_A_index.grd >> AMSR_E_L2A_Latitude_Jul2004.grd
cat AMSR_E_L2A_Latitude_200407031740_A_index.grd >> AMSR_E_L2A_Latitude_Jul2004.grd
cat AMSR_E_L2A_Latitude_200407041823_A_index.grd >> AMSR_E_L2A_Latitude_Jul2004.grd
cat AMSR_E_L2A_Latitude_200407051727_A_index.grd >> AMSR_E_L2A_Latitude_Jul2004.grd
cat AMSR_E_L2A_Latitude_200407061811_A_index.grd >> AMSR_E_L2A_Latitude_Jul2004.grd
cat AMSR_E_L2A_Latitude_200407071715_A_index.grd >> AMSR_E_L2A_Latitude_Jul2004.grd
cat AMSR_E_L2A_Latitude_200407081758_A_index.grd >> AMSR_E_L2A_Latitude_Jul2004.grd
cat AMSR_E_L2A_Latitude_200407091703_A_index.grd >> AMSR_E_L2A_Latitude_Jul2004.grd
cat AMSR_E_L2A_Latitude_200407101746_A_index.grd >> AMSR_E_L2A_Latitude_Jul2004.grd
cat AMSR_E_L2A_Latitude_200407111650_A_index.grd >> AMSR_E_L2A_Latitude_Jul2004.grd
cat AMSR_E_L2A_Latitude_200407111829_A_index.grd >> AMSR_E_L2A_Latitude_Jul2004.grd
cat AMSR_E_L2A_Latitude_200407121734_A_index.grd >> AMSR_E_L2A_Latitude_Jul2004.grd
cat AMSR_E_L2A_Latitude_200407131817_A_index.grd >> AMSR_E_L2A_Latitude_Jul2004.grd
cat AMSR_E_L2A_Latitude_200407141721_A_index.grd >> AMSR_E_L2A_Latitude_Jul2004.grd
cat AMSR_E_L2A_Latitude_200407151805_A_index.grd >> AMSR_E_L2A_Latitude_Jul2004.grd
cat AMSR_E_L2A_Latitude_200407161709_A_index.grd >> AMSR_E_L2A_Latitude_Jul2004.grd
cat AMSR_E_L2A_Latitude_200407171752_A_index.grd >> AMSR_E_L2A_Latitude_Jul2004.grd
cat AMSR_E_L2A_Latitude_200407181657_A_index.grd >> AMSR_E_L2A_Latitude_Jul2004.grd
cat AMSR_E_L2A_Latitude_200407191740_A_index.grd >> AMSR_E_L2A_Latitude_Jul2004.grd
```

```

cat AMSR_E_L2A_Latitude_200407201823_A_index.grd >> AMSR_E_L2A_Latitude_Jul2004.grd
cat AMSR_E_L2A_Latitude_200407211727_A_index.grd >> AMSR_E_L2A_Latitude_Jul2004.grd
cat AMSR_E_L2A_Latitude_200407221811_A_index.grd >> AMSR_E_L2A_Latitude_Jul2004.grd
cat AMSR_E_L2A_Latitude_200407231715_A_index.grd >> AMSR_E_L2A_Latitude_Jul2004.grd
cat AMSR_E_L2A_Latitude_200407241758_A_index.grd >> AMSR_E_L2A_Latitude_Jul2004.grd
cat AMSR_E_L2A_Latitude_200407251703_A_index.grd >> AMSR_E_L2A_Latitude_Jul2004.grd
cat AMSR_E_L2A_Latitude_200407261746_A_index.grd >> AMSR_E_L2A_Latitude_Jul2004.grd
cat AMSR_E_L2A_Latitude_200407271650_A_index.grd >> AMSR_E_L2A_Latitude_Jul2004.grd
cat AMSR_E_L2A_Latitude_200407271829_A_index.grd >> AMSR_E_L2A_Latitude_Jul2004.grd
cat AMSR_E_L2A_Latitude_200407281734_A_index.grd >> AMSR_E_L2A_Latitude_Jul2004.grd
cat AMSR_E_L2A_Latitude_200407291817_A_index.grd >> AMSR_E_L2A_Latitude_Jul2004.grd
cat AMSR_E_L2A_Latitude_200407301721_A_index.grd >> AMSR_E_L2A_Latitude_Jul2004.grd
cat AMSR_E_L2A_Latitude_200407311804_A_index.grd >> AMSR_E_L2A_Latitude_Jul2004.grd

```

11. An example of the Fortran code used to generate daily brightness temperature data at a well site

```

program write_BT_data

real*4  bt,xlon,xlat
integer*2  ibt

irecl = 4

lrecm = 2

open(10, file='AMSR_E_L2A_Longitude_Jul2003.grd',ACCESS='DIRECT',
      RECL=irecl, FORM='UNFORMATTED', status='old')
open(20, file='AMSR_E_L2A_Latitude_Jul2003.grd',ACCESS='DIRECT',
      RECL=irecl, FORM='UNFORMATTED', status='old')
open(30, file='AMSR_E_L2A_89.0V_Res.5_Jul2003.grd',ACCESS='DIRECT',
      RECL=lrecm, FORM='UNFORMATTED', status='old')

open(51,file='AMSR_E_L2A_V_BA_Cd_Jul2003.txt')
open(52,file='AMSR_E_L2A_V_BA_Ea_Jul2003.txt')
open(53,file='AMSR_E_L2A_V_BA_Ec_Jul2003.txt')
open(54,file='AMSR_E_L2A_V_FR_Cg_Jul2003.txt')
open(55,file='AMSR_E_L2A_V_FR_Df_Jul2003.txt')
open(56,file='AMSR_E_L2A_V_HA_Bd_Jul2003.txt')
open(57,file='AMSR_E_L2A_V_HA_Ca_Jul2003.txt')
open(58,file='AMSR_E_L2A_V_HO_Bd_Jul2003.txt')
open(59,file='AMSR_E_L2A_V_HO_Cd_Jul2003.txt')
open(60,file='AMSR_E_L2A_V_HO_Ce_Jul2003.txt')

```

```

open(61,file='AMSR_E_L2A_V_MO_Cc_Jul2003.txt')
open(62,file='AMSR_E_L2A_V_MO_Eh_Jul2003.txt')
open(63,file='AMSR_E_L2A_V_PG_Bc_Jul2003.txt')

irec = 1

nt = 486*300*50

do i=1, nt

  read(10,rec=irec,iostat=ios) xlon

  if(ios .ne. 0) then
    stop
  end if

  read(20,rec=irec) xlat
  read(30,rec=irec) ibt

  bt = ibt * 0.01 + 327.68

  if (bt .eq. 0.0) go to 888

111  format(3f8.2)

  dlat1 = abs(abs(xlat) - abs(39.5247))
  dlon1 = abs(abs(xlon) - abs(76.6450))

  if (dlat1 .le. 0.025 .and. dlon1 .le. 0.0325) write(51,111) xlon, xlat, bt

  dlat2 = abs(abs(xlat) - abs(39.3458))
  dlon2 = abs(abs(xlon) - abs(76.8569))

  if (dlat2 .le. 0.025 .and. dlon2 .le. 0.0325) write(52,111) xlon, xlat, bt

  dlat3 = abs(abs(xlat) - abs(39.3847))
  dlon3 = abs(abs(xlon) - abs(76.7222))

  if (dlat3 .le. 0.025 .and. dlon3 .le. 0.0325) write(53,111) xlon, xlat, bt

  dlat4 = abs(abs(xlat) - abs(39.5322))
  dlon4 = abs(abs(xlon) - abs(77.2325))

  if (dlat4 .le. 0.025 .and. dlon4 .le. 0.0325) write(54,111) xlon, xlat, bt

```

```

dlat5 = abs(abs(xlat) - abs(39.4214))
dlon5 = abs(abs(xlon) - abs(77.3178))

if (dlat5 .le. 0.025 .and. dlon5 .le. 0.0325) write(55,111) xlon, xlat, bt

dlat6 = abs(abs(xlat) - abs(39.6506))
dlon6 = abs(abs(xlon) - abs(76.2667))

if (dlat6 .le. 0.025 .and. dlon6 .le. 0.0325) write(56,111) xlon, xlat, bt

dlat7 = abs(abs(xlat) - abs(39.5328))
dlon7 = abs(abs(xlon) - abs(76.5072))

if (dlat7 .le. 0.025 .and. dlon7 .le. 0.0325) write(57,111) xlon, xlat, bt

dlat8 = abs(abs(xlat) - abs(39.3194))
dlon8 = abs(abs(xlon) - abs(76.9492))

if (dlat8 .le. 0.025 .and. dlon8 .le. 0.0325) write(58,111) xlon, xlat, bt

dlat9 = abs(abs(xlat) - abs(39.2458))
dlon9 = abs(abs(xlon) - abs(76.9308))

if (dlat9 .le. 0.025 .and. dlon9 .le. 0.0325) write(59,111) xlon, xlat, bt

dlat10 = abs(abs(xlat) - abs(39.1669))
dlon10 = abs(abs(xlon) - abs(76.9000))

if (dlat10 .le. 0.025 .and. dlon10 .le. 0.0325) write(60,111) xlon, xlat, bt

dlat11 = abs(abs(xlat) - abs(39.2206))
dlon11 = abs(abs(xlon) - abs(77.3783))

if (dlat11 .le. 0.025 .and. dlon11 .le. 0.0325) write(61,111) xlon, xlat, bt

dlat12 = abs(abs(xlat) - abs(39.0761))
dlon12 = abs(abs(xlon) - abs(76.9583))

if (dlat12 .le. 0.025 .and. dlon12 .le. 0.0325) write(62,111) xlon, xlat, bt

dlat13 = abs(abs(xlat) - abs(39.0308))
dlon13 = abs(abs(xlon) - abs(76.9375))

if (dlat13 .le. 0.025 .and. dlon13 .le. 0.0325) write(63,111) xlon, xlat, bt

```

888 continue

```

    irec = irec + 1

end do

stop
end

```

12. An example of the Fortran code used to generate monthly mean brightness temperature data at a well site

```

program write_BT_month_data

real*4  bt,xlon,xlat
integer*2 ibt

irecl = 4
irecm = 2

open(10, file='AMSR_E_L2A_Longitude_Jul2004.grd',ACCESS='DIRECT',
     RECL=irecl, FORM='UNFORMATTED', status='old')
open(20, file='AMSR_E_L2A_Latitude_Jul2004.grd',ACCESS='DIRECT',
     RECL=irecl, FORM='UNFORMATTED', status='old')
open(30, file='AMSR_E_L2A_89.0V_Res.5_Jul2004.grd',ACCESS='DIRECT',
     RECL=irecm, FORM='UNFORMATTED', status='old')

666  format(3f8.2)

open(51,file='AMSR_E_L2A_V_BA_Cd_Jul2004_M.txt')
open(52,file='AMSR_E_L2A_V_BA_Ea_Jul2004_M.txt')
open(53,file='AMSR_E_L2A_V_BA_Ec_Jul2004_M.txt')
open(54,file='AMSR_E_L2A_V_FR_Cg_Jul2004_M.txt')
open(55,file='AMSR_E_L2A_V_FR_Df_Jul2004_M.txt')
open(56,file='AMSR_E_L2A_V_HA_Bd_Jul2004_M.txt')
open(57,file='AMSR_E_L2A_V_HA_Ca_Jul2004_M.txt')
open(58,file='AMSR_E_L2A_V_HO_Bd_Jul2004_M.txt')
open(59,file='AMSR_E_L2A_V_HO_Cd_Jul2004_M.txt')
open(60,file='AMSR_E_L2A_V_HO_Ce_Jul2004_M.txt')
open(61,file='AMSR_E_L2A_V_MO_Cc_Jul2004_M.txt')
open(62,file='AMSR_E_L2A_V_MO_Eh_Jul2004_M.txt')

```

```
open(63,file='AMSR_E_L2A_V_PG_Bc_Jul2004_M.txt')
```

```
sbt01 = 0.0  
nbt01 = 0
```

```
sbt02 = 0.0  
nbt02 = 0
```

```
sbt03 = 0.0  
nbt03 = 0
```

```
sbt04 = 0.0  
nbt04 = 0
```

```
sbt05 = 0.0  
nbt05 = 0
```

```
sbt06 = 0.0  
nbt06 = 0
```

```
sbt07 = 0.0  
nbt07 = 0
```

```
sbt08 = 0.0  
nbt08 = 0
```

```
sbt09 = 0.0  
nbt09 = 0
```

```
sbt10 = 0.0  
nbt10 = 0
```

```
sbt11 = 0.0  
nbt11 = 0
```

```
sbt12 = 0.0  
nbt12 = 0
```

```
sbt13 = 0.0  
nbt13 = 0
```

```
irec = 1
```

```
nt = 486*300*30
```

```
do i=1, nt
```

```

read(10,rec=irec,iostat=ios) xlon

if(ios .ne. 0) then
  go to 999
end if
read(20,rec=irec) xlat
read(30,rec=irec) ibt

bt = ibt * 0.01 + 327.68

if (bt .eq. 0.0 .or. bt .lt. 250.0) go to 888

dlat1 = abs(abs(xlat) - abs(39.5247))
dlon1 = abs(abs(xlon) - abs(76.6450))

if (dlat1 .le. 0.025 .and. dlon1 .le. 0.0325) go to 101

dlat2 = abs(abs(xlat) - abs(39.3458))
dlon2 = abs(abs(xlon) - abs(76.8569))

if (dlat2 .le. 0.025 .and. dlon2 .le. 0.0325) go to 102

dlat3 = abs(abs(xlat) - abs(39.3847))
dlon3 = abs(abs(xlon) - abs(76.7222))

if (dlat3 .le. 0.025 .and. dlon3 .le. 0.0325) go to 103

dlat4 = abs(abs(xlat) - abs(39.5322))
dlon4 = abs(abs(xlon) - abs(77.2325))

if (dlat4 .le. 0.025 .and. dlon4 .le. 0.0325) go to 104

dlat5 = abs(abs(xlat) - abs(39.4214))
dlon5 = abs(abs(xlon) - abs(77.3178))

if (dlat5 .le. 0.025 .and. dlon5 .le. 0.0325) go to 105

dlat6 = abs(abs(xlat) - abs(39.6506))
dlon6 = abs(abs(xlon) - abs(76.2667))

if (dlat6 .le. 0.025 .and. dlon6 .le. 0.0325) go to 106

dlat7 = abs(abs(xlat) - abs(39.5328))
dlon7 = abs(abs(xlon) - abs(76.5072))

```

if (dlat7 .le. 0.025 .and. dlon7 .le. 0.0325) go to 107

dlat8 = abs(abs(xlat) - abs(39.3194))
dlon8 = abs(abs(xlon) - abs(76.9492))

if (dlat8 .le. 0.025 .and. dlon8 .le. 0.0325) go to 108

dlat9 = abs(abs(xlat) - abs(39.2458))
dlon9 = abs(abs(xlon) - abs(76.9308))

if (dlat9 .le. 0.025 .and. dlon9 .le. 0.0325) go to 109

dlat10 = abs(abs(xlat) - abs(39.1669))
dlon10 = abs(abs(xlon) - abs(76.9000))

if (dlat10 .le. 0.025 .and. dlon10 .le. 0.0325) go to 110

dlat11 = abs(abs(xlat) - abs(39.2206))
dlon11 = abs(abs(xlon) - abs(77.3783))

if (dlat11 .le. 0.025 .and. dlon11 .le. 0.0325) go to 111

dlat12 = abs(abs(xlat) - abs(39.0761))
dlon12 = abs(abs(xlon) - abs(76.9583))

if (dlat12 .le. 0.025 .and. dlon12 .le. 0.0325) go to 112

dlat13 = abs(abs(xlat) - abs(39.0308))
dlon13 = abs(abs(xlon) - abs(76.9375))

if (dlat13 .le. 0.025 .and. dlon13 .le. 0.0325) go to 113

go to 888

101 continue

sbt01 = sbt01 + bt
nbt01 = nbt01 + 1

go to 888

102 continue

sbt02 = sbt02 + bt
nbt02 = nbt02 + 1

go to 888

103 continue

$sbt03 = sbt03 + bt$
 $nbt03 = nbt03 + 1$

go to 888

104 continue

$sbt04 = sbt04 + bt$
 $nbt04 = nbt04 + 1$

go to 888

105 continue

$sbt05 = sbt05 + bt$
 $nbt05 = nbt05 + 1$

go to 888

106 continue

$sbt06 = sbt06 + bt$
 $nbt06 = nbt06 + 1$

go to 888

107 continue

$sbt07 = sbt07 + bt$
 $nbt07 = nbt07 + 1$

go to 888

108 continue

$sbt08 = sbt08 + bt$
 $nbt08 = nbt08 + 1$

go to 888

109 continue

sbt09 = sbt09 + bt
nbt09 = nbt09 + 1

go to 888

110 continue

sbt10 = sbt10 + bt
nbt10 = nbt10 + 1

go to 888

111 continue

sbt11 = sbt11 + bt
nbt11 = nbt11 + 1

go to 888

112 continue

sbt12 = sbt12 + bt
nbt12 = nbt12 + 1

go to 888

113 continue

sbt13 = sbt13 + bt
nbt13 = nbt13 + 1

888 continue

irec = irec + 1

end do

999 continue

abt01 = sbt01 / nbt01
abt02 = sbt02 / nbt02
abt03 = sbt03 / nbt03
abt04 = sbt04 / nbt04
abt05 = sbt05 / nbt05
abt06 = sbt06 / nbt06

```
abt07 = sbt07 / nbt07
abt08 = sbt08 / nbt08
abt09 = sbt09 / nbt09
abt10 = sbt10 / nbt10
abt11 = sbt11 / nbt11
abt12 = sbt12 / nbt12
abt13 = sbt13 / nbt13
```

```
write(51,666) abt01
write(52,666) abt02
write(53,666) abt03
write(54,666) abt04
write(55,666) abt05
write(56,666) abt06
write(57,666) abt07
write(58,666) abt08
write(59,666) abt09
write(60,666) abt10
write(61,666) abt11
write(62,666) abt12
write(63,666) abt13
```

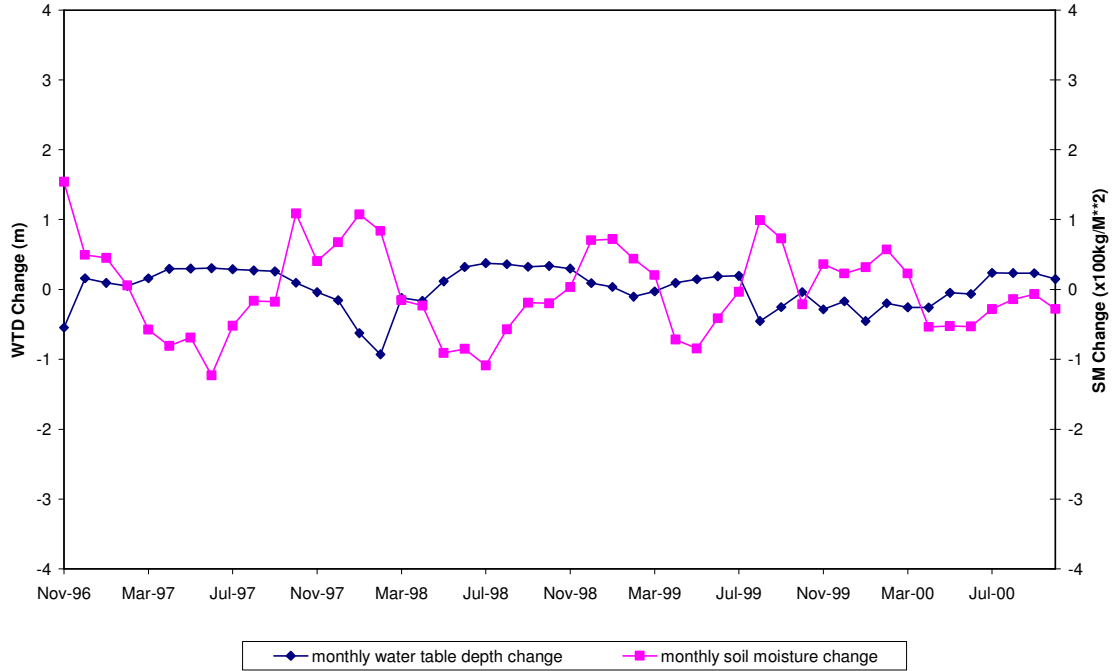
```
stop
end
```

Appendix B. Hydrologic Soil Group of Maryland (Courtesy Maryland Department of Planning)

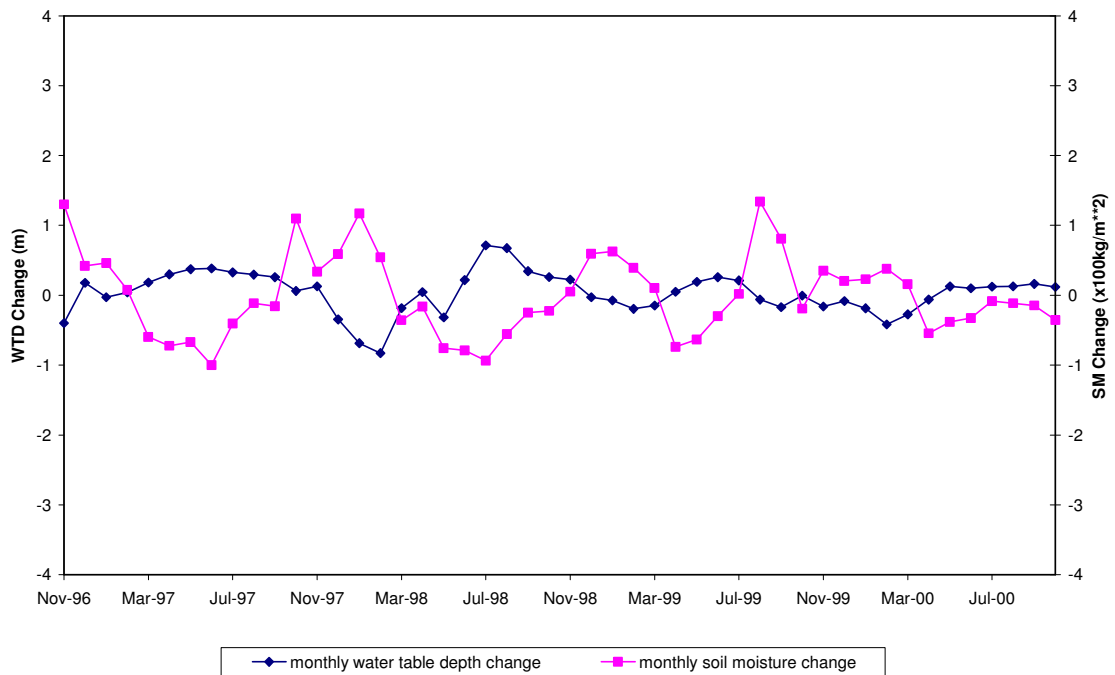
SOIL	TEXTUR	HYDGRP
A1,A1a,A1b,A1c	loamy sand; sand, sandy loam	A
A2	sand	A
B1,B1a,B1b,B1c	silt loam,loam, fine sandy loam, sandy loam, silty clay loam, clay loam,silty clay, clay	B
B2,B2a,B2b, B2c	silt loam, loam, gravelly loam, clay loam,silty clay loam	C
B3	clay, silty clay, silt loam, loam,loamy sand	C
C1,C1a,C1b,C1c	silt loam, loam, shaly silty loam, shaly loam, channery loam, channery silt loam, sandy loam	C
C2	silty clay loam, silty clay, clay	C
D1,D1a,D1b, D1c	shaly silt loam, shaly loam, silty clay loam, silty clay	C-D
E1, E1a,E1b	sandy loam, sandy clay, loam, loamy sand, sand	C
E2,E2a,E2b	silt loam, loam, silty clay loam, fine sandy loam, sandy clay loam	C
E3, E3a, E3b	silt loam, loam, silty clay loam	C
F1	loamy sand, sand	D
F2	sandy loam, fine sandy loam, sandy clay loam, loam, loamy sand	D
F3	silty clay loam, silty clay, clay, loam, silt loam	D
G1,G1a	silt loam, loam, fine sandy loam, sandy loam, silty clay loam	B-C
G2	silt loam, silty clay loam, silty clay, fine sandy loam, sandy loam, loam, muck	D
G3	variable	N/A
H1,H1a,H1b,H1c	Too variable to rate. Determine the specific soil series name from detailed soil map and use the information for the group that the series is in.	
H2,H2a,H2b,H2c	Too variable to rate. Determine the specific soil series name from detailed soil map and use the information for the group that the series is in.	

Appendix C. Comparison of Time Series of Water Table Change and Soil Moisture Variation at the 13 Well Sites in Piedmont Plateau, MD

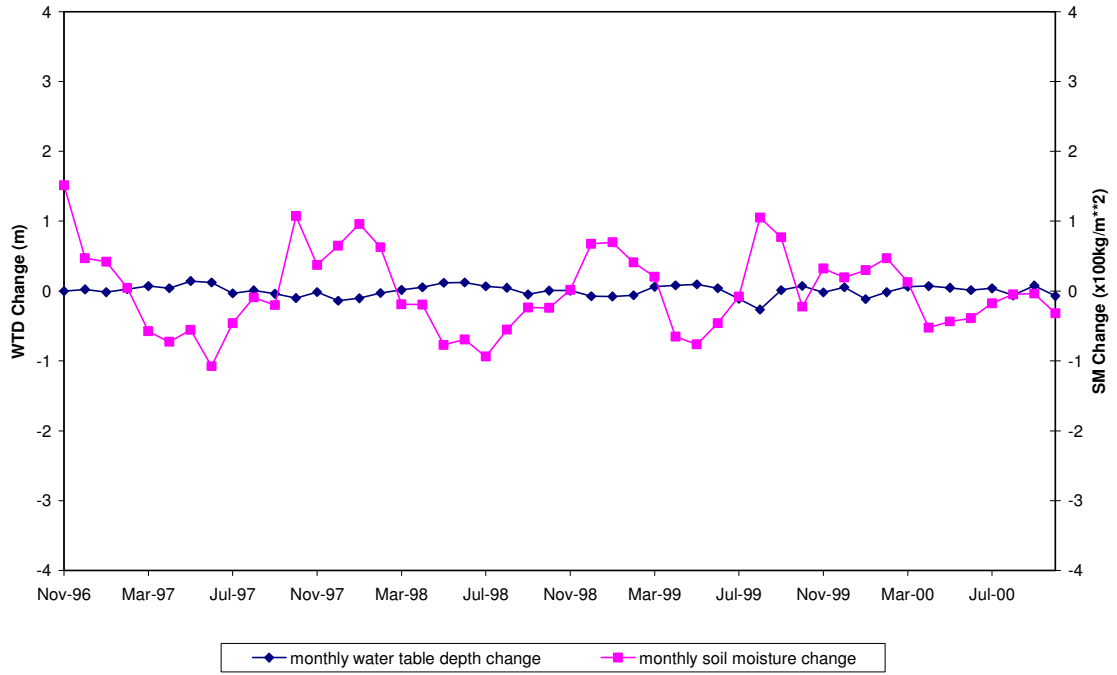
Monthly Variation in Water Table Depths and Soil Moisture Contents (at BA_Cd_26)



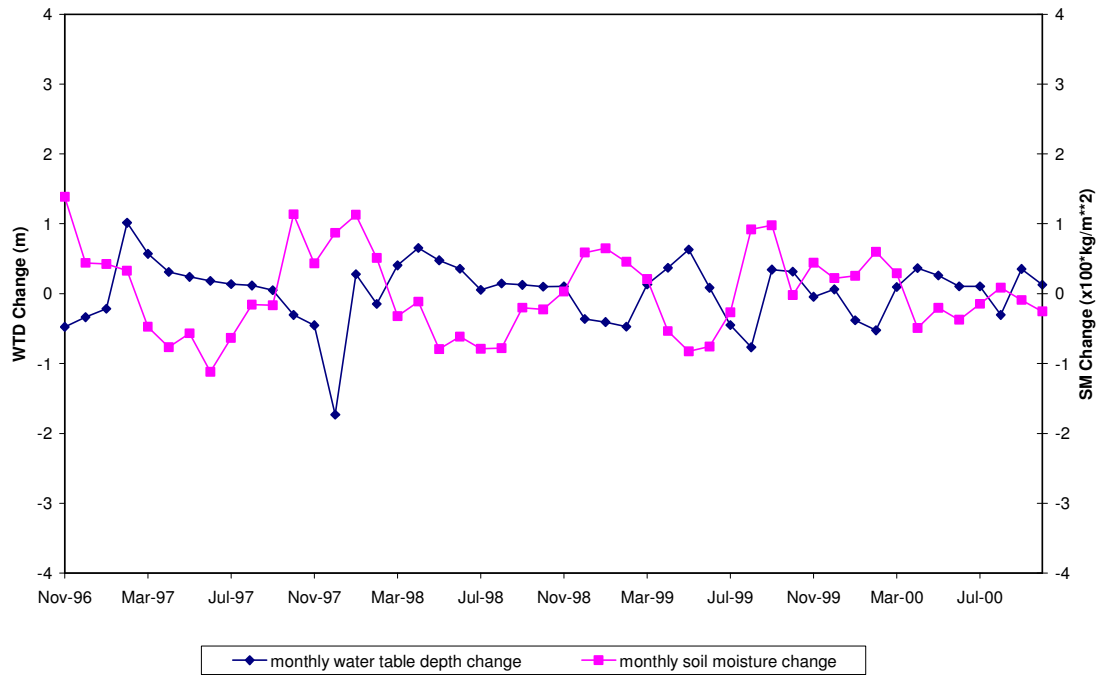
Monthly Variation in Water Table Depths and Soil Moisture Contents (at BA_Ea_18)



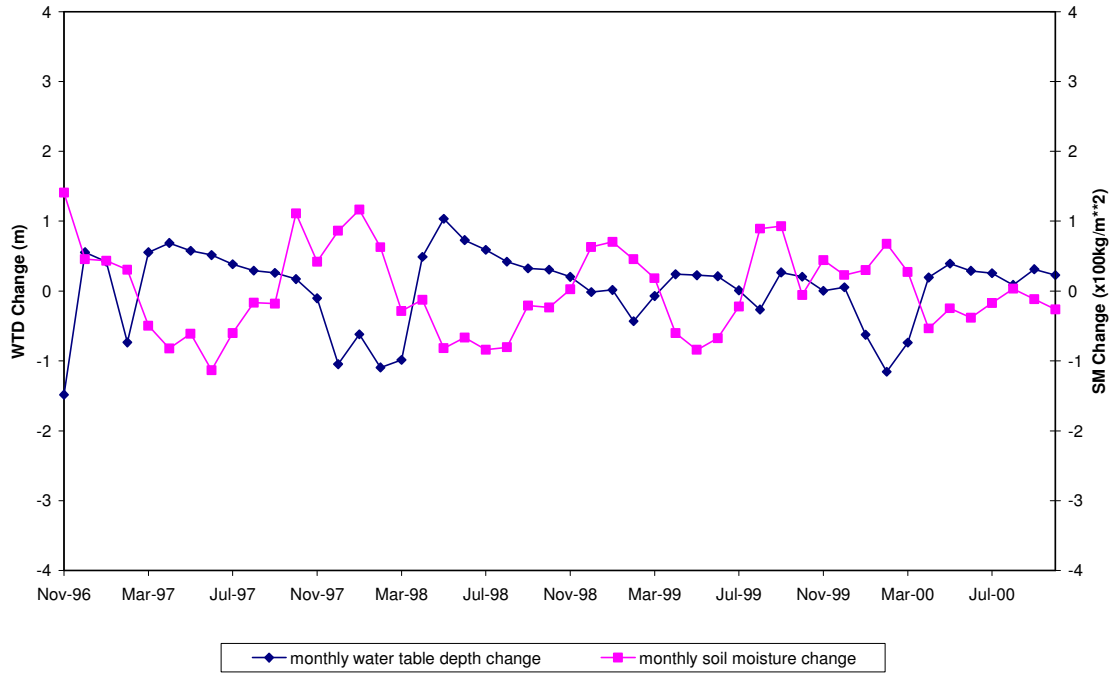
Monthly Variation in Water Table Depths and Soil Moisture Contents (at BA_Ec_43)



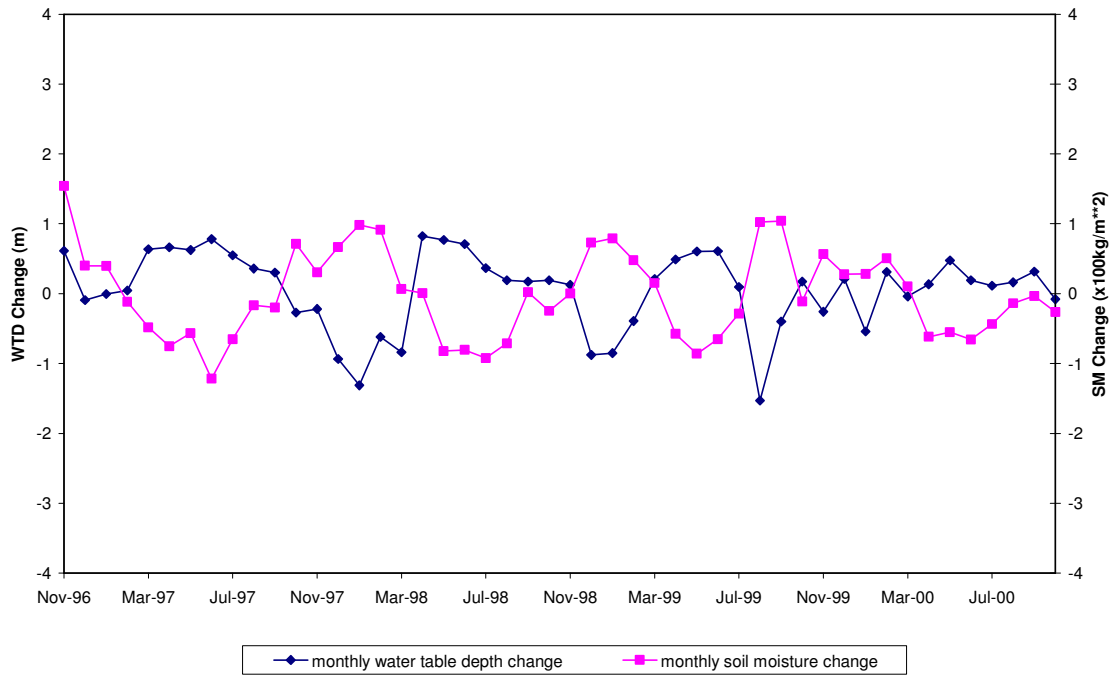
Monthly Variation in Water Table Depths and Soil Moisture Contents (at FR_Cg_1)



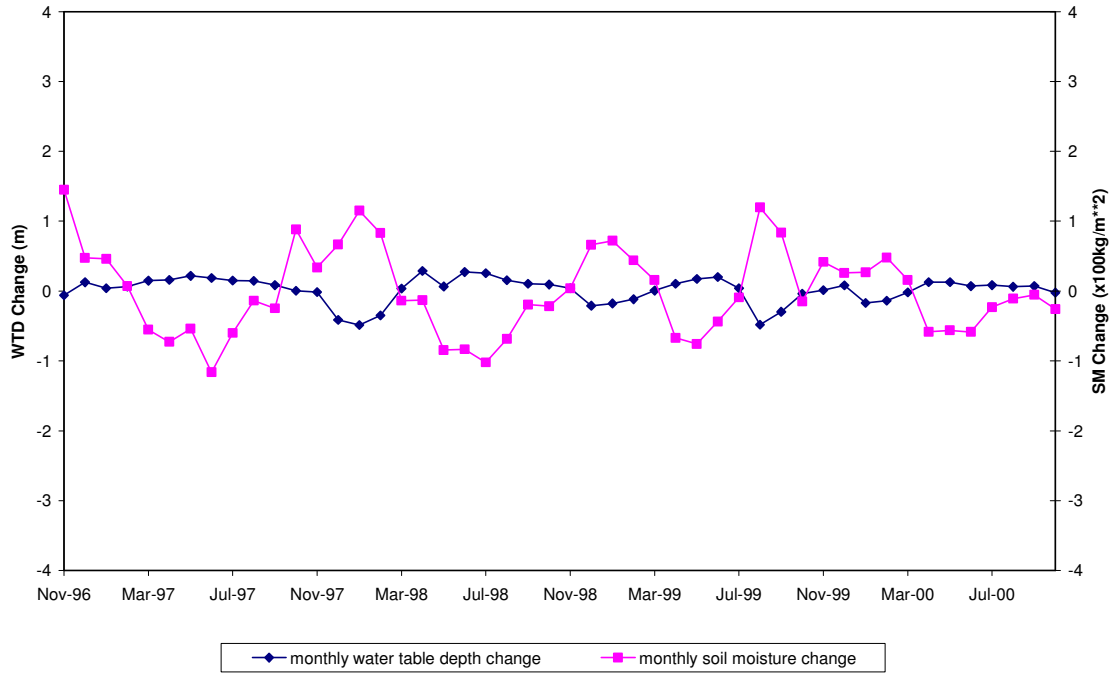
Monthly Variation in Water Table Depths and Soil Moisture Contents (at FR_Df_35)



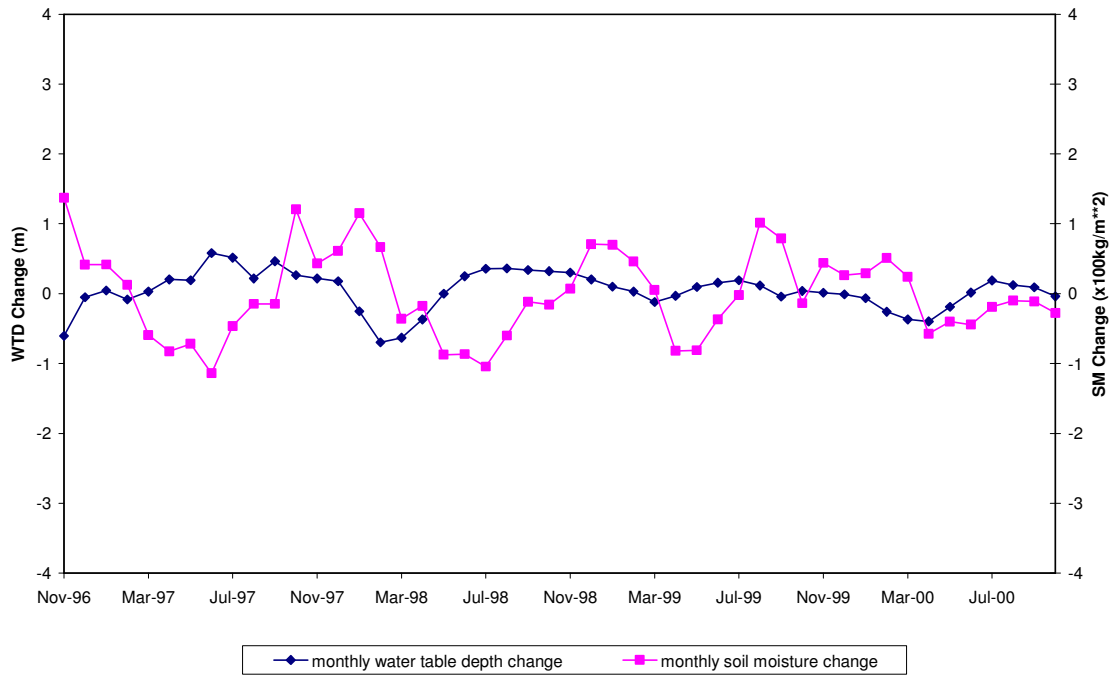
Monthly Variation in Water Table Depths and Soil Moisture Contents (at HA_Bd_31)



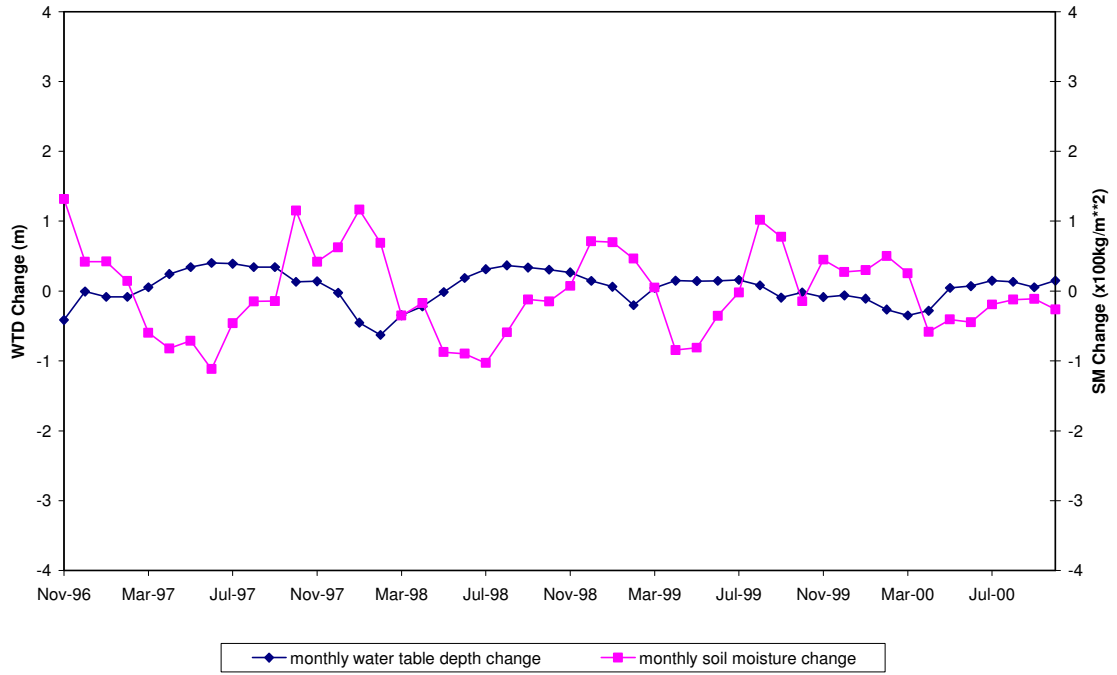
Monthly Variation in Water Table Depths and Soil Moisture Contents (at HA_Ca_23)



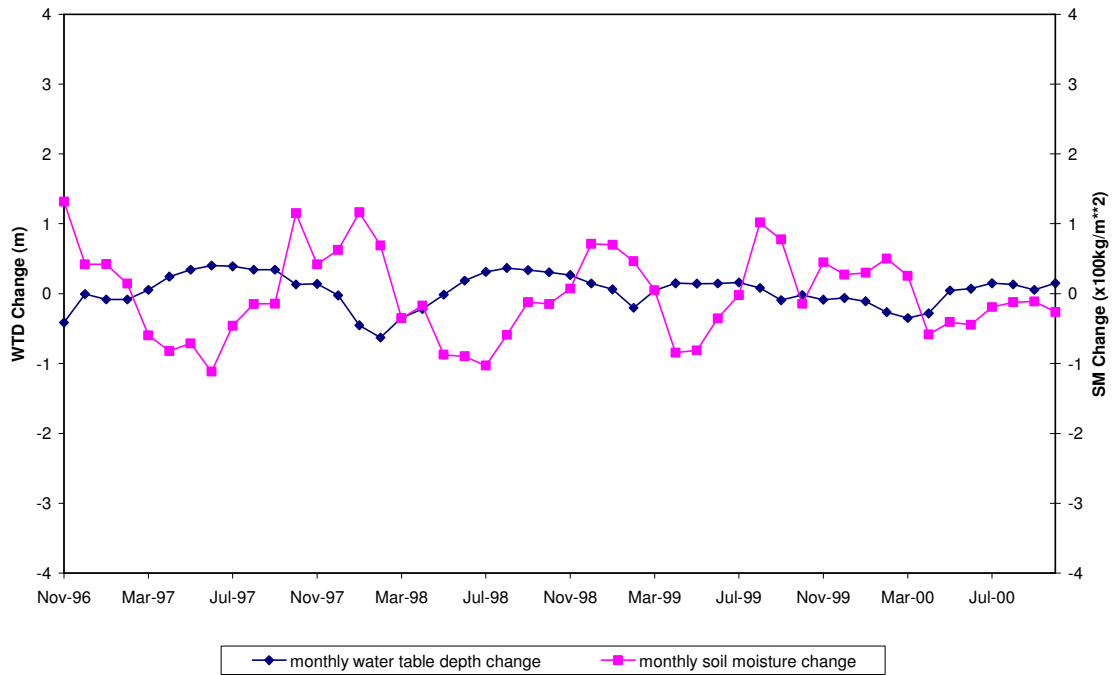
Monthly Variation in Water Table Depths and Soil Moisture Contents (at HO_Bd_1)



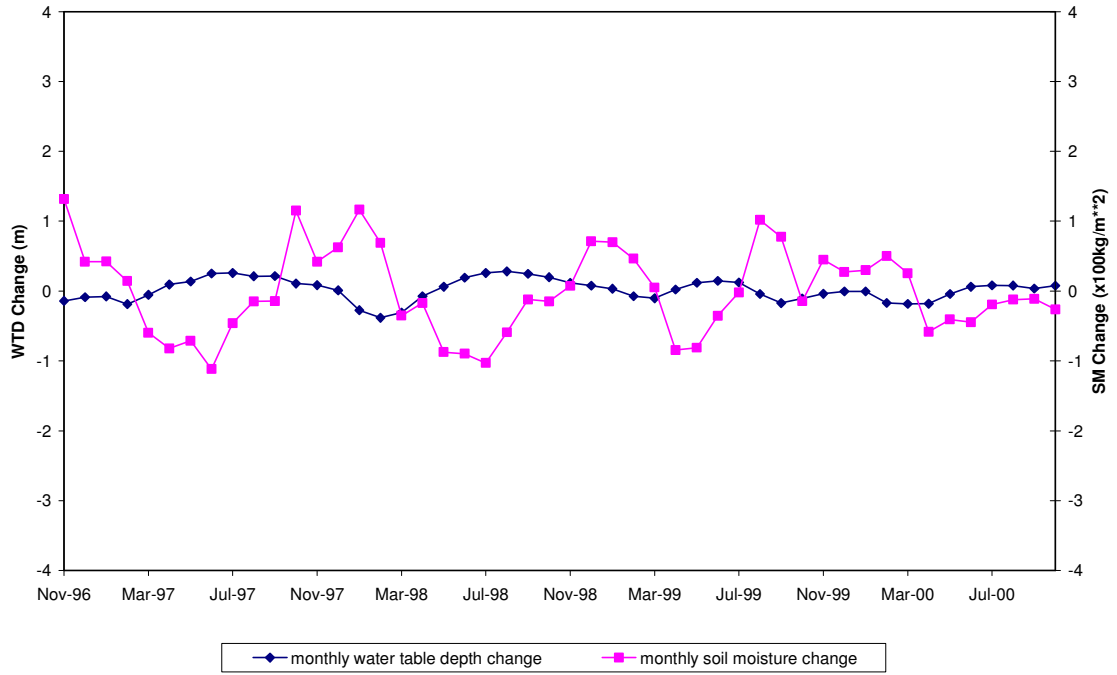
Monthly Variation in Water Table Depths and Soil Moisture Contents (at HO_Cd_79)



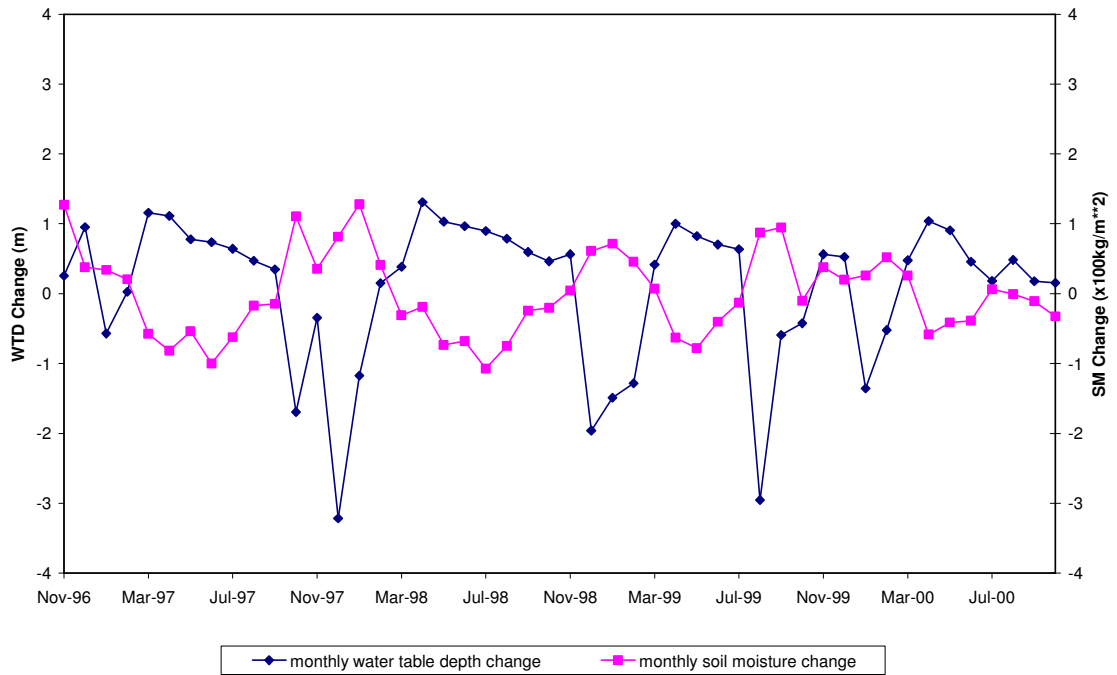
Monthly Variation in Water Table Depths and Soil Moisture Contents (at HO_Ce_38)



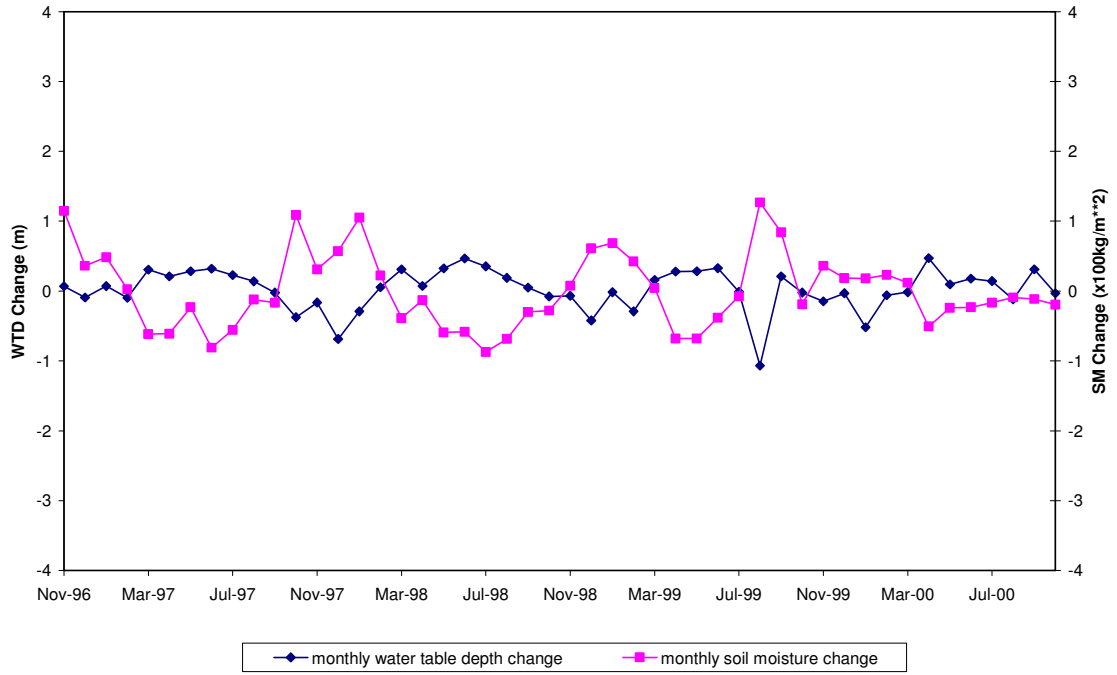
Monthly Variation in Water Table Depths and Soil Moisture Contents (at MO_Cc_14)



Monthly Variation in Water Table Depths and Soil Moisture Contents (at MO_Eh_20)

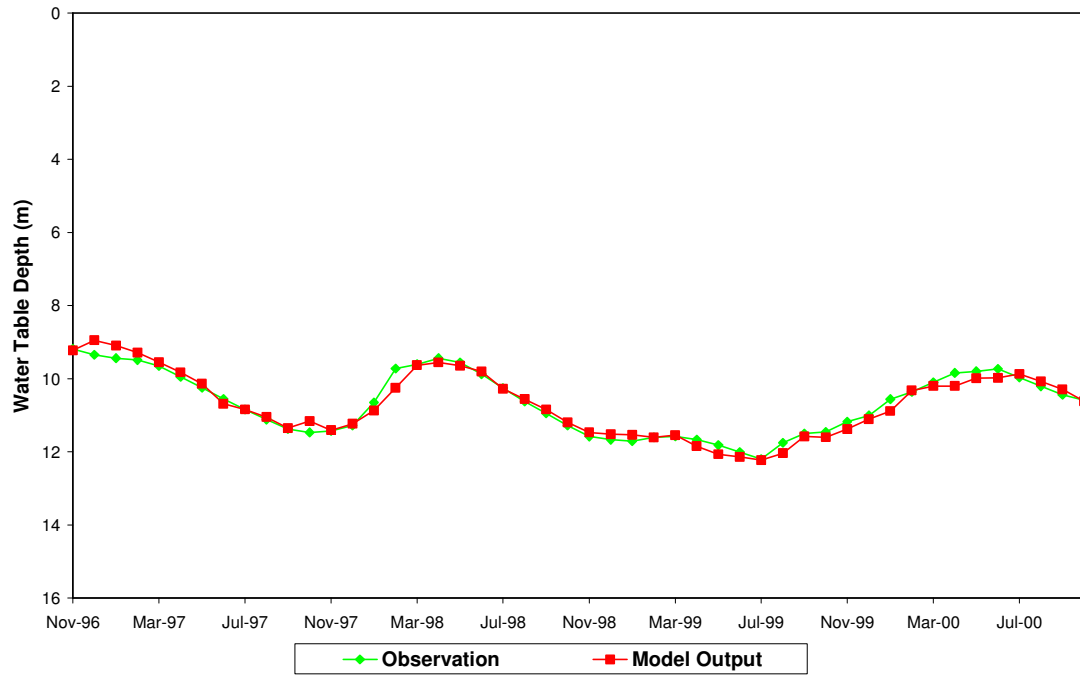


Monthly Variation in Water Table Depths and Soil Moisture Contents (at PG_Bc_16)

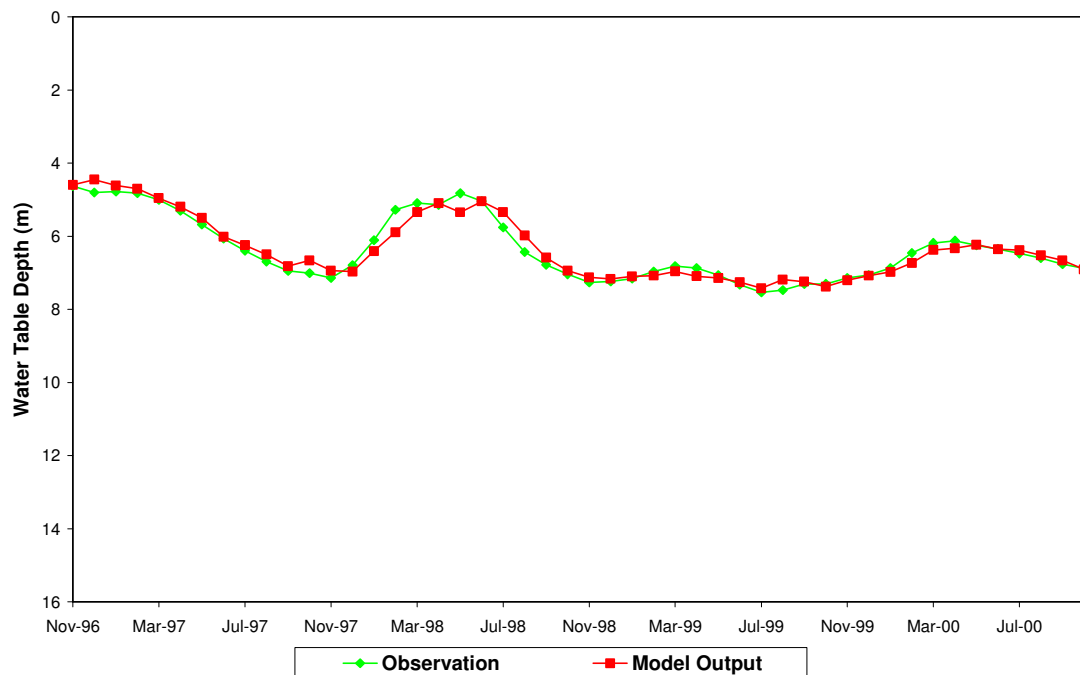


Appendix D. Comparison of Training Outputs and Observations at 12 Available Wells in Piedmont Plateau, Maryland

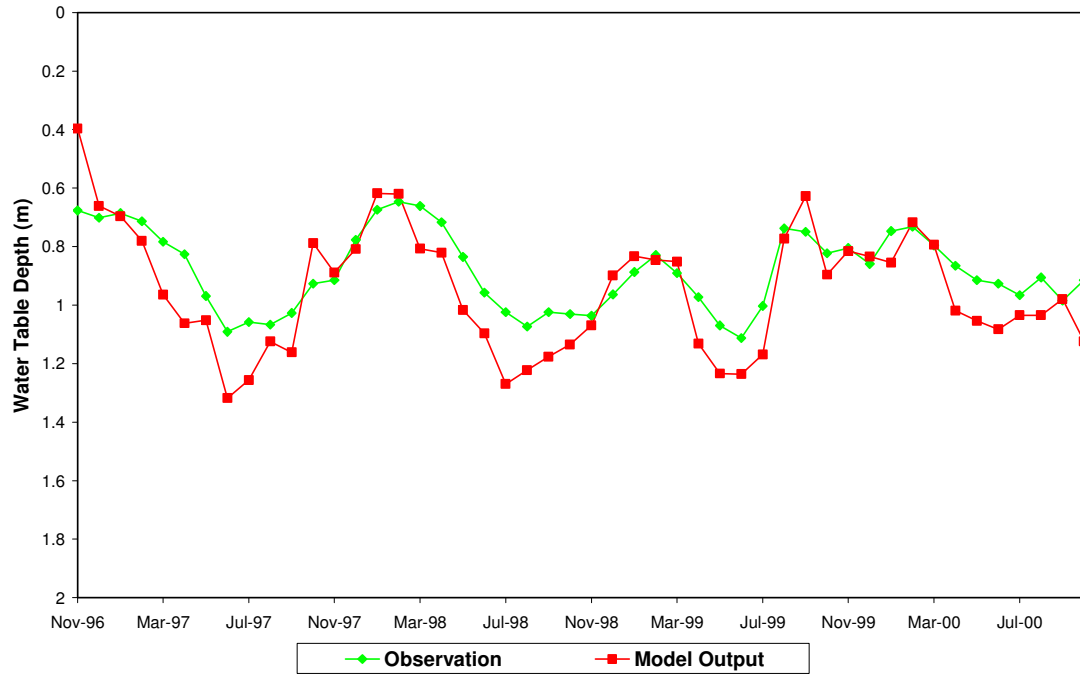
Comparison of Model Output and Observation at BA Cd 26



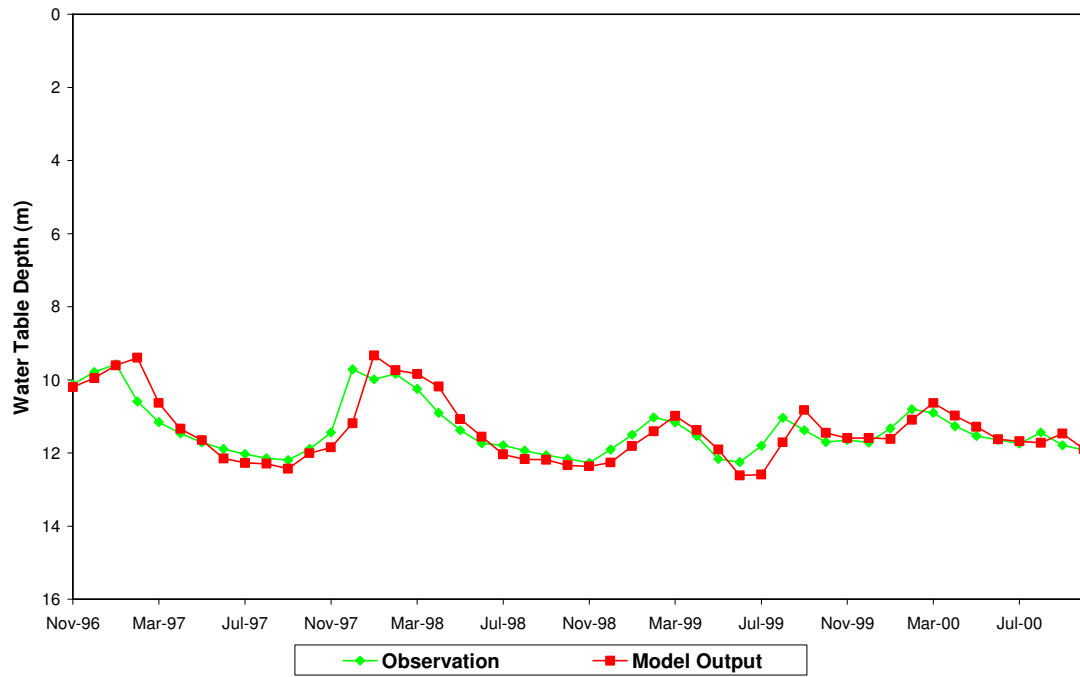
Comparison of Model Output and Observation at BA Ea 18



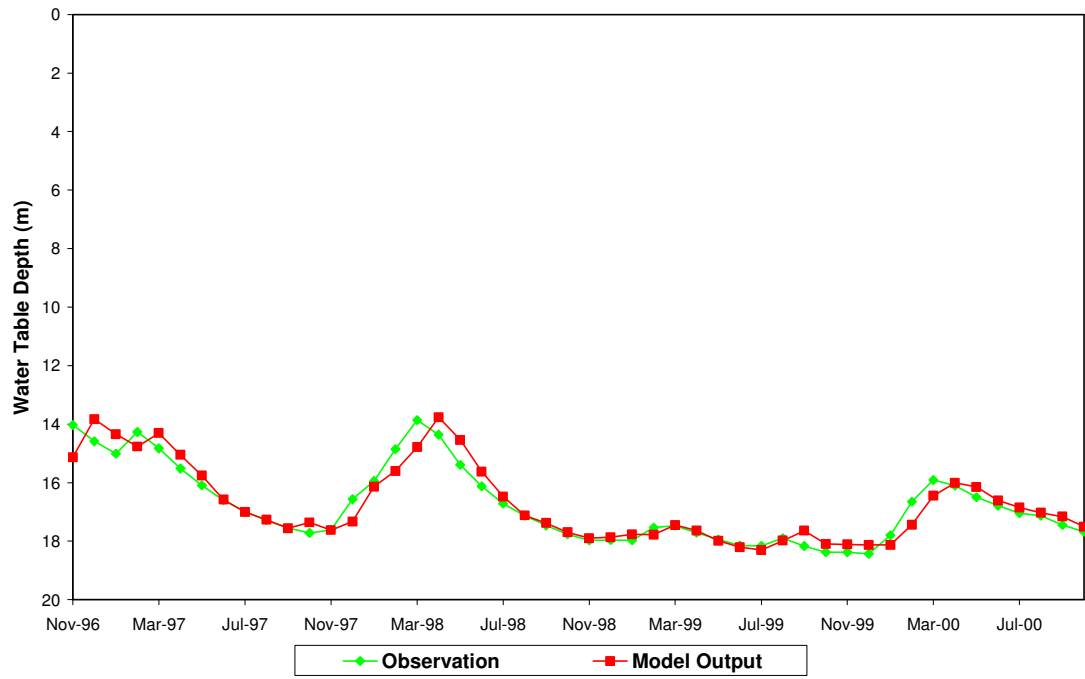
Comparison of Model Output and Observation at BA Ec 43



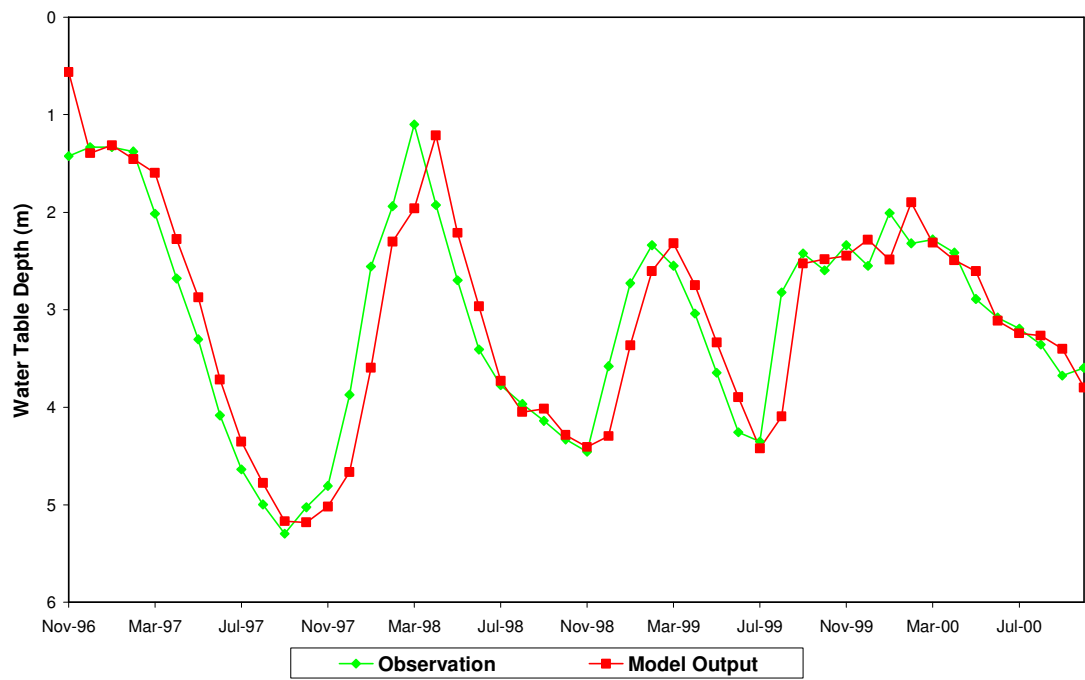
Comparison of Model Output and Observation at FR Cg 1



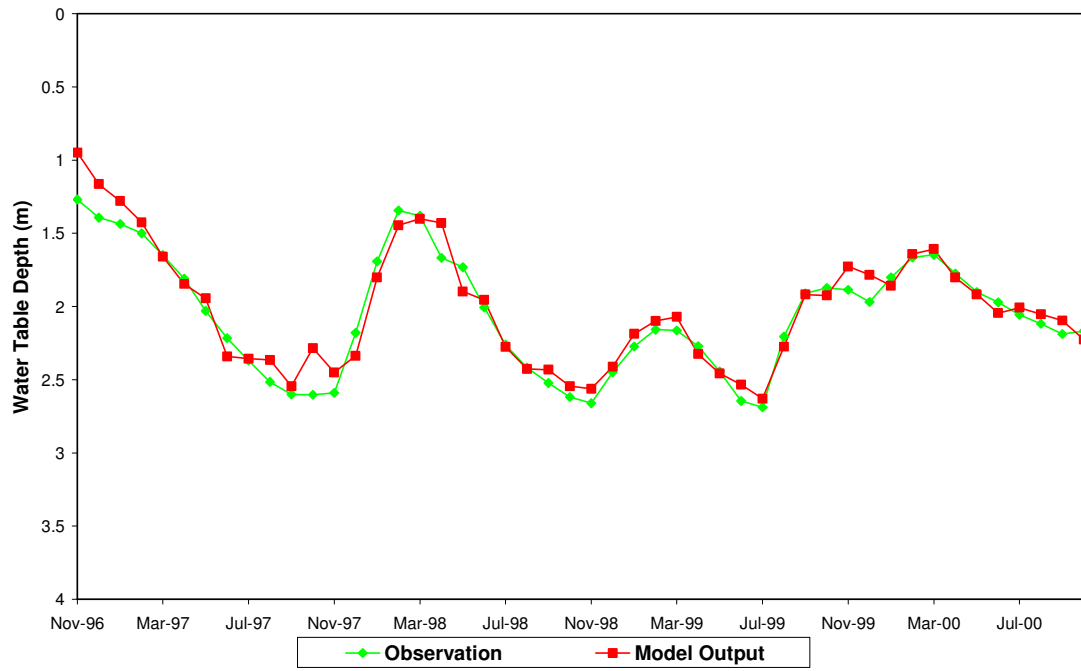
Comparison of Model Output and Observation at FR Df 35



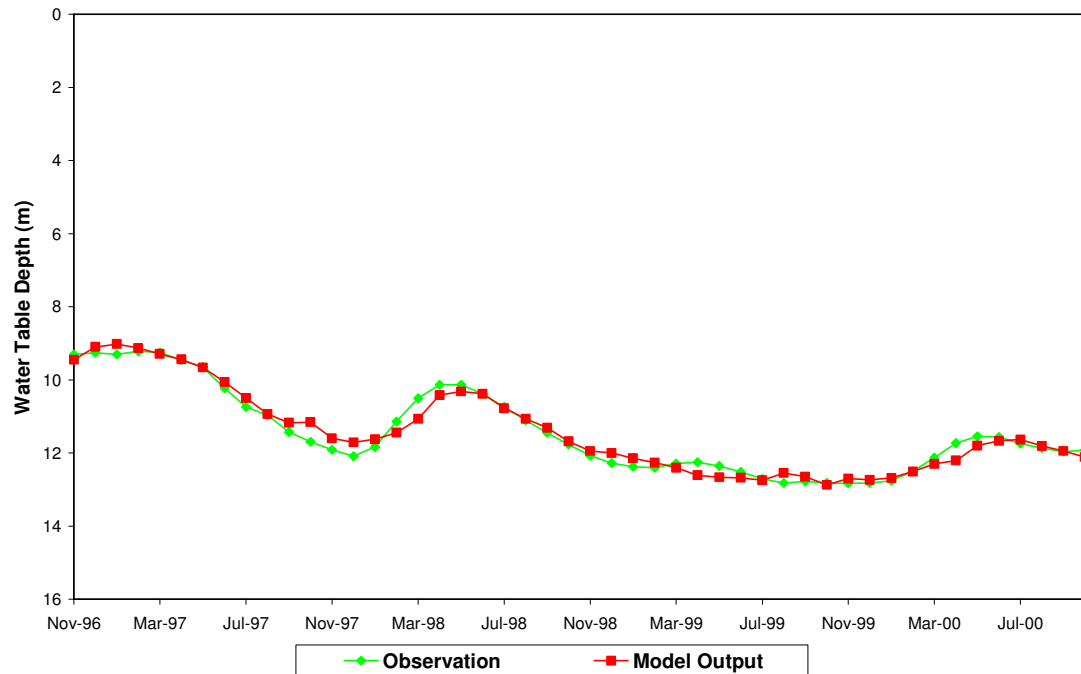
Comparison of Model Output and Observation at HA Bd 31



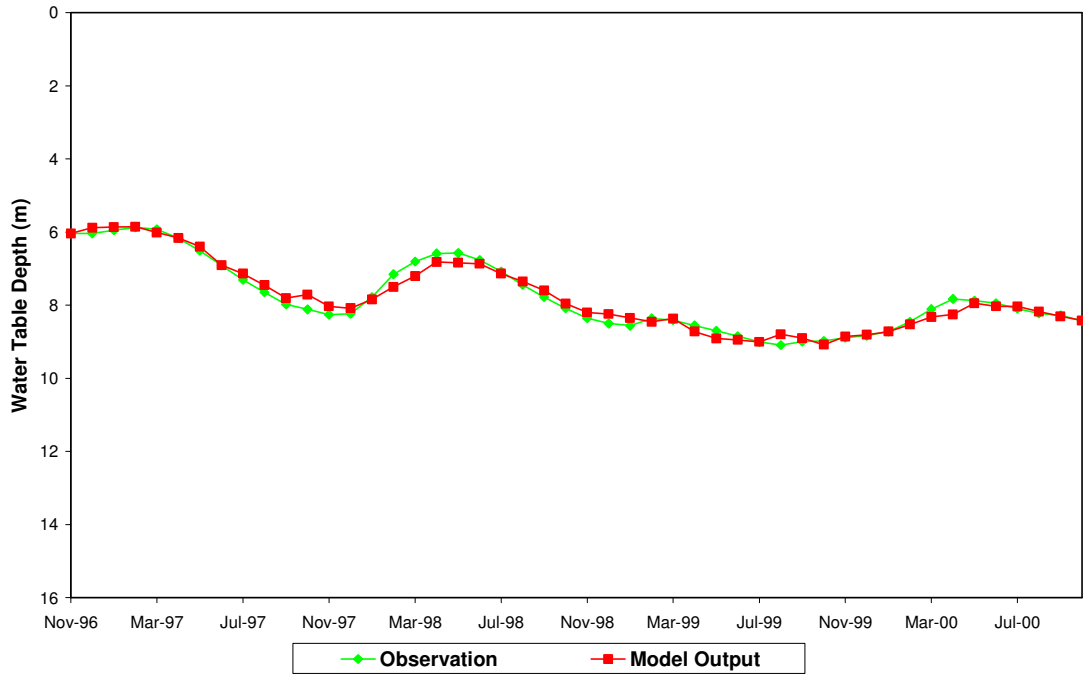
Comparison of Model Output and Observation at HA Ca 23



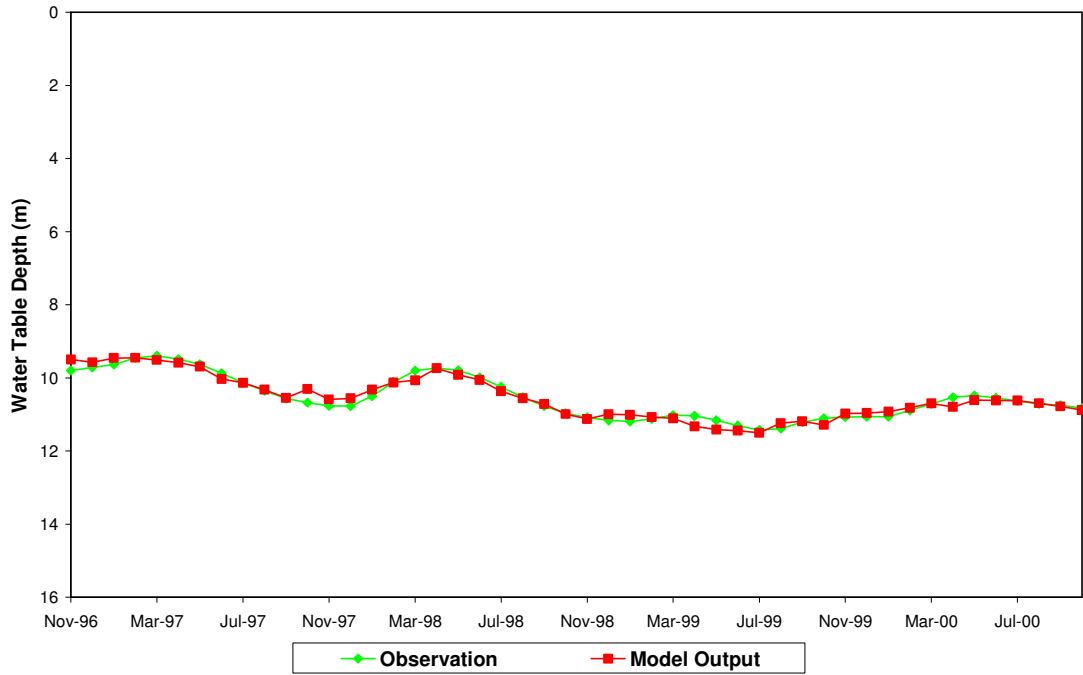
Comparison of Model Output and Observation at HO Bd 1



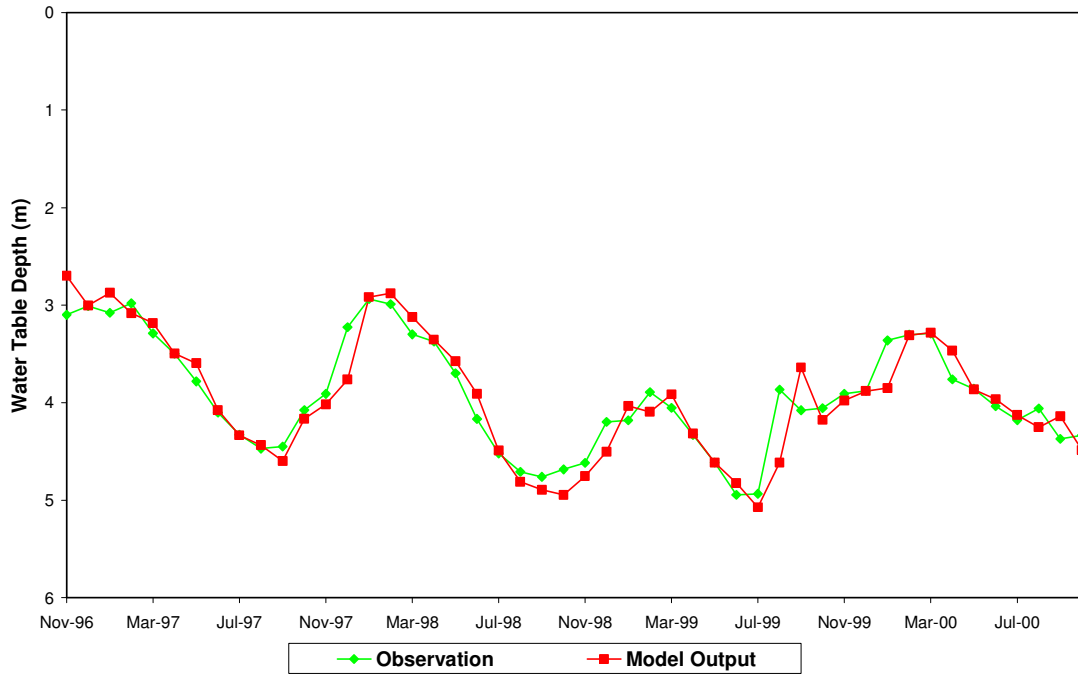
Comparison of Model Output and Observation at HO Cd 79



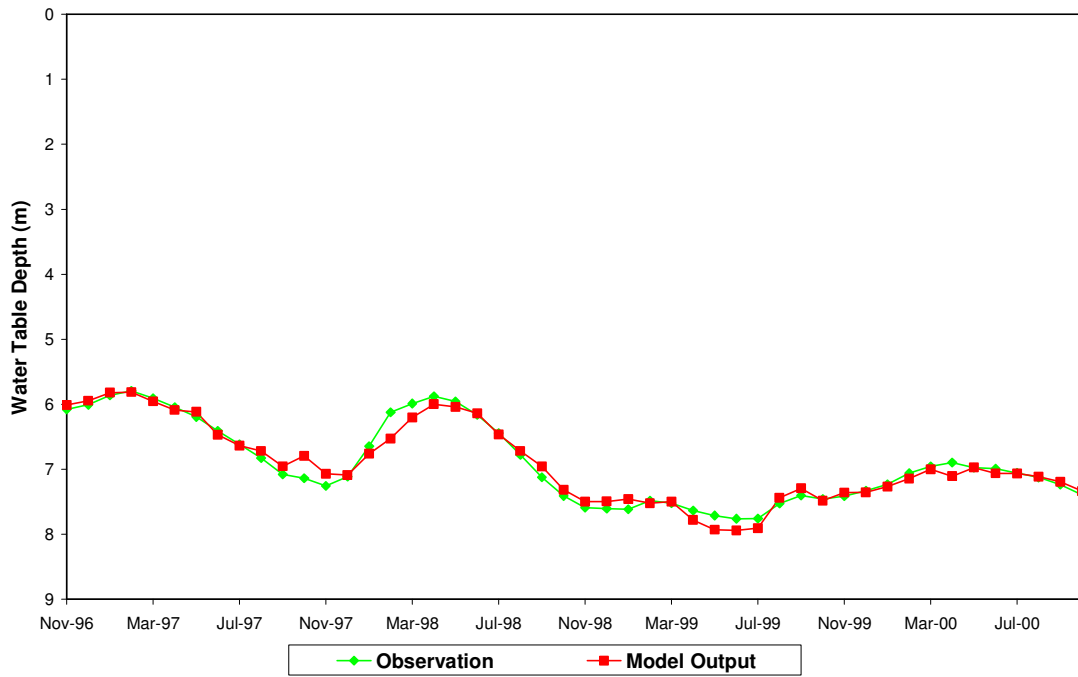
Comparison of Model Output and Observation at HO Ce 38



Comparison of Model Output and Observation at MO Eh 20

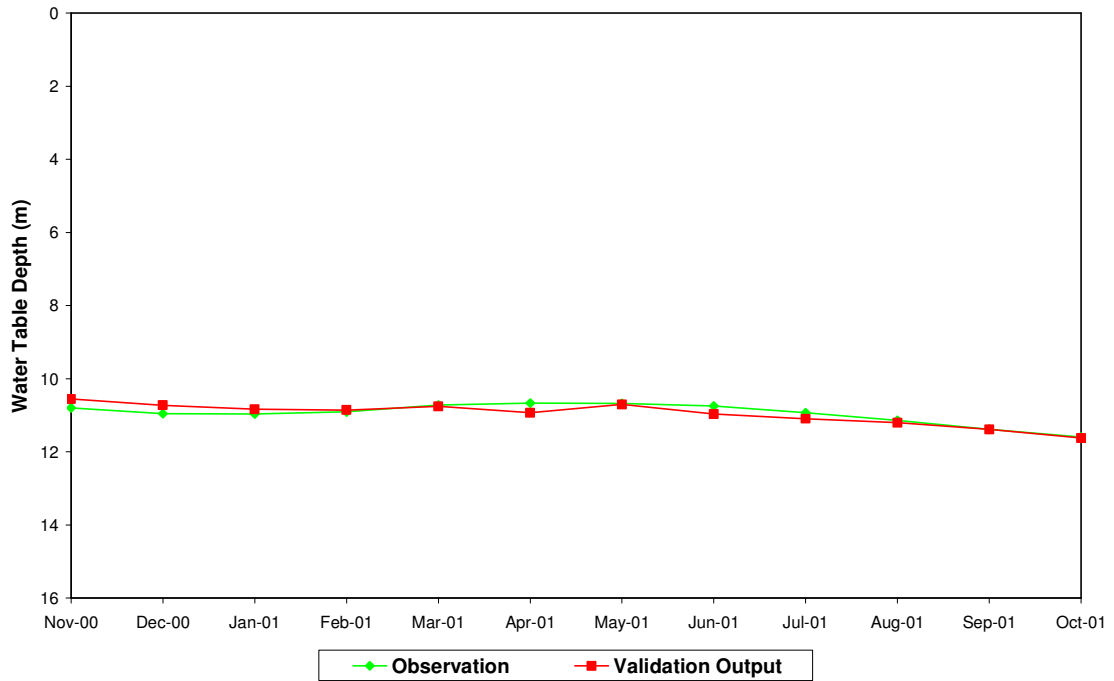


Comparison of Model Output and Observation at PG Ec 16

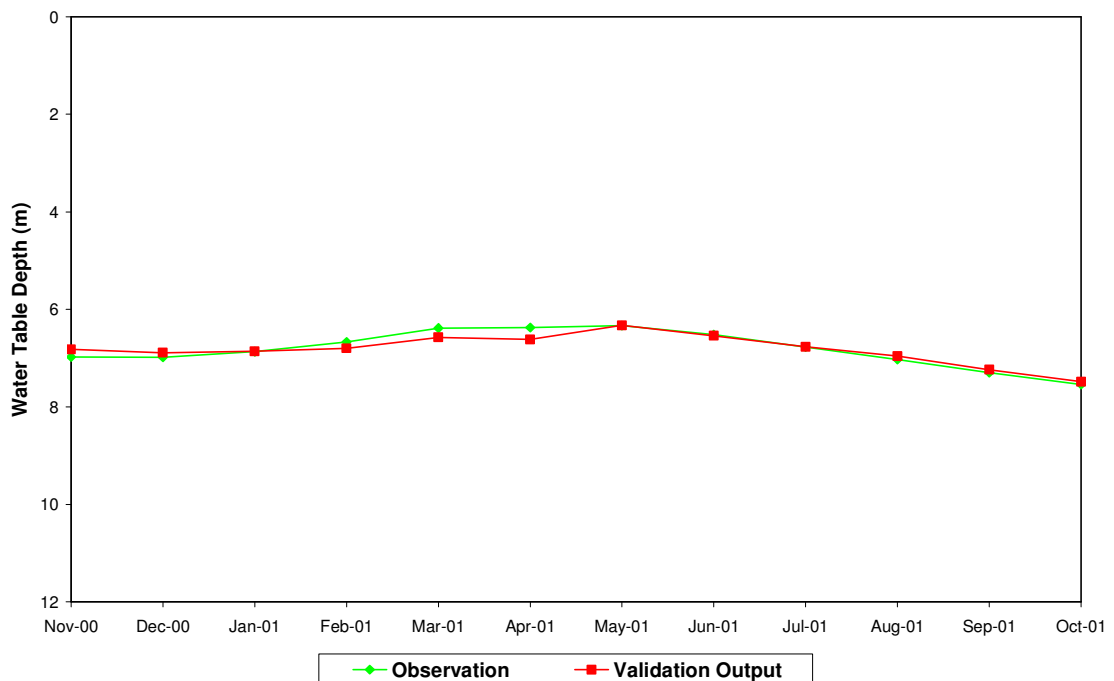


Appendix E. Comparison of Validation Outputs and Observations at 12 Available Wells in Piedmont Plateau, Maryland

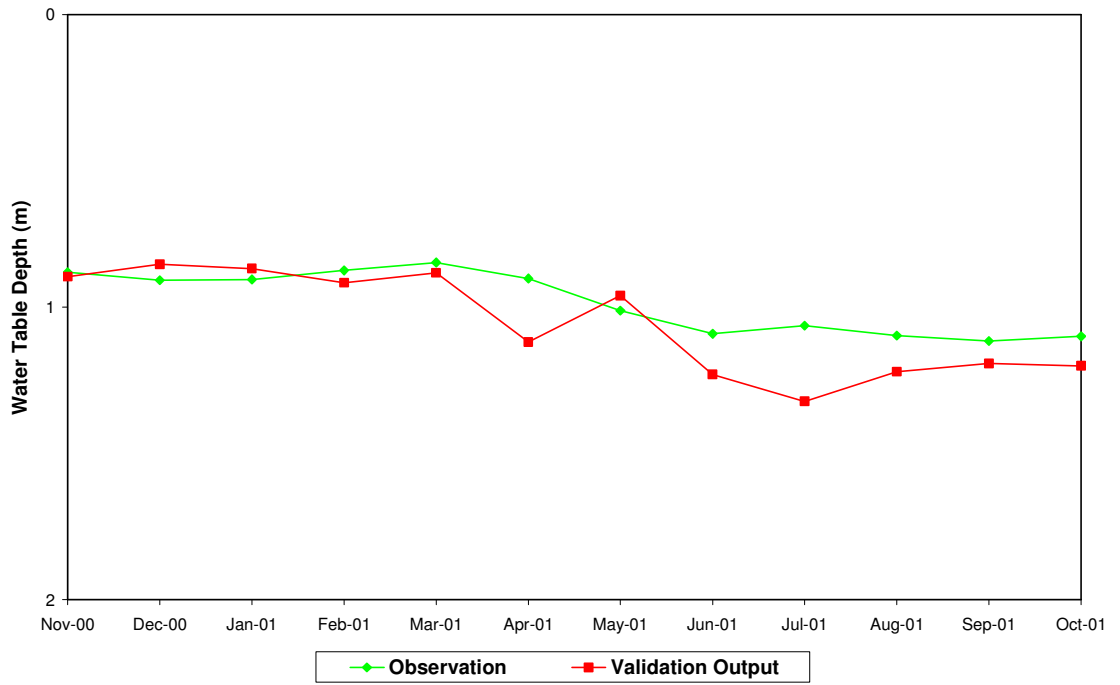
Comparison of Validation Output and Observation at BA Cd 26



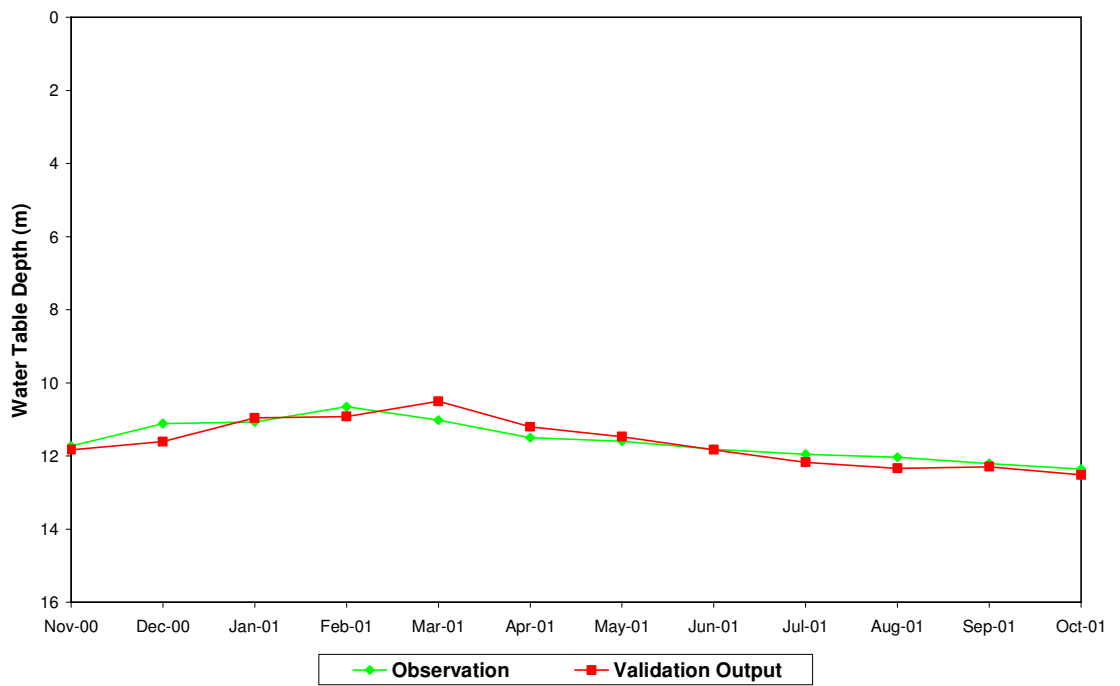
Comparison of Validation Output and Observation at BA Ea 18



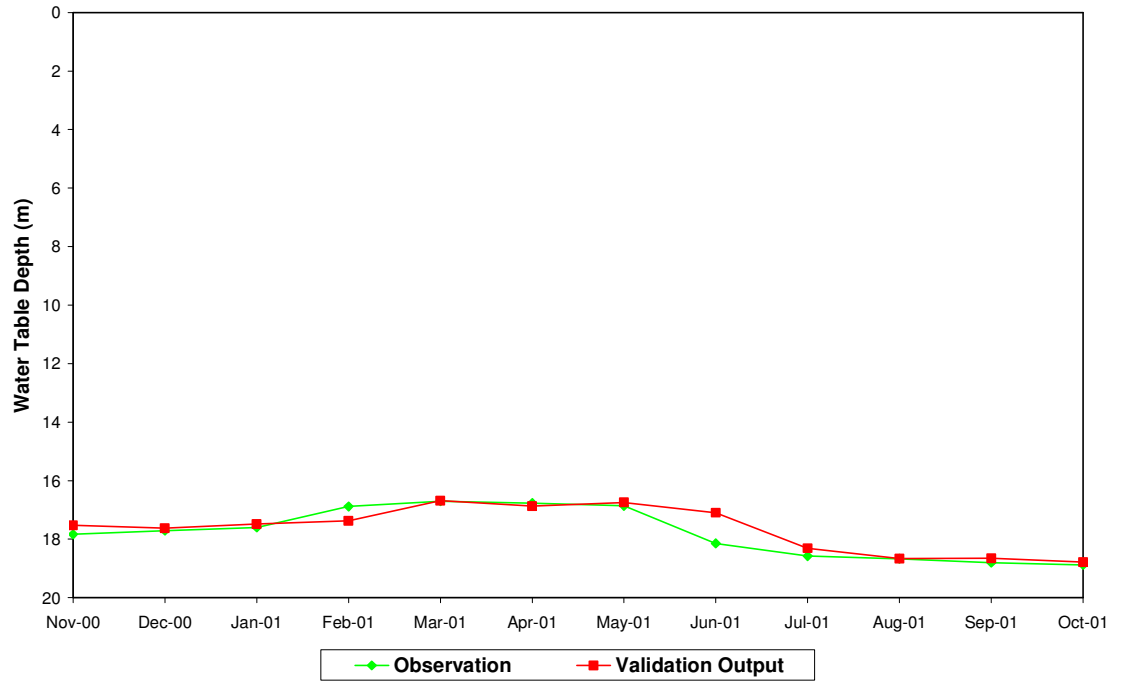
Comparison of Validation Output and Observation at BA Ec 43



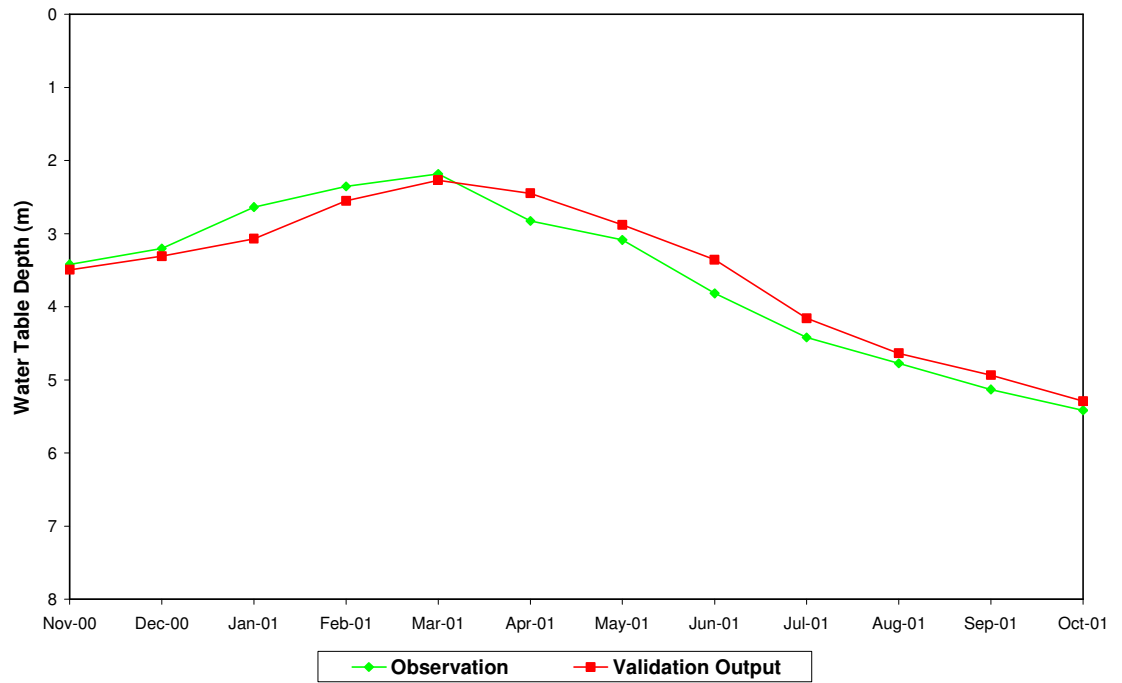
Comparison of Validation Output and Observation at FR Cg 1



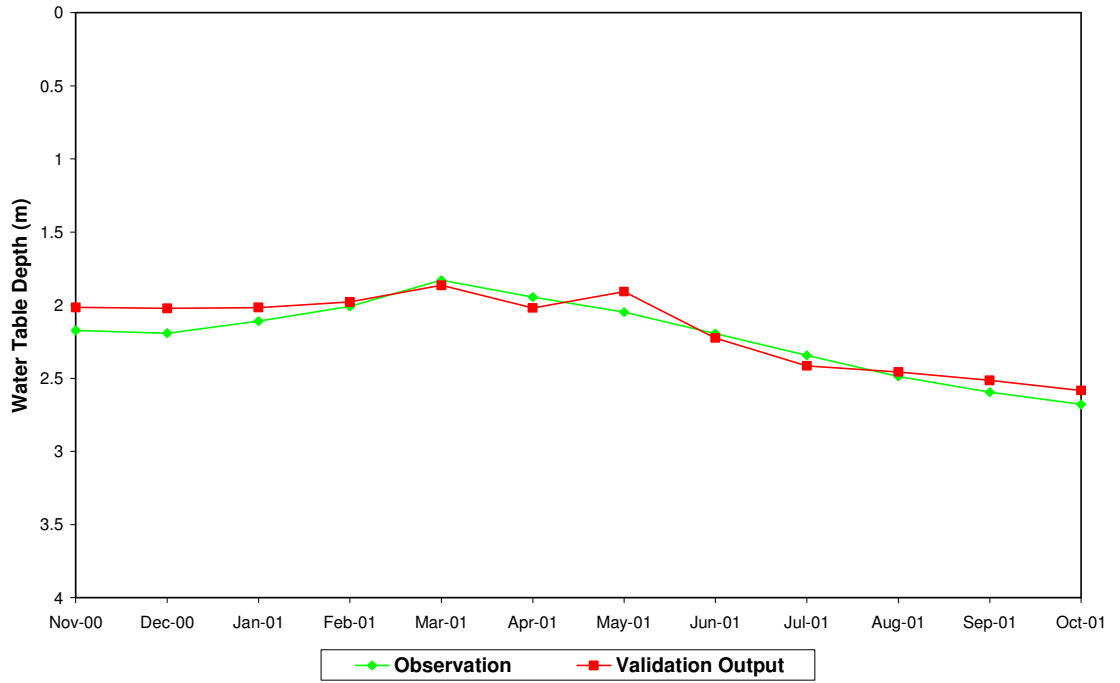
Comparison of Validation Output and Observation at FR Df 35



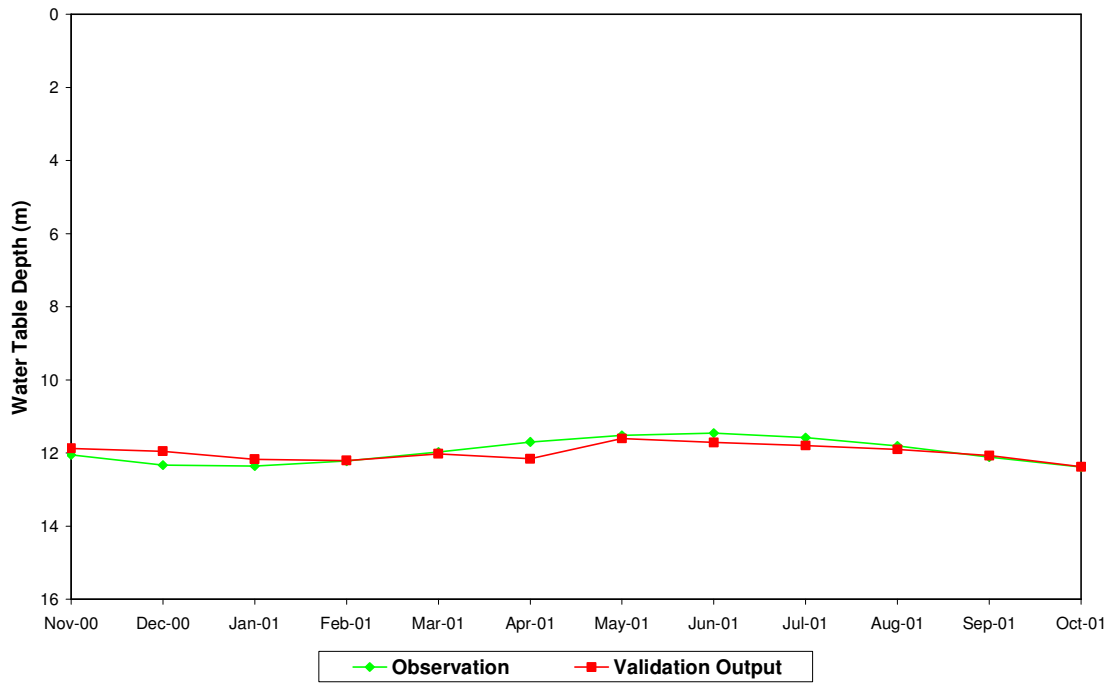
Comparison of Validation Output and Observation at HA Bd 31



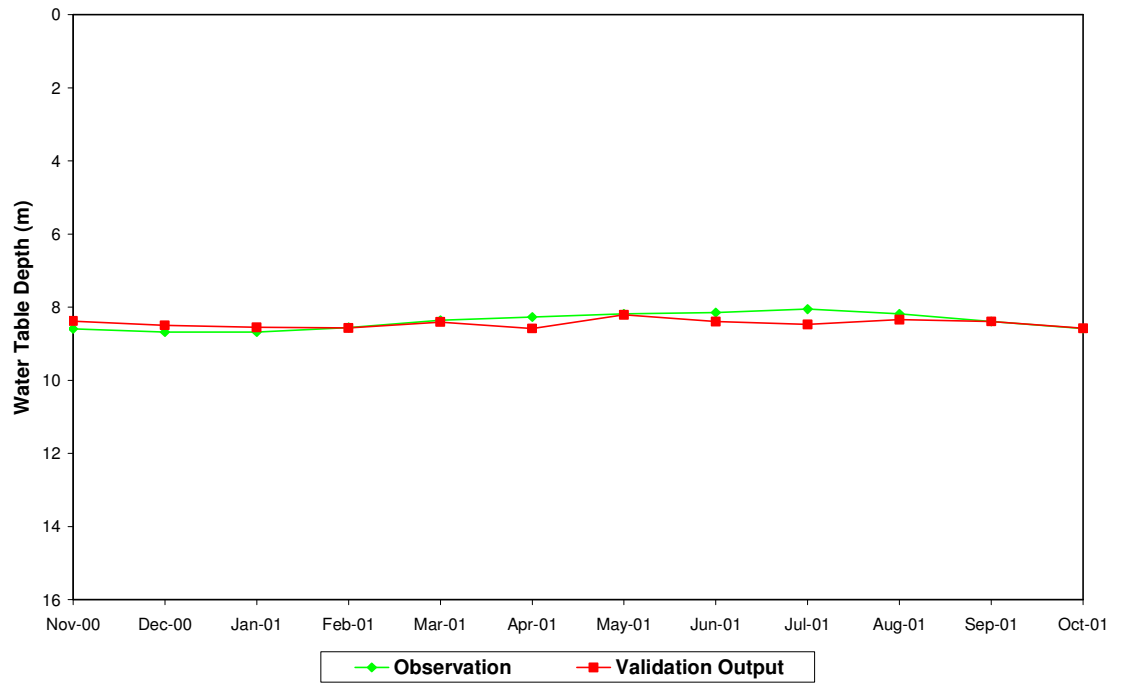
Comparison of Validation Output and Observation at HA Ca 23



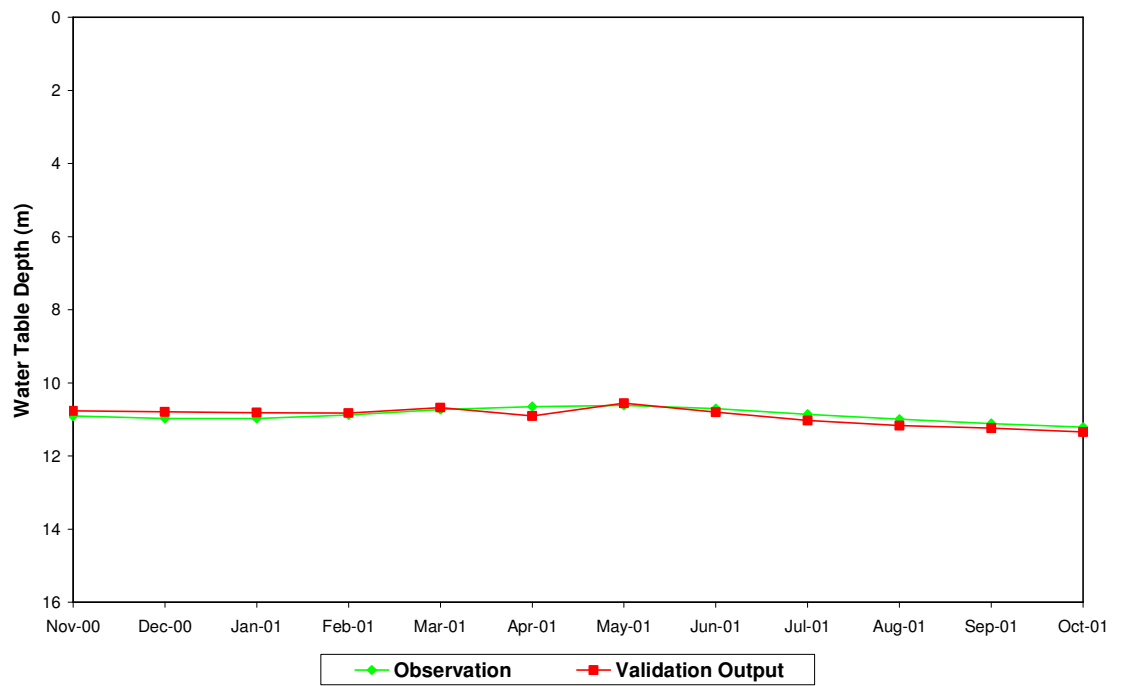
Comparison of Validation Output and Observation at HO Bd 1



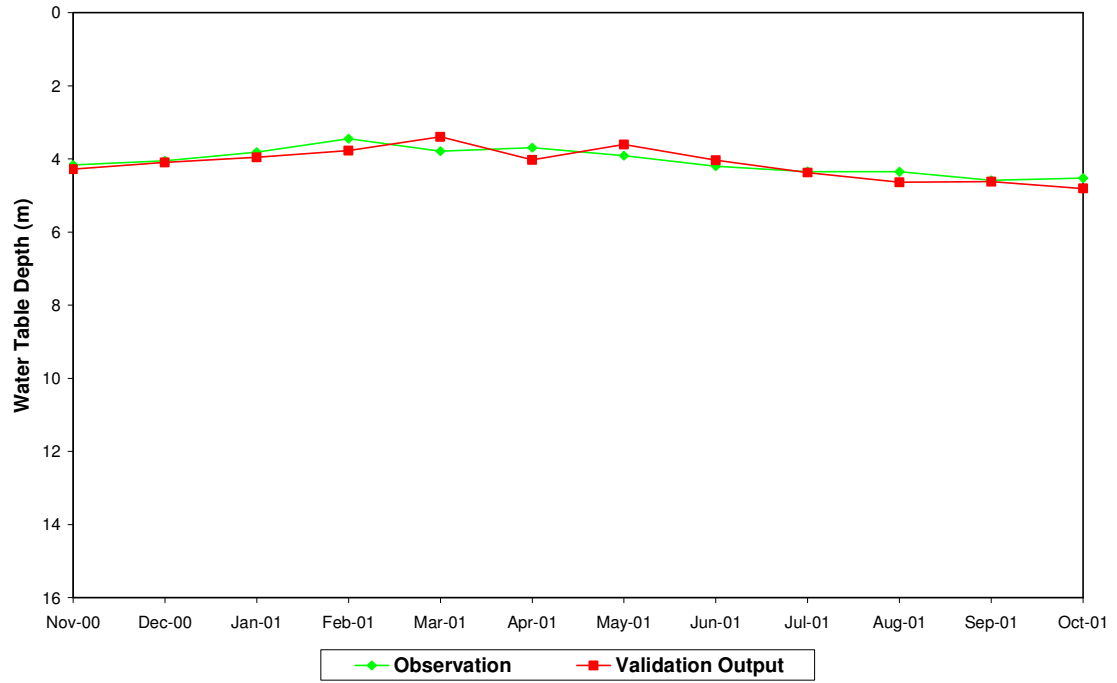
Comparison of Validation Output and Observation at HO Cd 79



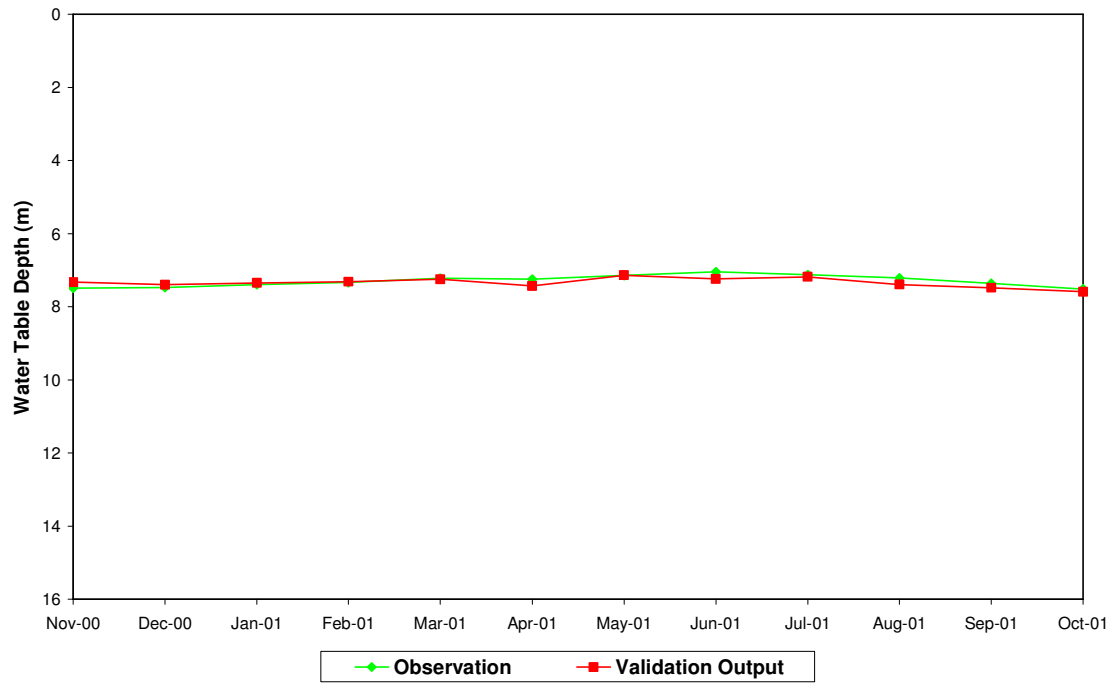
Comparison of Validation Output and Observation at HO Ce 38



Comparison of Validation Output and Observation at MO Eh 20



Comparison of Validation Output and Observation at PG Bc 16



References

- Affandi, A. K., K. Watanabe, and H. Tirtomihardjo. 2007. Application of An Artificial Neural Network to Estimate Groundwater Level Fluctuation, *Journal of Spatial Hydrology*, 7(2): 17-32.
- Anderson, M. P., and W. W. Woessner. 1992. *Applied Groundwater Modeling: Simulation of Flow and Advective Transport*, Academic Press, San Diego, CA, pp.381.
- Antar, M. A., I. Elassiouti, and M. N. Allam. 2006. Rainfall-runoff modeling using artificial neural networks technique: a Blue Nile catchment case study. *Hydrological Processes*, 20(5): 1201-1216.
- ASCE Task Committee on Application of Artificial Neural Networks in Hydrology, *Artificial Neural Networks in Hydrology*. 2000. I: Preliminary Concepts, *Journal of Hydrologic Engineering*, 115 – 123.
- Ashcroft, P., and F. Wentz. 2006. Updated Daily. *AMSR-E/Aqua L2A Global Swath Spatially-Resampled Brightness Temperatures V002*, Mar 2008. Boulder, Colorado USA: National Snow and Ice Data Center. Digital media.
- Ator S. W., and M. J. Ferrari. 1997. Nitrate and selected pesticides in ground water of the mid-Atlantic region, *Water-Resource Investigations Report 97-4139*, USGS.
- Belcher, H. W., and G. E. Merva. 1991. Water table management at Michigan State University, *Pap. Am. Soc. Agric. Eng.*, 19 p.
- Belisle W. R., N. Rajbhandhari, T. Tsegaye, A. Fahsi, A. Manu, Y. Liu, G. Robertson, T. L. Coleman, T. Jackson, P. O'Neill, and M. Collins. 1997. An ideal brightness temperature algorithm for estimating soil profile water status: Part I-algorithm development, *Earth Surface Remote Sensing*, 3222: 180-185.
- Bengtson, R. L., R. S. Garzon, and J. L. Fouss. 1993. A fluctuating water-table model for the management of a controlled-drainage subirrigation system, *Transaction of the ASAE*, 36 (2): 437-443.
- Brunet, R.-C., K. B. Astin, S. Dartiguelongue, and P. Brunet. 2008. The mineralisation of organic nitrogen: relationship with variations in the water-table within a floodplain of the river Adour in Southwest France, *Water Resources Management*, 22(3): 277-289.
- Chen, J. M., B. J. Yang, and R. H. Zhang. 1989. Soil thermal emissivity as affected by its water content and surface treatment, *Soil Science*, 148(6): 433-435.
- Chescheir, G. M., R. W. Skaggs, J. W. Gilliam, and R. O. Evans. 1995. Effects of water table management on water quality, *ASAE*, 3: 61-64.

- Collins, K. M. 2008. Maryland Climate and Historical Temperature Trend Analysis. Master thesis, University of Maryland, College Park, MD.
- Coppola Jr., E. A., A. J. Rana, M. M. Poulton, F. Szidarovszky, and V. W. Uhl. 2004. A neural network model for predicting aquifer water level elevations, *Ground Water*, 43(2): 231-241.
- Coulibaly, P., F. Anctil, R. Aravena, and B. Bobee. 2001. Artificial neural network modeling of water table depth fluctuations, *Water Resource Research*, 37(4): 885-896.
- Crow W. T., and E. F. Wood. 2003. The assimilation of remotely sensed soil brightness temperature imagery into a land surface model using Ensemble Kalman filtering: a case study based on ESTAR measurements during SGP97, *Advances in Water Resources*, 26(2): 137-149.
- Dibike, Y. B., and D. P. Solomatine. 2001. River flow forecasting using artificial neural networks, *Physics and Chemistry of the Earth, part B – Hydrology, Oceans, and Atmosphere*, 26(1): 1-7.
- Dillow, J. J. A., and E. A. Greene. 1999. Ground water discharge and nitrate loadings to the coastal bays of Maryland, *Water-Resource Investigations Report 99-4167*, U. S. Geological Survey.
- EPA. Sep 1998. Climate change and Maryland, Environmental Protection Agency, September, 236-F-98-0071.
- Fausett, L. 1994. *Fundamentals of Neural Networks: Architectures, Algorithms, and Applications*, Prentice-Hall, Englewood Cliffs, NJ.
- Fausey, N. R., A. D. Ward, and L. C. Brown. 1991. Water table management and water quality research in Ohio, *Pap. Am. Soc. Agric. Eng.*, 13 p.
- Freeman, J. A., and D. M. Skapura. 1991. *Neural Networks: Algorithms, Applications, and Programming Techniques*, Addison-Wesley Publishing Company, Reading, MA. 401 p.
- Gallant, S. I. 1993. *Neural Network Learning and Expert Systems*, The MIT Press, Cambridge, MA.
- Gambrell, R. P., J. W. Gilliam, and S. B. Weed. 1975. Denitrification in subsoils of the North Carolina coastal plain as affected by soil drainage, *Journal of Environmental Quality*, 4(3): 311-316.
- Gautam, M. R., K. Watanabe, and H. Saegusa. 2000. Runoff analysis in humid forest catchment with artificial neural network, *Journal of Hydrology*, 235: 117-136.

Graupe, D. 1997. Principles of Artificial Neural Networks. In *Advanced Series on Circuits and Systems – Vol.3*, World Scientific Publishing Company, NJ.

Groundwater Indicators. 2001. Montgomery County, Maryland.

Guix-Hebrard, N., M. Voltz, W. Trambouze, F. Garnier, J. P. Gaudillere, and P. Lagacherie. 2007. Influence of water table depths on the variation of grapevine water status at the landscape scale, *European Journal of Agronomy*, 27(2-4): 187-196.

Gundogdu, K. S., S. T. A. Aslan. 2007. Effects of irrigation system management turnover on water table depth and salinity of groundwater, *Journal of Environmental Biology*, 28(2, Suppl. S): 455-459.

GWPC. 1999. *Ground Water Report to Congress – Summary of State Ground Water Conditions*, Ground Water Protection Council.

Hanks R. J., and R. W. Hill. 1980. Modelling crop responses to irrigation in relation to soils, climate and salinity. Inter. Irrig. Inform. Center, Publ. No. 6, Bet Dagan.

Hanks, R. J. 1992. *Applied Soil Physics: Soil Water and Temperature Applications*, Springer-Verlag, New York, 176 p.

Hanna, K. N. 2006. Integrated Economic Decision Support System Model For Determining Irrigation Application And Projected Agricultural Water Demand On A Watershed Scale. PhD thesis, University of Maryland, College Park, MD.

Haykin, S. 1999. *Neural Networks: A Comprehensive Foundation*, Prentice Hall, Upper Saddle River, NJ. 842 p.

Hebb, D. O. 1949. *The Organization of Behavior*, Wiley, New York.

Hefting, M., J. C. Clement, D. Dowrick, A. C. Cosandey, S. Bernal, C. Cimpian, A. Tatur, T. P. Burt, and G. Pinay. 2004. Water table elevation controls on soil nitrogen cycling in riparian wetlands along a European climatic gradient, *Biogeochemistry*, 67: 113-134.

Hillel, D. 1982. *Introduction to Soil Physics*, Academic Press, San Diego, CA, 364 p.

Hsu, K., H. V. Gupta, and S. Sorooshian. 1995. Artificial neural network modeling of the rainfall-runoff process, *Water Resource Research*, 31(10): 2517-2530.

Hutson, S. S., N. L. Barber, J. F. Kenny, K. S. Linsey, D. S. Lumia, and M. A. Maupin. 2004. *Estimated Use of Water in the United States in 2000*, U. S. Geological Survey. Circular 1268.

Jackson, T. J. 1993. Measuring surface soil moisture using passive microwave remote sensing, *Hydrological Processes*, 7(2): 139 – 152.

- Jain, A., and S. Srinivasulu. 2004. Development of effective and efficient rainfall-runoff models using integration of deterministic, real-coded genetic algorithms and artificial neural network techniques, *Water Resource Research*, 40(w04302).
- Jensen, M. E., Robb, D. C. N., and Franzoy, C. E. 1970. Scheduling irrigation using climate-crop soil data, *ASCE, Journal of Irrigation and Drainage Division*, 96(IR1): 25-38.
- Jeong, D.-I., and Y. O. Kim. 2005. Rainfall-runoff models using artificial neural networks for ensemble streamflow prediction. *Hydrological Processes*, 19(19): 3819-3835.
- Joginder, S., R. Kumar, and S. Rajinder. 1981. Ground water regression model for prediction of water table India, *J. Res. Haryana. Agric Univ. Hissar, India*, 11(4): 528-533.
- Ju Q., Z. Yu, Z. Hao, C. Zhu, and D. Liu. 2007. Third International Conference on Natural Computation: Hydrologic Simulations with Artificial Neural Networks, pp. 22-27.
- Kalita, P. K., and R. S. Kanwar. 1993. Effect of water-table management practices on the transport of nitrate-N to swallow groundwater, *Trans. ASAE*, 36(2): 413-422.
- Kanwar, R. S. 1990. Water table management and groundwater quality research at Iowa State University, *Pap. Amer. Soc. Agric. Eng.*, 10 p.
- Karayiannis, N. B., and A. N. Venetsanopoulos. 1993. *Artificial Neural Networks: Learning Algorithms, Performance Evaluation, and Applications*, Kluwer Academic Publishers, Boston, MA.
- Karunanithi, N., W. J. Grenney, D. Whitley, and K. Bovee. 1994. Neural networks for river flow prediction, *Journal of Computing In Civil Engineering, ASCE*, 8(2): 201-220.
- Kim, G., and A. P. Barros. 2001. Quantitative flood forecasting using multisensor data and neural networks, *Journal of Hydrology*, 246: 45-62.
- Kliewer, B. A., and Gilliam J. W. 1995. Water table management effects on denitrification and nitrous oxide evolution, *Soil Science Society of America Journal*, 59(6): 1694-1701.
- Lagace, R., R. W. Skaggs, and J. E. Parsons. 1982. Predicting water table drawdown for two-dimensional drainage Boussinesq equations, *Advances in drainage: proceedings, Fourth National Drainage Symposium*, 13-14: 6-15.

LDAS. 2008. Mosaic Model Output Information, Land Data Assimilation System. Goddard Space Flight Center, NASA. [Online]. Available WWW: <http://ldas.gsfc.nasa.gov/LDAS8th/Mosaic.LDAS.output.htm>

Liaghat, A., and S. O. Prasher. 1996. A lysimeter study of grass cover and water table depth effects on pesticide residues in drainage water, *Trans. ASAE*, 39(5): 1731-1738.

Lingireddy, S., and G. M. Brion. 2005. *Artificial Neural Networks in Water Supply Engineering*. Published by ASCE Publications.

Maier, H. R., and G. C. Dandy. 1996. The use of artificial neural networks for the prediction of water quality parameters, *Water Resource Research*, 32(4): 1013-1022.

Manglik, A., and S. N. Rai. 2000. Modeling of water table fluctuations in response to time-varying recharge and withdrawal, *Water Resources Management*, 14(5): 339-347.

Maryland at a glance. 2008. [Online]. Available WWW: <http://www.msa.md.gov/msa/mdmanual/01glance/html/Climate>.

Maryland Department of Agriculture. 2001. *Agriculture in Maryland: Summary for 2000-2001*. 54 p.

Maryland Department of State Planning. 1973. *Natural soil groups of Maryland*. Tech. Serv. Publ. No. 199, 153 p.

McCarthy, E. J., and R. W. Skaggs. 1991. A simplified model for predicting drainage rates for changing boundary conditions, *Trans. ASAE*, 34(2): 443-448.

McCarthy, J. J., O. F. Canziani, N. A. Leary, D. J. Dokken, and K. S. White. 2001. *Climate Change 2001: Impacts, Adaptation, and Vulnerability*, Cambridge University Press, Cambridge, UK.

McCulloch, W. S., and W. Pitts. 1943. A Logical Calculus of the Ideas Immanent in Nervous Activity, *Bulletin of Mathematical Biophysics*, 5: 115-33.

Mitchell, K., P. Houser, E. Wood, J. Schaake, D. Tarpley, D. Lettenmaier, W. Higgins, C. Marshall, D. Lohmann, M. Ek, B. Cosgrove, J. Entin, Q. Duan, R. Pinker, A. Robock, F. Habets, and K. Vinnikov. 1999. GCIP Land Data Assimilation Systems (LDAS) project now underway, *GEWEX News*, World Climate Research Programme.

Mitchell, K., C. Marshall, D. Lohmann, M. Ek., Y. Lin, P. Grunmann, P. Houser, E. Wood, J. Schaake, D. Lettenmaier, D. Tarpley, W. Higgins, R. Pinker, A. Robock, B. Cosgrove, J. Entin, and Q. Duan. 2000. The collaborative GCIP land data assimilation (LDAS) project and supportive NCEP uncoupled land-surface modeling initiatives, 15th AMS Conference on Hydrology, 9-14.

- MSCO, 2008. Maryland State Climatologist Office. [Online]. Available WWW: <http://www.atmos.umd.edu/~climate/>
- Munster, C. L., R. W. Skaggs, and V. R. Pemmireddy. 1996. Effect of water table management on the fate of the pesticide aldicarb, *Trans. ASAE*, 39(1): 55-66.
- Narayan, U., V. Lakshmi, and E. G. Njoku. 2004. Retrieval of soil moisture from passive and active L/S band sensor (PALS) observations during the Soil Moisture Experiment in 2002 (SMEX02), *Remote Sensing of Environment*, 92(4): 483-496.
- NASA, 2008. The Community Noah-Surface Model, NASA. [Online]. Available WWW: http://gcmd.nasa.gov/records/NOAA_NOAH.html
- Nash, M. H., L. A. Daugherty, B. A. Buchanan, and B. W. Hunyadi. 1994. The effect of groundwater table variation on characterization and classification of gypsiferous soils in the Tularosa Basin, New Mexico, *Soil Science Society of America*, 35(4): 102-110.
- National Engineering Handbook*. 1985. Section 4, Hydrology, US Department of Agriculture.
- NCEP CFS, 2008. Climate Forecast System, National Centers for Environmental Prediction, NOAA. [Online]. Available WWW: <http://cfs.ncep.noaa.gov/>
- Nelson, M. M., and W. T. Illingworth. 1991. *A Practical Guide to Neural Nets*, Addison-Wesley, Reading, MA.
- NSIDC. 2008. Distributed Active Archive Center, National Snow and Ice Data Center. [Online]. Available WWW: <http://nsidc.org/daac/projects/passivemicro/amsre.html>
- Ogawa K., T. Schmugge, and S. Rokugawa. 2006. Observations of soil moisture dependence of thermal infrared emissivity on soil moisture, *Geophysical Research Abstracts*, 8 (04996).
- Pacanowski, R. C., and S. M. Griffies, cited 1998: MOM 3.0 manual. NOAA/GFDL. [Online]. Available WWW: http://www.gfdl.noaa.gov/smg/MOM/web/guide_parent/guide.parent.html
- Pan, G., C. Wang, H. Wang, and G. Tian. 2000. Microwave emissivity retrieval from SSM/I data over land in China, *Proceedings, IGARSS 2000*, 2: 923 – 925.
- Parker, D. B., *Learning Logic*. Apr 1985. Technical Report TR-47, Center for Computation Research in Economics and Management Science. MIT, Cambridge, MA.

Pellarin, T., J.-P. Wigneron, J.-C. Calvet, and P. Waldteufel. 2003. Global soil moisture retrieval from a synthetic L-band brightness temperature data set, *Journal of Geophysical Research*, 108(D12), 4364.

Peng, P. Xie. 2006. The NCEP Climate Forecast System, *Journal of Climate*, 19(15): 3483-3517.

Philip, J. R. 1957. The theory of infiltration: 4. Sorptivity and algebraic infiltration equations, *Soil Science*, 84: 257-264.

Phillips, S. W., M. J. Focazio, and L. J. Bachman. 1999. Discharge, nitrate load, and residence time of ground water in the Chesapeake Bay Watershed, US Geological Survey. Fact Sheet, FS-150-99.

QNET 2000, Vesta Services, Inc., Winnetka, IL.

Rabunal J. R., and J. Dorrado. 2006. *Artificial Neural Networks in Real-life Applications*. Ideal Group Inc. p.375.

Rai, S. N., and A. Manglik. 1999. Modeling of water table variation in response to time-varying recharge from multiple basins using the linearized Boussinesq equation, 220(3/4): 141-148.

Rai, S. N., and R. N. Singh. 1992. Water-table fluctuations in an aquifer system owing to time-varying surface infiltration and canal recharge, *Journal of Hydrology*, 136(1-4): 381-387.

Rajurkar, M. P., U. C. Kothyari, and U. C. Chaube. 2002. Artificial neural networks for daily rainfall-runoff modeling, *Hydrological Sciences*, 47(6): 865-877.

Rajurkar, M. P., U. C. Kothyari, and U. C. Chaube. 2004. Modeling the daily rainfall-runoff relationship with artificial neural network, *Journal of Hydrology*, 285(1-4): 96-113.

Ramirez, J. A., and B. Finnerty. 1996. Precipitation and water-table effect on agricultural production and economics, *ASCE*, 122(3): 164-171.

Ranjan, S. M., and R. Srinivasan. 1997. Prediction of two-year peak stream discharges using neural networks, *American Water Resources Association*, 33(3): 625-630.

Roulet, N. T. 1991. Surface level and water table fluctuations in a subarctic fen, *Arctic Alpine Research*, 23(3): 303-310.

Rumelhart, D. E., G. E. Hinton, and R. J. Williams. 1986. Learning Internal Representations by Error Propagation. In D. E. Rumelhart & J. L. McClelland, eds., *Parallel Distributed Processing*, vol. 1, chapter 8, Anderson and Rosenfeld, 675-695.

- Saha S., S. Nadiga, C. Thiaw, J. Wang, W. Wang, Q. Zhang, H. M. van den Dool, H.-L. Pan, S. Moorthi, D. Behringer, D. Stokes, M. Pena, S. Lord, G. White, W. Ebisuzaki, P. Sajikumar, N., and B. S. Thandaveswara. 1999. A non-linear rainfall-runoff model using an artificial neural network, *Journal of Hydrology*, 216: 32-55.
- Salehi F., S. O. Prasher, S. Amin, A. Madani, S. J. Jebelli, H. S. Ramaswamy, C. Tan, and C. F. Drury. 2000. Prediction of annual nitrate-N losses in drain outflows with artificial neural networks, *Trans. ASAE*, 43(5): 1137-1143.
- Sarwar, T., and R. S. Kanwar. 1996 NO₃-N and metolachlor concentrations in the soil water as affected by water table depth, *ASAE*, 39(6): 2119-2129.
- SCAN. 2008. Soil Climate Analysis Network, Natural Resources Conservation Service, USDA. [Online]. Available WWW: <http://www.wcc.nrcs.usda.gov/scan/>
- Schmugge, T., P. Gloersen, T. Wilheit, and F. Geiger. 1974. Remote Sensing of Soil Moisture with Microwave Radiometers. *Journal of Geophysical Research*, 79(2): 317 – 323.
- Schmugge, T. 1978. Remote Sensing of Surface Soil Moisture, *Journal of Applied Meteorology*, 17(10): 1549 – 1557.
- Schmugge, T. 1990. Measurements of surface soil moisture and temperature. In *Remote Sensing of Biosphere Functioning* (R.J. Hobbs, and H.A. Mooney, Eds.). Springer-Verlag, New York.
- Schmugge, T. 1998. Applications of Passive Microwave Observations of Surface Soil Moisture, *Journal of Hydrology*, 212 – 213: 188 – 197.
- Schoneman, R. A., H. I. Nightingale, and B. Varnell. 1992. Winter Subsurface drip installation, PAP. American Society of Agricultural Engineering, 5 p.
- Selker, J. S., C. K. Keller, and J. T. McCord. 1999. *Vadose Zone Processes*, Lewis Publishers, Boca Raton, FL, 339 p.
- Shepherd G. M., and C. Koch. 1990. Introduction to synaptic circuits. In *The Synaptic Organization of the Brain*, G. M. Spepherd, ed., pp. 3-31, Oxford University Press, New York.
- Shirmohammadi, A., K. S. Yoon, W. J. Rawls, and O. H. Smith. 1997. Evaluation of curve number procedures to predict runoff in GLEAMS, *Journal of the American Water Resources Association*, 33(5):1069-1076.

- Shirmohammadi, A., I. Chaubey, R. D. Harmel, D. D. Bosch, R. Munoz-Carpena, C. Dharmarsi, A. Sexton, M. Arabi, M. L. Wolfe, J. Frankenberger, C. Graff, and T. M. Sohrabi. 2006. Uncertainty in TMDL Models. *Trans. ASABE*, 494: 1033-1049.
- Shukla, M. B., R. Kok, S. O. Prasher, G. Clark, and R. Lacroix. 1996. Use of artificial neural networks in transient drainage design, *Trans. ASAE*, 39(1): 119-124.
- Singh, R. N., S. N. Rai, and R. N. Ramaua, 1991. Water-table fluctuation in a sloping aquifer with transient recharge, *Journal of Hydrology*, 126(3-4): 315-326.
- Skaggs, R. W. 1980. DRAINMOD, Reference Rep., Raleigh, North Carolina State University.
- Skaggs, R. W., and A. Nassehzadeh-Tabrizi. 1982. Optimizing drainage system design for corn costs, income, North Carolina, *Advances in drainage: proceedings, Fourth National Drainage Symposium*, 13-14.
- Skaggs, R. W. 1991. Modeling water table response to subirrigation and drainage, *Trans. ASAE*, 34(1): 169-175.
- Solley, W. B., R. R. Pierce, and H. A. Perlman. 1998. Estimated use of water in the United States in 1995, U. S. Geological Survey. Circular 1200.
- Song , Z., L. Li, J. Kong, and H. Zhang. 2007. A new analytical solution of tidal water table fluctuations in a coastal unconfined aquifer, *Journal of Hydrology*, 340(3-4): 256-260.
- Srivastava, P., J. N. McNair, T. E. Johnson. 2006. Comparison of process-based and artificial neural network approaches for streamflow modeling in an agricultural watershed, *Journal of the American Water Resources Association*, 42 (3) : 545–563.
- Stanley, C. D., and G. A. Clark. 1995. Effect of reduced water table and fertilizer levels on subirrigated tomato production, *Applied Engineering in Agriculture*, 11(3): 385-388.
- Stephens, D. B.1996. *Vadose Zone Hydrology*, Lewis Publishers, Boca Raton, FL.
- Teloglou, I. S., T. S. Zissis, and D. N. Karamouzis. 1997. Water table fluctuation in soils overlying semi-confined aquifers in response to time-varying replenishment, *Journal of Hydrology*, 202(1-4): 78-94.
- Thiaw, C., and S. Saha. 2007. CFS CMIP T1126L64 Free Coupled Runs: Time Series of Monthly and Daily Data in the EMC/NCEP CFS public server. [Online]. Available WWW: http://cfs.ncep.noaa.gov/cmip126_cfs_data.doc
- Thomas, D. L., P. G. Hunt, and J. W. Gilliam.1992. Water table management for water quality improvement, *Journal of Soil and Water Conservation*, 47(1): 65-70.

Thorpe, N., and A. Shirmohammadi. 2005. Herbicides and Nitrates in Ground Water of Maryland and Childhood Cancers: A Geographic Information Systems Approach. *J. of Environmental Science and Health, Part C*. Vol 23, 261-278.

UNDP, UNEP, World Bank, and WRI. 2000. *World Resources 2000-2001*. World Resources Institute, Washington DC.

UNEP GEO Team. 2002. *Global Environment Outlook 3*, Division of Early Warning and Assessment (DEWA), United Nations Environment Programme, Nairobi, Kenya.

Upadhyaya, A., and H. S. Chauhan. 2001. Water table fluctuations due to canal seepage and time varying recharge, *Journal of Hydrology*, 244(1/2), 1-8.

USGS. 1999. Maryland, US Geological Survey. Fact Sheet 021-99.

USGS. 2000. Physiographic Province Map of Maryland, Delaware, and the District of Columbia, US Geological Survey. [Online]. Available WWW: <http://md.water.usgs.gov/groundwater/physiomaps/>

USGS. 2001. *Water Resources Data : Maryland and Delaware Water Year 2001, volume 2. Ground-Water Data*, US Geological Survey. Water-Data Report MD-DE-01-2.

USGS. 2008. Where is Earth's water located? US Geological Survey. [Online]. Available WWW: <http://ga.water.usgs.gov/edu/earthwherewater.html>

Walker. P.N. 1970. Water in Maryland: a review of the Free State's liquid assets, Maryland Geological Survey Educational Series Report No. 2, 52 p.

Wang, J. R., and B. J. Choudhury. 1981. Remote Sensing of Soil Moisture Content over Bare Field at 1.4 GHz, *Journal of Geophysical Research*, 86(C6): 5277 – 5282.

Wasserman, P. D. 1989. *Neural Computing: Theory and Practice*, Van Nostrand Reinhold, NY, NY.

Werbos, P. J. 1974. Beyond Regression: New Tools for Prediction and Analysis in the Behavioral Sciences. PhD thesis, Harvard, Cambridge, MA.

Werbos, P. J. 1990. Backpropagation Through Time: What It Does and How to Do It, *IEEE*, 78(10): 1550-1560.

Wesseling, J. 1974. Crop growth and wet soils, *Agronomy*, 17: 7-37.

Wheeler, J. C. 1995. Freshwater Use in Maryland. US Geological Survey. Fact Sheet 98-115.

Widrow, B., and M. A. Lehr. 1992. 30 Years of Adaptive Neural Networks: Perceptron, Madaline, and Backpropagation. In *Neural Networks – Theoretical Foundations and Analysis* edited by Clifford Lau, 27-53, IEEE, NY, NY.

Wu, J. S., J. Han, S. Annambhotla, and S. Bryant. 2005. Artificial neural networks for forecasting watershed runoff and stream flows, *Journal of Hydrologic Engineering*, 10(3), 216-222.

Yakowitz, S. 1976., Model free statistical methods for water table prediction, *Water Resources Research*, 12(5): 836-844.

Yang, C. C., S. O. Prasher, and R. Lacroix. 1996. Applications of artificial neural networks land drainage engineering, *Trans. ASAE*, 39(2): 525-533.

Yang, C. C., S.O. Prasher, R. Lacroix, S. Sreekanth, N. K. Patni, and L. Masse. 1997. Artificial neural network model for subsurface-drained farmlands, *Journal of Irrigation and Drainage Engineering – ASCE*, 123(4): 285-292.

Yang, C. C., C. S. Tan, and S. O. Prasher. 2000. Artificial neural networks for subsurface drainage and subirrigation systems in Ontario, Canada, *Journal of the American Water Resources Association*, 36(3): 609-618.

Zhang Q., and S. J. 1997. Stanley, Forecasting raw-water qualityparameters for the north Saskatchewan river by neural network modeling, *Water Research*, 31(9): 2340-2350.

Zealand, C. M., D. H. Burn, and S. P. Simonovic. 1999. Short term streamflow forecasting using artificial neural networks. *Journal of Hydrology*, 214(1-4): 32-48.